McKelvey School of Engineering Theses & Dissertations

McKelvey School of Engineering

5-14-2024

# Coupling Treatment Technologies with Bioelectrochemical Systems to Optimize Resource Recovery from Wastewater

Matthew Stephen Ferby
*Washington University – McKelvey School of Engineering*

WASHINGTON UNIVERSITY IN ST. LOUIS

McKelvey School of Engineering

Department of Energy, Environmental and Chemical Engineering

Dissertation Examination Committee:
Zhen He, Chair
Young-Shin Jun
Xinhua Liang
Fangqiong Ling
Srikanth Singamaneni

Coupling Treatment Technologies with Bioelectrochemical Systems to Optimize Resource
Recovery from Wastewater
by
Matthew Ferby

A dissertation presented to
the McKelvey School of Engineering
of Washington University in
partial fulfillment of the
requirements for the degree
of Doctor of Philosophy

May, 2024
St. Louis, Missouri

## Table of Contents

# List of Figures

# List of Tables

**Acknowledgements**

First, I want to thank God for his unwavering hand over my life. This was not easy. At many points I thought this was impossible. Thankfully, God is the doer of impossible things, so here I am because He is.

Next, I would like to thank my advisor and chair Dr. Zhen He. I first met Dr. He in passing at the 2016 Virginia Tech HBCU/MSI Research Summit. We had a three minute conversation that ended with him handing me information about a paper on Bioelectrochemical systems. From there, we talked every month about attending Viginia Tech for graduate school. One in person meeting, one prospective student weekend, and one acceptance letter later, I committed to Tech and the Environmental Biotechnology and Bioenergy Laboratory (EBBL). Dr. He has been the most supportive advisor, and I cannot imagine navigating this experience without him. His grace, understanding, guidance, drive, and consideration will never go unacknowledged. Thank you for everything, Dr. He. I could not have done this without you.

I also have great gratitude for the members of my dissertation committee – Drs. Young-Shin Jun, Fangqiong Ling, Xinhua Liang, and Srikanth Singamaneni. I want to thank you all for your expertise and time in serving as committee members. Your individual knowledge helped improve my research questions, experimental design, and overall outcomes. I will forever be appreciative.

Next, I want to thank the people I have had the pleasure of meeting at Florida Agricultural & Mechanical University and North Carolina Agricultural & Technical State University. The quantity and quality of people are great, and I would be remiss if I missed anyone. So, to everyone I met via the Marching '100', Rampage Step Team, Eternal Legendary Kingz, ASCE, Cooper Hall (RA Staff & Step Team), Aggie Suites, Tau Beta Pi, Tau Sigma, Student Government and ENGAGE2BE: I thank each of you for your participation in my life.

To the "unsung heroes" at Virginia Tech and Washington University in St. Louis, I say thank you. (VT) Beth Lucas, Jody Smiley, Dr. Aaron J. Prussin II, Dr. Jack Lesko, Holly Lesko, Dr. Tremayne Waller, Renee Cloyd, Lindy Cromwell, (WashU) Monique Spears, Kim Coleman, Megan Morrissey, Tammy Haney, Cindy Alvarez, and Kourtney Shaw. From fellowships to special programming to room reservations, I thank you all for being there time and time again in the many capacities that have cultivated a wonderful matriculation through my graduate degree programs.

To my many friends and many networks at Virginia Tech, I thank you for keeping my head up. Mathue, Meredith, Kory, Haniyyah, the Civil & Environmental Engineering department, New Horizons Graduate Scholars, Janey, Senam, Katrina, Wendell, Daniel, Dwayne, Jalen, Javier, TeAirra, AJ, the Via Scholars, and the Black Graduate Student Organization (BGSO). You all, and many other friends, were phenomenal people to share Blacksburg with from 2017-2019.

To my many friends and many networks at Washington University in St. Louis, I thank you for encouraging me to the finish line. Personally thank you shoutouts to Kaseba, Tyler, Ashlynn, Bryce, Alexandria, Tiana, the Black Graduate Student Association (BGSA), Yao, Weiyi, Jackie, Maria, and the Environmental Engineering Student Association (EnvESA) for the encouragement. All of you and my time in St. Louis, Missouri (2020-2024) will remain in my memories forever.

EBBL, Thank You! Lab mates – Pranav, Yu, Jessie, Harry, Mohan, Syeed, Shiqiang, Akshay, Yanran, Fubin, Zixuan, Bing, Yue, Kaichao, Shruti, Jiasi, and Po – Thank You! The amount of trouble shooting, building, designing, and lab maintenance we have been through together seems surreal. But each of those moments helped solidify you all's places in my life. The kindness, laughter, and consideration will fuel me in my career. To Rohan, Daran, Das, and Wes, thank you for all your help on completing my doctoral work as undergraduate and graduate rotation researchers. It was a pleasure learning and growing with each of you.

To Marjorie Cutter (mother), Marlaina Beaty (sister), and Ellen Ferby (step-mother), I am sure that none of this would be possible if God did not intentionally craft my life to include you. No matter the circumstance, you all served as unconditional, infinite supplies of hope and support. I am empowered to navigate this life I have been given without fear or worry because of you. I will forever position myself to do the best I can because of and for you. Each of you, in your own way, helped me to realize that I am strong, smart, capable, and resilient. And because there are not enough words to express the amount of gratitude I have for each of you, I say thank you with every ounce of my being and I love you from the deepest depth of my heart.

To Stephen Ferby (father), I want to thank you for being present in my life. The laughs and good times of yesteryear to today have helped tremendously during the tough days. To Marcus Ferby (brother), thanks for being there and supporting me in all my endeavors. Also, thank you for being my riding partner on the dozens of rollercoasters throughout our lives. To Rodney Beaty (brother-in-law), Malia Beaty (niece), and Mina Beaty (niece), thank you for your support and the individual joys you bring to our family. I cannot wait to continue to grow and learn as a family. I love each of you.

Finally, I want to say thank you to my extended family, incredible friends (Kneisha, Crystall, Erica, Nashira, Magenta, Spencer, Sekou, and more) and wise individuals that have guided me on this tough journey. Each of you has been a pivotal force in my story. I hold a special place in my heart for all of you.

Matthew Stephen Ferby

*Washington University in St. Louis*

*May 2024*

Dedicated to my ancestors for beating all odds, my grandparents – Horace L. and Willie Mae Cutter (maternal), Nathaniel and Bobbie J. F. Lea (paternal), John, Helen, and Mamie I. Miller (step-maternal) – for raising those that raised me, and God for keeping us all.

ABSTRACT OF THE DISSERTATION

Coupling Treatment Technologies with Bioelectrochemical Systems to Optimize Resource

Recovery from Wastewater

by

Matthew Ferby

Doctor of Philosophy in Energy, Environmental and Chemical Engineering

Washington University in St. Louis, 2024

Professor Zhen He, Chair

Wastewater is a common waste produced from municipal, agricultural, and industrial processes. As the world's population increases, the amount of wastewater produced globally is expected to reach approximately 450 billion $m^3$ in the next two decades. Issues surrounding water, food, and energy accessibility will also become more imminent as the population grows. Interestingly, wastewater is an unconventional source of resources including water, nutrients (e.g., $NH_4^+$ and $PO_4^{3-}$), and energy. However, conventional wastewater treatment processes focus primarily on the removal of containments rather than the recovery of resources.

Bioelectrochemical systems (BES) have the ability to recover resources from wastewater. These engineered systems take advantage of microbial oxidation of organics to generate electricity. Incorporation of ion exchange membranes can also promote the separation of nutrients. Two common types of BES are microbial fuel cells (MFCs) and microbial electrolysis cells (MECs). However, shortcomings including relatively low energy production and high material costs oftentimes deter justification of BES implementation over conventional methods. Other processes and technologies such as forward osmosis (FO), membrane contactor (MC), and thermoelectric

generators (TEGs) have similar issues when comparing the advantages and disadvantages of the recovery system. Coupling BES with other recovery approaches could potentially achieve synergy and optimize resource recovery from wastewater. However, systematic investigation of BES coupled systems to understand their potential as effective recovery systems is insufficient.

This dissertation has three research objectives: (1) investigate forward osmosis as a pretreatment step for microbial fuel cell treatment, (2) explore membrane contactor integration with microbial fuel cell technology as a sustainable resource recovery method, and (3) investigate thermoelectric generators as an alternative power supply for microbial electrolysis cells.

1. Investigate forward osmosis as a pretreatment step for microbial fuel cell treatment. Chapter 2 describes methods used for removal and recovery of reverse fluxed solutes during FO operation. Chapter 3 investigates two draw solutes (NaCl and $NH_4HCO_3$) for FO water recovery and the effects that draw solutes have on coupled MFC performance. Holistic evaluations based on energy consumption, COD removal, ammonium removal and recovery, and water recovery were used to compare the coupled systems.

2. Explore membrane contactor integration with microbial fuel cell technology as a sustainable resource recovery method. Chapter 4 explores MC as a non-energy intensive approach to recover volatile fatty acids (VFAs) and ammonium. The effect osmotic distillation has on VFA and ammonium recovery, economic feasibility, and optimal operation conditions are explored as well. Chapter 5 incorporates MC into MFC treatment to compare air stripping and membrane separation as ammonium recovery methods. Different system configurations and parameters were analyzed to determine optimal operation conditions.

3. Investigate thermoelectric generators as an alternative power supply for microbial electrolysis cells. Chapter 6 presents TEGs as an alternative energy source that can be used to power an MEC for hydrogen generation. First, the TEGs were characterized for performance based on temperature gradient and recirculation rate of the hot and cold sources. Then, the TEG powered MEC was evaluated based on variables including Coulombic efficiency, hydrogen production rate, and maximum power density.

Overall, this dissertation seeks to better understand the synergy that can be achieved by coupling BES with membrane processes and alternative energy sources, as well as how we evaluate these systems in terms of their effectiveness. It also seeks to provide insight on challenges that need to be addressed for real world implementation of these coupled systems.

# Chapter 1
# Introduction

## 1.1  The State of Wastewater

Water is the most important resource on the face of the planet and is necessary in industries such agricultural, pharmaceutical, and energy. However, population growth and concurrent increases in water demand run the risk of limiting our access to water. Consequently, this will also produce more wastewater. It has been estimated that the approximately 300 billion $m^3$ of wastewater produced globally will increase 26% by 2030 and 51% by 2050 [1]. These issues combined will demand novel wastewater handling to offset water stress issues. Wastewater is a complex waste that can be composed of organic matter, nutrients (e.g., nitrogen and phosphorus), heavy metals, pharmaceuticals, and other toxins [2, 3]. Conventional wastewater treatment is usually sufficient to eliminate solid and organic contaminants so natural waterways will not be polluted. This approach to  wastewater handling process, however, does not take advantage of the value-add products that are in wastewater. The development of wastewater processes that can treat wastewater, recover resources, and decrease energy consumption needs to be heavily considered.

Resource recovery has gained attention in the wastewater field because of its potential to counteract the energy cost of wastewater treatment. Various engineering processes such as anaerobic digestion [4], microfiltration, nanofiltration, and reverse osmosis [5] have shown to be effective in recovering nutrients and water from wastewater. For example, one study achieved more than 95% removal of total dissolved salts while operating at 36 LMH water flux. One major challenge that exists is the high energy demand required for their implementation [6]. A common

approach to lessen this energy demand is by using an alternative energy source. The digestion of wastewater sludge is a conventional method for fuel production in the form of biogas. Several approaches including substrate selection and microbiome engineering have been suggested to increase methane generation [7]. Despite the advancement of these technologies, they typically are only applicable for the recovery of a single resource. New technologies that have wide applicability, good efficacy, adaptability, and low energy requirements will help make the implementation of novel approaches more attainable.

## 1.2  Bioelectrochemical Systems

### 1.2.1  History and Types of Bioelectrochemical Systems

Bioelectrochemical systems (BES) are engineered systems that produce electricity through the natural oxidation of organic matter. First, microbes inoculated in the anode chamber oxidize organic matter at the anode electrode [8]. This oxidation releases electrons that flow to the cathode electrode to reduce an electron acceptor. The configuration of the BES determines the electron acceptor that is used. There are four main types of BES including microbial fuel cells (MFC), microbial electrolysis cells (MEC) (Fig. 1.1), microbial electrosynthesis systems (MES), and microbial desalination cells (MDC). BES are oftentimes identified as more sustainable wastewater treatment systems compared to conventional methods because of energy recovery from the estimated 1.93 kWh m$^{-3}$ of stored energy that is in wastewater [9]. BES have been shown to generate electricity from low concentration [10] to high concentration [11, 12] wastewaters with varying compositions of other contaminants [13-15].

**(A) Microbial Fuel Cell**          **(B) Microbial Electrolysis Cell**
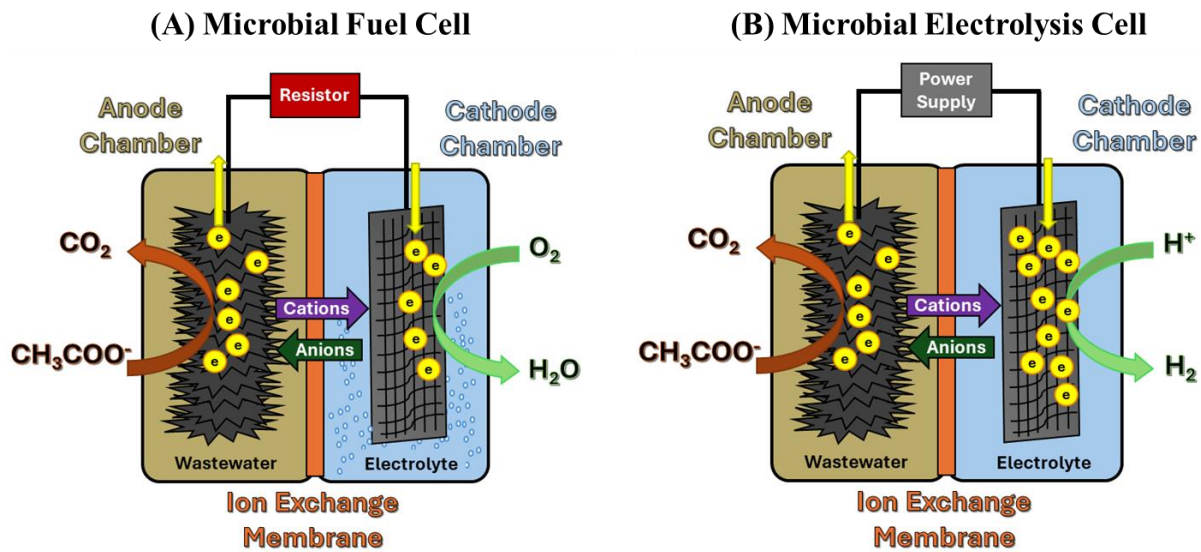
**Figure 1.1** Schematics of two bioelectrochemical systems: (A) microbial fuel cell and (B) microbial electrolysis cell.

## 1.2.2 Specific Function of Microbial Fuel Cells and Microbial Electrolysis Cells

MFCs are the fundamental configuration of BES. MFCs are inoculated with electrogens that oxidize organic matter and reduce oxygen as an electron acceptor. The most well-known bacteria in MFCs are *Geobacter* because of the presence of oxygen [16]. Early studies of MFCs were able to achieve current and power density outputs of 1.21 A m$^{-2}$ and 0.28 W m$^{-2}$, respectively. Since then, studies have explored single and dual chamber configurations to increase MFC performance and capabilities. For example, cylindrical MFCs have been shown to decrease internal resistance of the system which increased the maximum power density to 3.32 ± 0.04 W m$^{-2}$ [17]. The incorporation of an ion exchange membrane can promote the selective removal of key anions (e.g., $PO_4^{3-}$) that move towards the positive anode electrode or key cations (e.g., $NH_4^+$) that move towards the negative cathode electrode [18, 19]. Additionally, MFC technology has also been

incorporated into municipal wastewater treatment systems to investigate their applicability in real world systems [20]. Variability in MFC performance is due to factors including organic loading rate, nutrient loading rate, electrode fabrication, cathodic electrolyte and materials used to build the MFC [21]. Modeling efforts have shown that predicting the performance comes with its own challenges as well. Using kinetic equations and microbial make up to determine the COD removal, pH, Electrical conductivity, current of the MFC based on initial conditions has been investigated [22]. Recently, investigators are using the technology as a biosensor [23]. The evolution of this technology has shown that it can meet the demand of nutrient and energy recovery while being a robust solution for many problems.

MECs are have the additional benefit of generating hydrogen gas by reducing protons [24]. Instead of having a thermodynamically favorable redox reaction like MFCs, MECs require a power source to overcome the overpotential of the hydrogen evolution reaction. This is due to the 0.14 V that is not achieved by the oxidation of organic matter in the anode chamber [25]. MECs also require a special catalyst to help facilitate electron transfer from the cathode to the hydrogen protons. Hydrogen gas generation has great attention due to its potential use as a green fuel source compared to traditional oil. Platinum is the most common catalyst used in MECs because of its high surface area and low contribution to resistance due to material in the system [26]. Systems with Pt electrode have achieved 0.8 $m^3$ $H_2$ $m^{-3}$ $d^{-1}$ hydrogen yields combined with additional strategies to enhance hydrogen gas production to 1.3 $m^3$ $H_2$ $m^{-3}$ $d^{-1}$ in the cathode chamber [27]. MECs have also been shown to be applicable for the treatment of fermentation products, sludge and food waste while maintaining good hydrogen gas yield [28]. The power source used in most MEC studies is a traditional power supply. Other studies have explored more renewable energy source such as wind [29], solar [30], and hydro [31] power.

### 1.2.3 Challenges of Microbial Fuel Cells and Microbial Electrolysis Cells

Despite the advantageous qualities of BES, they have some disadvantages that make the technology less attractive for resource recovery. MFCs still have relatively low energy production compared to traditional energy sources. Treatment of low strength wastewaters also reveals a challenge for MFC. Due to low organic concentrations, MFCs that treat municipal wastewater have only show maximum power densities and average Coulombic efficiencies of less than ~20 W m$^{-3}$ and 18%, respectively. Another common problem is the internal resistance of BES. Increasing the internal resistance via insufficient electrolytes, materials used for constructing the BES, immature biofilms or microbiomes will decrease electrical performance [32]. For MEC specifically, high material cost for catalyst such as platinum and the need for an external power source are considered significant challenges. Platinum is a well established material that is able to facilitate electron transfer for the generation of hydrogen gas but it has negative environmental impacts (i.e., toxicity and material degradation by common wastewater constituents), that deter from its use in real systems [33]. Additionally, it is estimated that MECs will consume an additional 0.56 kWh m$^{-3}$ compared to MFC, which will drive up the energy consumption of the system [34]. This has been suggested to be a factor only for lower applied voltages [35], but the energy efficiency drops promoting the over use of energy. The handling or use of hydrogen gas produced by MECs has also been questioned. A shared concern for the technology is in scaling up the systems [36-39]. Increasing the size of the system will require more materials that increase resistance within the system, decrease access to substrate (e.g., oxygen or organics), and major operational and capital cost. These are just a few issues that need to be systematically investigated and resolved before BESs are a viable technology.

# 1.3   Other Technologies for Wastewater Treatment

## 1.3.1  Forward Osmosis

Forward osmosis is a membrane process that is employed to recover water from a wastewater source. This water recovery method operates similarly to the natural phenomenon. Water moves across a semipermeable membrane from a low saline solution (feed) to a highly saline solution (draw) due to a difference in their osmotic pressures [40]. The most common membranes used in FO studies are cellulous triacetate (CTA) and thin film composites (TFC) [41]. Various salts  and other matter have been used to generate the draw solution. This was first considered for wastewater treatment using a NaCl draw solute. Now, novel magnetic particles and fertilizer have been identified as sustainable draw solutes for FO operation. The most appealing trait of FO treatment is its low energy demand. Reverse salt flux is an inevitable occurrence in FO treatment. RSF is the movement of salt from the draw moving into the feed [42]. Draw solutes reverse flux differently based on their characteristics (e.g., hydrated radius, oxidation state, volatility). This can cause internal and external concentration polarization which decreases the effects of osmotic pressure differences to motivate water transport across the membrane [40]. Membrane fouling is also a disadvantage of FO that decreases water flux. Fouling has been shown to occur due to solution membrane interactions that cause build up on or within the membrane structure [43].

## 1.3.2 Membrane Contactor

Membrane Contactor (MC) is a treatment option that has had growing interest because of its good recovery and low energy consumption (Figure 1.2). Carbon capture from the atmosphere has been

6

the main application considered for MC [44-46]. Other pollutants such as sulfur dioxide, alcohols, ammonia, and volatile fatty acids (VFAs) have been considered in recent studies for MC separation from air and aqueous waste streams. Polypropylene (PP), polytetrafluoroethylene (PTFE), and polyvinylidene fluoride (PVDF) are three types of membranes used for MC separation. Unlike membrane distillation (MD) which requires a thermal gradient to recover water, MC operates if a pH gradient exist so that the gaseous form is released from the feed and absorbed in the aqueous form in the permeate. Despite the lack of additional energy demand like comparable methods such as MD and electrodialysis (ED), high recovery of nutrients such as ammonium and VFAs. For example, a PP-polyethylene hollowfiber member was able to achieve 99% ammonium recovery (feed pH>11) [47]. Selectivity, membrane fouling and decreased recovery times of larger compounds such as VFAs raises concern in its overall effectiveness. This was is made evident in one study that showed VFA migration rates increase for acetate (0.04 to 0.43 mg cm$^{-2}$ h$^{-1}$) when 20 V was applied [48]. Recent studies have begun to investigate scaling up MC to understand performance of large systems[49].

### 1.3.3 Thermoelectric Generators

Thermoelectric generators (TEGs) are an alternative energy source that convert heat energy into electrical energy. TEGs are double plated, semiconductor composites that require a temperature gradient between the two interfaces to work. The two types of semiconductors (n-type and p-type) are connected in series. The movements of electrons due to the temperature gradient is known as the Seebeck Effect. Industrial machinery, auto manufacturing [50], network sensors [51], and aerospace systems have already investigated TEGs as potential energy generators. Thermal conductivity is the passage of heat from the hot source to the cold source, which decreases the

temperature gradient and the TEG voltage output. Factors including TEG composite material and TEG structure can alter the effects of thermal conductivity [52]. For example, higher thermal conductivity was observe in one study when particle sizes were 250 nm ($0.13 \text{ W m}^{-1} \text{ K}^{-1}$) to 5 nm ($0.13 \text{ W m}^{-1} \text{ K}^{-1}$) [53]. While TEG fabrication techniques are used to mitigate thermal conductivity, some studies utilize the drawback to have better thermal to electrical energy conversion performance [54].
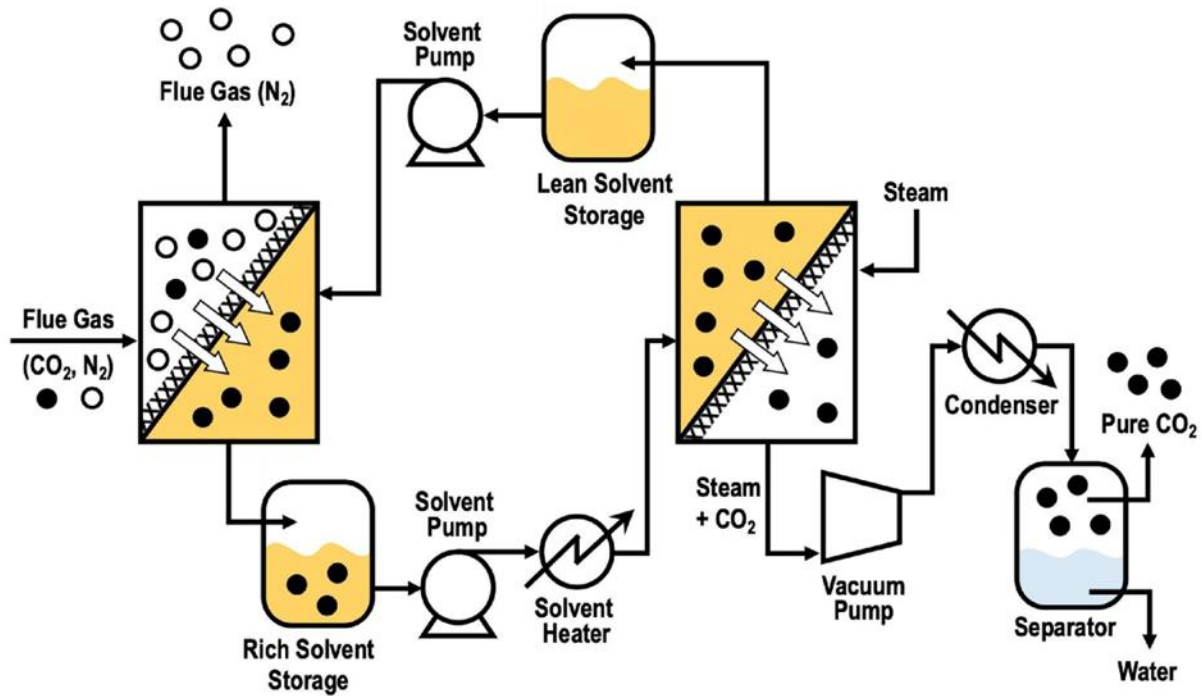


**Figure 1.2** Process flow diagrams of membrane contactors for $CO_2$ capture from flue gas. Figure utilized from a previous study with permission [55].

**Table 1.1** Treatment option and technology advantages and disadvantages

| Treatment Option or Technology | Advantages | Disadvantages |
|---|---|---|
| Microbial Fuel Cell | • Sustainable chemical to electrical energy conversion [21]<br>• Various application for various wastewaters [36, 37]<br>• Nutrient Removal and Recovery with use of ion exchange membranes [36, 56]<br>• Mixed microbial communities provide robust treatment [57] | • Relatively low energy production [36, 37]<br>• Overpotential issues [21]<br>• Internal resistance due to material and electrolyte [21]<br>• Scaling up issues [36, 37] |
| Microbial Electrolysis Cell | • Hydrogen generation [24, 33, 58]<br>• Various application for various wastewaters [58]<br>• Nutrient removal due to high electron flow to cathode [38, 59] | • Requires high-cost material (e.g., platinum) [33, 38]<br>• External power source [39]<br>• Scaling up issues [38, 39] |
| Forward Osmosis | • Fresh water recovery from wastewater [40, 60, 61]<br>• Concentrate contaminants [60, 62]<br>• Less energy intensive than other membrane processes (e.g., RO and NF) [40, 61] | • Reverse Solute Flux [40, 43]<br>• Internal and External Polarization [40]<br>• Membrane Fouling [43, 61]<br>• Irreversible membrane fouling [43] |
| Membrane Contactor | • Nutrient, volatile fatty acid, gas, and alcohol recovery [63, 64]<br>• Athermal separation process [63]<br>• Low investment and labor for scaled up systems [44, 65]<br>• Metal removal capabilities [63, 66] | • Selective Separation [67]<br>• Membrane Fouling [44, 64]<br>• Plasticization decreasing permeability [44, 68] |
| Thermoelectric Generator | • Sustainable energy source (heat to electrical) [69, 70]<br>• Only requires small temperature gradients [71, 72]<br>• Long term stability [71] | • Requires adequate heat source/heat gradient [73]<br>• Low conversion efficiency [72, 74]<br>• High production cost [70]<br>• Knowledge gap in systematic application studies [69] |

# 1.4 Outline

The technologies presented have a variety of advantages and disadvantages that can promote or deter from their individual implementation into the real world (Table 1.1). The purpose of the work compiled in this dissertation is to further understand the synergistic behaviors between BES and other technologies. Coupling these systems will seek to improve BES performance and optimize resource recovery from wastewater. In order to achieve that goal, this work has been separated into 7 chapters covering 3 main objectives: First, the difference of draw solute removal and recovery is explored in a systematic review (Chapter 2). Draw solutes have different properties that affect how they are handled after FO treatment. Physical, chemical, and biological removal are oftentimes employed to attenuate salt accumulation. Solute recovery via air stripping or membrane processes are applied to create a circular system that regenerates the draw solution necessary for water recovery during FO. Next, $NH_4HCO_3$ and NaCl are evaluated as draw solutes for a FO+MFC system (Chapter 3). The coupled system is evaluated using 5 parameters: energy consumption, chemical oxygen demand (COD) removal, ammonium removal rate, ammonium recovery rate, and water recovery. This study also elucidates the implications of draw solute selection for coupled FO+MFC systems. The second objective investigated the use of MC incorporated into MFC. First, pure MC was utilized to recover VFAs and ammonium using a hollow fiber membrane (Chapter 4). The effects of osmotic distillation on resource recovery across a gas permeable membrane were explored. This study also utilized multi-criteria decision making to determine the optimal operation conditions to recovery VFAs and ammonium. Then, the MFC integrated with MC was evaluated for its ability to recover ammonium compared to air stripping (Chapter 5). Different configurations were considered to optimize ammonium recovery during MFC operation. Aeration and absorption solution strength were evaluated on their effectiveness to promote ammonium recovery from the

catholyte. The third objective explored how to achieve more sustainable hydrogen production from MEC treatment. TEGs were used as the power source for the treatment of a synthetic brewery wastewater in the MEC (Chapter 6). The TEGs were characterized under different temperature gradients, recirculation rates, and heat sources and sinks. The TEG-MEC was also compared to a traditional MEC powered by a power supply to determine the benefits of the alternative energy source.

# 1.5 Attributions

All authors are credited for their expertise in their respective areas that helped develop and complete this work.

Zhen (Jason) He, Ph.D.

(Principal Investigator)

Department of Energy, Environmental and Chemical Engineering, Washington University in St. Louis. St. Louis, Missouri, 63112, USA.

Chapters 2-6

Shiqiang Zou, Ph.D.

Department of Civil and Environmental Engineering, Auburn University. Auburn, Alabama, 36849, USA.

Chapter 2-3

# Chapter 2

# Reduction of Reverse Solute Flux Induced Solute Buildup in the Feed Solution of Forward Osmosis

**Abstract**

Forward osmosis (FO) has shown advancement towards recovery of useful water from various waste streams. A major issue that arises is the accumulation of salts due to reverse solute flux (RSF) from a draw solution into a feed solution that can result in several negative effects such as decreased water flux and inhibiting biological activities. This paper aims to provide a concise discussion and analysis of methods that can help to alleviate the effects of solute build up. New parameters, solute removal/recovery rate (SRR) and removal/recovery ratio (ReR), are proposed to help better define the performance of reducing solute buildup and employed in case studies to evaluate the selected reduction methods. Solute removal can be accomplished by physical separation, chemical precipitation, and biological removal. Recovery of solutes, one step beyond removal, is discussed and demonstrated by using bioelectrochemical systems and electrodialysis as examples. This work has highlighted the concerns associated with solute buildup and encouraged further exploration of effective tools to mitigate solute buildup for improved performance of FO-based water/wastewater systems.

**Keywords:** Forward osmosis; salinity buildup; concentrating effect; reverse solute flux; solute removal or recovery

## 2.1 Introduction

The perception of wastewater being a waste has been altered to it being a resource due to burgeoning technologies and processes for recovering valuable resources (e.g., energy and fresh water) from wastewater [75]. Recovery of useful water from wastewater, for potable or non-potable use, will help to address the challenge of water shortage, especially in the area where freshwater supply is limited [76]. To accomplish wastewater reuse, emerging membrane technologies such as forward osmosis (FO) can play an important role. FO is a system that relies on the natural osmosis phenomenon and a semi-permeable membrane to extract water driven by an osmotic pressure gradient [61]. Various wastewaters such as municipal [77, 78], agricultural [79, 80], medical, and mining [81] wastewaters have been examined in FO studies to determine best application practices for wastewater treatment and reuse. FO technologies have also been investigated to concentrate heavy metals, such as copper, mercury, and lead, within specific wastewaters to facilitate further resource recovery [82]. Bench-scale FO experiments have evolved to pilot-scale tests that utilize fertilizer as draw solutes to eliminate the need for regeneration [83-85].

Despite the promise for water/wastewater treatment, practical applications of FO are still limited by some challenges. Among them, reverse solute flux (RSF) is an inherent limitation of FO membranes but has received less attention than membrane fouling. RSF describes the movement of draw solute (DS) permeating through FO membrane from a draw solution to a feed solution [86]. The most commonly used membranes in FO studies include thin film composites

(TFCs) and cellulose triacetate (CTA). It has been suggested that RSF can be influenced by the deposition of materials on the surface via interaction with the feed solution's constituents and DS [87]. In addition, the amount of RSF depends on DS characteristics and operating conditions, as well. For example, the RSF of NaCl DS (approximately 2.34 gMH) can be very different from other inorganic DS such as $MgCl_2$ and $MgSO_4$ (approximately 2.86 and 1.20 gMH, respectively) under similar experimental conditions [88]. The most notable direct effects of RSF include loss of DS and decrease in water flux. For example, when 1 M $NH_4HCO_3$ DS was used to recover water from treated leachate, the water flux decreased from 3.3 LMH to less than 0.6 LMH after 3.5 hours of operation due to rapid loss of DS via RSF. Therefore, reducing RSF is critically important to FO operation, and the mitigation tactics such as membrane fabrication/modification and selection of suitable DS have been discussed in a recent review paper [89].

Besides direct effects, RSF can also lead to unfavorable consequences such as the accumulation of DS in the feed solution (i.e., the solute buildup). Note that solute buildup or DS buildup from RSF is a part of salinity buildup in an FO operation, as the latter also includes the concentrating effect (CE) of other substances in the feed solution caused by membrane rejection (Fig. 2.1). For a standalone FO process, a higher-salinity solution from both RSF and CE could lead to increased fouling issue on the FO membrane [90], leading to deteriorated water extraction performance caused by potential pore blockage, additional water transport resistance, and enhanced concentration polarization [91, 92]. Efforts have been made to quantify and predict these phenomena [93], but the lack of application of this mathematical model demands additional research to establish validity. Quantifying the salinity buildup will be important to understand how to properly treat DS-polluted feed solution [94]. For an integrated FO process with biological treatment (e.g., osmotic membrane bioreactor - OMBR), continuous solute/salinity buildup would

inhibit microbial activities, resulting in decreased wastewater treatment performance. For instance, integration of FO with anaerobic membrane bioreactor exhibited a highest RSF of 12.21 gMH when $KNO_3$ fertilizer was selected as DS, leading to severe solute buildup and 75% less of methane production compared to the control system [95]. The accumulation of NaCl DS in the feed solution resulted in decreased $NH_4^+$ removal (40% reduction) due to microbial inhibition [96]. Therefore, proper strategies to control the solute buildup due to RSF will be of strong interest and importance.
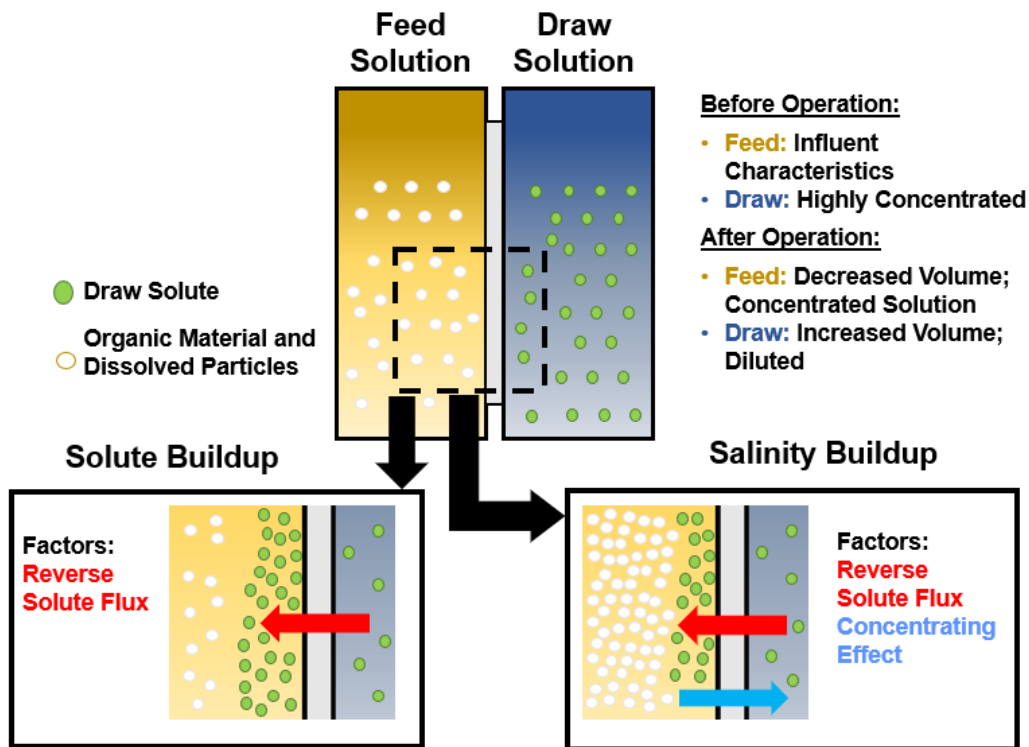


**Figure 2.1** Differences between solute buildup and salinity buildup in FO based systems as it relates to dissolved particles permeating across FO membranes.

Although some efforts have been invested to reduce solute buildup in the feed solution, there is a significant gap in literature on comprehensive description and assessment of solute removal and recovery technologies and their effectiveness. The main objective of this paper is to provide a concise discussion and analysis of those technologies that can help reduce solute buildup

15

towards optimal performance and water recovery in FO-based systems. The terms "salinity" and "solute" are used interchangeably in the present paper, assuming that the initial solute compound in the feed solution can be negligible. There is also a need to better compare solute accumulation and develop a quantification parameter to evaluate solute removal/recovery. Because of a lack of necessary information in the literature, we have created two case studies with appropriate assumptions to demonstrate the necessity of reporting RSF and solute removal or recovery in FO systems. Some discussions were limited to the examples of OMBRs because a few studies on this subject provide enough details for us to analyze and discuss. We also went beyond removal and discussed potential methods for solute recovery that may be reused directly or indirectly in FO applications via bioelectrochemical and electrochemical techniques as examples of recovery methods. It should be noted that this paper is about the mitigation of a key effect of RSF – accumulation of reverse-fluxed draw solute, instead of mitigation of RSF that has been discussed before.

## 2.2  Quantification of Solute Buildup

### 2.2.1  Common FO Parameters

Water flux ($J_w$, L m$^{-2}$ h$^{-1}$, LMH) is to quantify the amount of water that can be recovered from a feed solution and described by Eq. (1).

$$J_W = \frac{V_f - V_i}{A \times \Delta t}$$

(1)

where $V_f$ and $V_i$ represent the final and initial volumes (L) of the draw solution, respectively; A is the surface area (m$^{-2}$) of the membrane that water permeates across; and $\Delta t$ is the operation time (h$^{-1}$).

Reverse solute flux (RSF) ($J_S$, g m$^{-2}$ h$^{-1}$, gMH) presents the amount of DS that permeates the FO membrane to the feed solution and can be calculated by using Eq. (2).

$$J_S = \frac{C_f V_f - C_i V_i}{A \times \Delta t} \tag{2}$$

where $C_f$ and $C_i$ are the final and initial concentration (g L$^{-1}$) of solute in the draw solution, respectively.

Specific reverse solute flux (SRSF) is used to compare the movement of solute to movement of water [97], and expressed as Eq. (3).

$$SRSF = \frac{J_S}{J_w} \tag{3}$$

Membrane rejection ($R$) is determined under a condition of continuous operation by using the feed and permeate concentrations of a pollutant of interest [98] and can be calculated by using Eq. (4)

$$R = \frac{C_F - C_P}{C_F} \times 100\% \tag{4}$$

where $C_F$ and $C_P$ (mol L$^{-1}$) are the concentrations in the feed solution and permeate (draw solution), respectively. In batch FO systems, it is more appropriate to use total mass of the DS in the solution to calculate the rejection or RSF-water flux ratio described by Jin et al. (2011) [99].

The driving force for FO is based on the osmotic pressures ($\pi$) of the feed and draw solutions [100], calculated using Eq. (5)

$$\pi = iMRT, \tag{5}$$

where the variables are the gas constant ($R$), the solution's van't Hoff factor ($i$), M (mol L$^{-1}$), and temperature, $T$.

Other FO parameters that have been discussed in previous studies include solute buildup (SBU) and concentrating effect (CE). Both variables are used as a mean to define solute concentration in the feed solution. SBU and CE are listed as Eqs. (A.1 and A.2) and are provided in the supplementary materials (Appendix A).

## 2.2.2 Solute Reduction or Recovery

While the above parameters can quantitatively describe the performance of an FO process, a parameter to evaluate solute reduction or recovery is still missing. Herein, we proposed the solute reduction/recovery rate (SRR) to help establish a measure that can be used to compare the efficacy of solute reduction or solute recovery between FO studies. SRR (g m$^{-2}$ h$^{-1}$) is derived from Eq. (2) to show how much of solute is removed or recovered compared to how much permeates the membrane from the draw solution, expressed in Eq. (6).

$$SRR = \frac{m_{DS,recovered}}{A \times t} \; or \; \frac{m_{DS,removed}}{A \times t} \tag{6}$$

where $m_{DS,\,recovered}$ (g) is the mass of DS that is recovered from the feed solution, and $m_{DS,\,removal}$ is the mass of DS that is removed from the feed solution. How the mass is determined is based on the recovery or removal technique and vary between different measurement and quantitative approaches. The solute recovery/removal ratio (ReR) can be quantified by using Eq. (7).

$$ReR = \frac{SRR}{RSF} * 100\% \tag{7}$$

This ratio (%) can describe the amount of DS that is removed or recovered from the feed solution compared to the amount of DS that is reverse-fluxed. A potential obstacle in applying the SRR

equation is how to quantify DS. Inorganic DS are commonly quantified by using conductivity measurement [101, 102]. Organic DS are increasingly being considered as an attractive alternative for FO water treatment [103-105], but conductivity measurement is less reliable to quantify organic DS. Total carbon or chemical oxygen demand (COD) is suggested to better quantify the concentration of organic DS [106].

In this paper, two case studies in section 3.1 and 3.2 were created to understand the potential application of SRR and ReR. We did not extend those parameters to other sections because of lacking necessary data/information (e.g., RSF data) in literature; this should not be interpreted as that those parameters are not applicable to other (abiotic) removal/recovery processes.

## 2.3 Removal of Accumulated Solute

### 2.3.1 Physical (membrane) removal of solute

The migrated solutes via RSF can be removed by physical separation, mostly via membrane filtration (Table 2.1), for example coupling microfiltration (MF) or ultrafiltration (UF) with FO [107]. Physical separation is possible because MF/UF membrane pore sizes are selective in allowing reverse-fluxed DS in the feed solution to flow across the membrane while rejecting larger constituents such as suspended biomass. This selectivity allows overly accumulated solutes to leave the bulk (feed) solution, creating a permeate solution containing solutes. In an OMBR, MF was installed to reduce the concentration of salt in the biological system (feed side) (Fig. 2.2A). When the MF flow rate increased from 1 to 2 L d$^{-1}$, the mixed liquor electrical conductivity was reduced by half and remained stable for over 40 days, as shown in Fig. 2.2B [108]. The decreased solution conductivity could help to reduce fouling propensity with decreased adsorption of carbon material [109] and reduce the formation of biofilms on membranes [110]. Decreasing the

conductivity of the feed solution via physical separation would also help to maintain a greater osmotic pressure difference between the feed and draw solutions, resulting in more water flux. It was reported that in the absence of physical removal, water flux was observed to decrease by nearly 50% when the conductivity of the feed solution increased from 268 to 8270 $\mu S\ cm^{-1}$ after 7 days of operation; introducing MF has helped to retain the conductivity around 700 $\mu S\ cm^{-1}$ with a lessened decline in water flux for a duration of 60 days [122]. A pilot scale system showed relatively comparable results (4.8 LMH and steady conductivity of 1.6 mS $cm^{-1}$) to that of the bench scale studies and thus verified the effectiveness of physical removal for potentially large-scale implementation of FO technology.

To better understand the performance of physical separation, we employed SRR and ReR in a defined case based on data from the published literature and some assumptions under steady state conditions. In this case, an OMBR with an effective volume of 8.5 L utilized MF to remove the reverse-fluxed DS ($MgCl_2$) (Fig. 2.3A) [123]. The data from the period when MF was in operation were used in the SRR and ReR calculation. We assumed an MF water flux of 8.44 LMH and an effective membrane area of 0.0754 $m^2$ based on the data of MF flux versus FO flux [124] and osmotic pressure data for different draw solutes at 1 M [61]. The permeate $Mg^{2+}$ concentration was 4.06 mg $L^{-1}$, which resulted in an SRR of 0.034 gMH. The source of DS used to calculate the proposed paraments (SRR and ReR) is the reverse fluxed $Mg^{2+}$ ions. The reported RSF was 0.03 gMH and thus ReR is slightly greater than 100% (0.034/0.03). This ReR value suggests that the use of MF could recover all the $Mg^{2+}$ ions present in the mixed liquor; clearly, this is an ideal case. To clarify, the ReR could exceed 100% when the DS used for FO is already present the feed solution. This can be misleading as more DS will be recovered from the feed than what is

**Table 2.1** Mitigation of salinity buildup via solute removal in FO studies

| Conf.[a] | Method | Mode | Membrane | Area[b] | Product | DS | Conc.[b] | $J_w$[b] | FS | Cond.[b] | Ref. |
|---|---|---|---|---|---|---|---|---|---|---|---|
| *Physical* | | | | | | | | | | | |
| AeOMBR | MF | Continuous | CTA | 560 | - | NaCl | 1 | 5.5 | Synthetic | 5 | [109] |
| AeOMBR | UF | Continuous | CTA | 12,000 | - | NaCl | 0.44 | 4.8 | Domestic | 1.6 | [111] |
| AeOMBR | MF | Continuous | CTA | 720 | $Ca_3(PO_4)_2$ | Brine | 0.5 | 5.0 | Domestic | 6.5 | [112] |
| Cross-Flow | MF | Semi-Cont. | CTA | 138 | - | NaCl | 1 | 1.7 | Digestate | 0.7 | [113] |
| AeOMBR | MF | Continuous | CTA&TFC | 392 | $Ca_3(PO_4)_2$ $Mg_3(PO_4)_2$ | NaCl | 1 | 7.4 | Domestic | 10 | [114] |
| AeOMBR | MF | Continuous | CTA | - | $Ca_3(PO_4)_2$ | NaCl | 0.5 | 3.5 | Sewage | 10.5 | [115] |
| AnOMBR | MF | Continuous | CTA | 250 | $Ca_3(PO_4)_2$ $Mg_3(PO_4)_2$ | NaCl | 0.5 | 3 | Digestate | 3.5 | [116] |
| *Chemical* | | | | | | | | | | | |
| Cross-Flow | Precipitation | Batch | CTA | 140 | $MgNH_4PO_4$ | $MgCl_2$ | 1.5 | 6 | Digestate | - | [117] |
| Cross-Flow | Precipitation | Batch | TFC | 15 | $MgNH_4PO_4$ | $NH_4HCO_3$ | 1 | 4 | Digestate | - | [118] |
| Cross-Flow | Precipitation | Batch | CTA | 30 | $MgNH_4PO_4$ | $Na_2CO_3$ | 0.5 | 2.5 | Digestate | - | [119] |
| Cross-Flow | Precipitation | Batch | CTA | 98 | $CaCO_3$ | $Na_2CO_3$ | 4 | 1.5 | Leachate | - | [120] |
| *Biological* | | | | | | | | | | | |
| AeOMBR | Nitritation-Anammox | Continuous | CTA | 100 | - | $NH_4HCO_3$ | 1 | 2.5 | Synthetic | 1.8 | [42] |
| AeOMBR | Nitritation-Anammox | Continuous | CTA | 100 | - | $NH_4HCO_3$ | 0.5 | 2.3 | Synthetic | 1.3 | [121] |

a The configurations include aerobic or anaerobic submerged osmotic membrane bioreactor (AeOMBR or AnOMBR) and cross-flow FO.
b The units for membrane area, draw concentration, average water flux ($J_w$), and stable feed conductivity (Cond.) are $cm^2$, mol $L^{-1}$, LMH, and mS $cm^-$
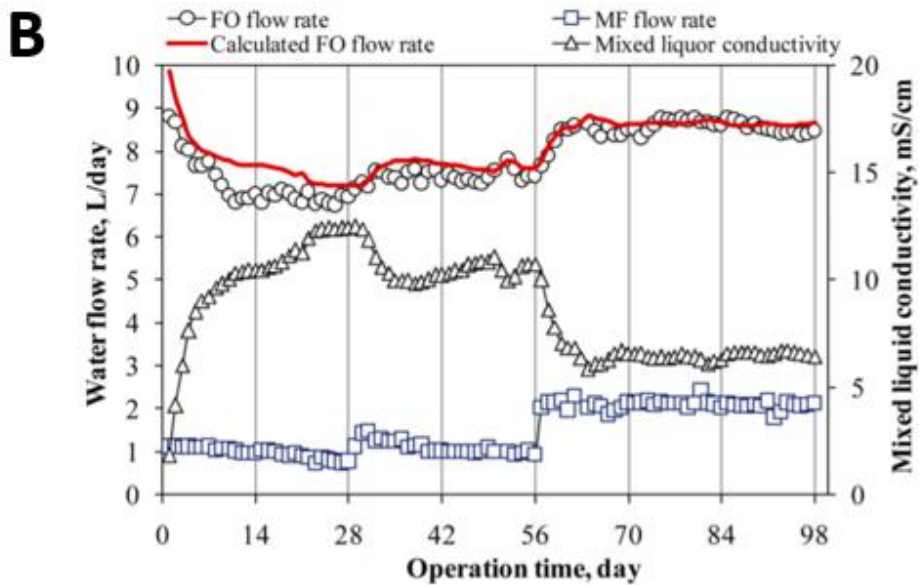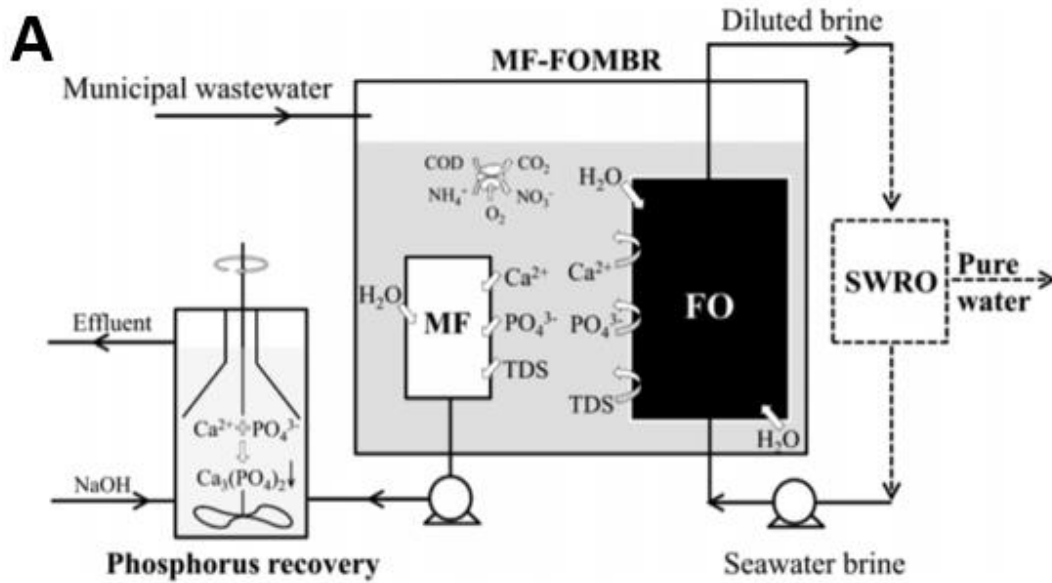
**Figure 2.2** Indirect mitigation of salinity buildup: (A) solute removal by an integrated microfiltration process; and (B) salinity decrease effect as microfiltration flow rate increases. Figures are adapted with permission from ref. [112].

22
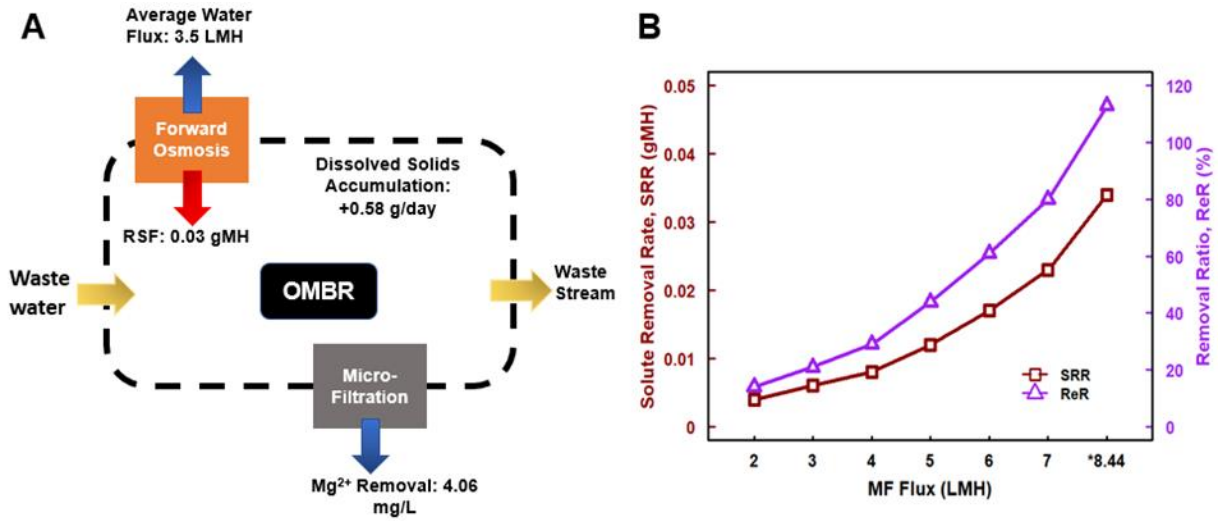
**Figure 2.3** A case study of physical removal of the accumulated solutes: (A) system balance in an osmotic membrane bioreactor (OMBR) with water flux, reverse salt flux, and removal rates being included to show SRR and ReR parameter's applicability to comparable FO-related studies; and (B) SRR and ReR values under varying MF flux operation (data sourced from ref. [123]).

contributed by RSF. MF flux, permeate DS concentration, and DS concentration in the feed solution before treatment should be presented in salinity buildup investigations as they will allow direct calculation of SRR and ReR without referencing other studies.

It is expected that operational changes or material adjustments will yield different SRR and ReR values. Thus, we performed a predication of SRR and ReR by varying water flux and RSF (Fig. 2.3B). If the waste stream via MF is slower than reported in the case study, then it is expected that less DS will be removed from the bulk (feed) solution. For example, a lower flux of 7 LMH yields a lower SRR (0.023 gMH) and ReR (80%), compared to the defined case (8.44 LMH). As the MF flux becomes significantly lower, the solute concentration may increase due to the increased FO membrane fouling [125, 126]. At a MF flux of 2 LMH, SRR is only 0.004 gMH with

14% ReR. Thus, a higher water flux would be preferred, though at the cost of more energy consumption. The water flux that produces a 100% ReR should not be exceeded to avoid the system being overworked. Moving forward, SRR calculations can make researchers aware of how much solute needs to be removed to maintain an environment for optimal operation of FO-based systems. If a different DS is used and results in different RSF, then a quick mathematical manipulation of the ReR equation could show how SRR needs to be adjusted and the required MF flux.

Using physical separation to mitigate salinity buildup comes with some limitations. Energy consumption and operational costs for FDFO-NF systems differ greatly when CTA (40.5% and $0.81/m^3$) or TFC (71.8% and $0.46/m^3$) membranes are used [127]. While the CTA membrane has a higher cost, its ability to remove DS is better than TFC at the same cost. Choosing a CTA membrane would most likely have a higher SRR and ReR and be better at reducing salinity buildup. This would be greatly adjusted by membrane fouling [128], yielding lower SRR and ReR due to reduced passage of solutes across the membrane. The DS molecular size can affect both RSF and ReR [129] and thus a high concentration of DS from RSF would lead to a poor performance of removal via filtration. Use of larger DS (e.g., potassium sorbate) will greatly reduce RSF and minimize the need for DS removal [130]. Another area of concern is the lack of attention placed on treatment or handling of the filtration permeate (the removed DS). A combination of fouling and poor selectivity of MF or UF membrane (due to relatively larger pore sizes) leads to the passage of impurities, making it difficult for direct permeate reuse [79]. Reuse of the permeate should be prioritized over disposal, because the solute concentrations [113, 124] would make post-treatment/disposal of permeate very challenging.

## 2.3.2 Chemical precipitation

Under suitable conditions (e.g., pH, temperature, and chemical compound ratio), salts, metal ions, and nonmetal ions can form precipitation with DS [131]. In contrast to physical separation, removing precipitates via filtration can be simpler than removing ionic forms of common elements, such as nitrate, ammonium, and sulfate [132, 133]. This is particularly evident considering that permeate ion treatment sometimes includes precipitation [123]. Chemical precipitation has been incorporated into FO, for example 92% phosphate removal was achieved from concentrated digestate [134]. In another study, calcium carbonate precipitated during the treatment of oil sand produced water in both FO and pressure retarded osmosis [135]. Struvite ($MgNH_4PO_4 \cdot 6H_2O$) is a common precipitate occurred in wastewater studies because of $NH_4^+$ and $PO_4^{3-}$ being common constituents, as well as widely used DS along with $Mg^{2+}$. For example, $MgCl_2$ was studied as a DS and the $Mg^{2+}$ ions migrated via RSF to the feed solution containing both $NH_4^+$ and $PO_4^{3-}$ to form struvite [117]. An added benefit was discovered when heavy metals, such as $Cu^{2+}$ and $Pb^{2+}$, were show to absorb onto struvite precipitates [136]. Externally added $Mg^{2+}$ ions were an option using $NH_4^+$-based DS, in which reversed-fluxed ammonium combined with phosphate in the feed solution to produce struvite [118]. This still presents opportunities for improvement since salinity buildup is not directly targeted and precipitation would only occur with supplemented resources that may not be available in the feed.

To evaluate SRR and ReR for solute removal via chemical precipitation, we used one of our prior studies as a case study, which formed struvite precipitation from a direct FO system used to dewater pig wastewater (Fig. 2.4A) [119]. To calculate SRR and ReR, only $Mg^{2+}$ that migrated via RSF and was precipitated in struvite was considered "removed". This case study utilized a batch operation with 60% water recovery. The SRR is calculated to be 0.388 gMH based on the

average water flux of 3.1 LMH, the amount of struvite that is precipitated, and the operation time. At RSF of 1.55 gMH, an ReR of 25% is obtained. Variability in nutrient rich feed solutions will ultimately require different reaction times and pH adjustments [137] to increase the formation of struvite, with increased complexity depending on the DS used for FO. This means that the key parameters such as SRR, water flux and RSF are expected to fluctuate with decreased $MgCl_2$ concentration [88], but this will allow more control with salinity buildup, resource usage, and operation time optimization.

Improving the removability of the solute is significantly dependent on decreasing RSF. In this case study, the amount of reverse fluxed $Mg^{2+}$ could decrease with enhanced RSF mitigation. According to Eq. 6 and 7, it is clear that decreasing the FO treatment time and the amount of DS moving across the membrane into the feed will increase both SRR and ReR. In particular, solute permeation across the FO membrane is the major variable, without affecting water recovery, which could be controlled to yield higher SRR and ReR (Fig. 2.4B). ReR can nearly double (from 25% to 45.6%) with only a 32% reduction in RSF. This would occur because less of the reverse fluxed $Mg^{2+}$ would remain dissolved in the feed solution compared to the amount of $Mg^{2+}$ that is used to form struvite. There is a potential to increase SRR with optimized FO membrane fabrication to minimize the residual DS in the feed solution. This is impactful as ReR would reflect an ideal percentage (>90%) when all the reverse fluxed DS is removed as solids. An additional limiting factor is the amount of $NH_4^+$ and $PO_4^{3-}$ that are required for struvite formation, and they may be supplied from either DS or constituents already in the feed solution. Insufficient supply of those elements could result in a significant decrease of ReR regardless of the reduced RSF. Other precipitates, such as $Mg_3(PO_4)_2$ and $CaNH_4PO_4$, may also form and be able to remove DS from the feed solution [138].

The feasibility of using chemical precipitation as a solute removal method in FO is dependent on the composition of the concentrated feed solution and the type of DS. In some cases, composition of the concentrated feed solution may decrease the efficacy of the method, resulting in lower SRR and ReR values (Fig. 2.4B). For example, if an $NH_4^+$ based DS was used in the study by Wu et al. [119], then the amount of struvite precipitated compared to the RSF of $NH_4^+$ would have been unbalanced because of a low $Mg^{2+}$ concentration. It is plausible seeing that different magnesium-phosphate and ammonium-phosphate ratios would show different removal rates of the ions from the bulk solution during struvite formation [139]. This issue branches off into underutilization of available nutrients present in the solution as an additional concern for chemical precipitation. This is observed in the case study that 75% of the DS is not removed from the system and the other 25% is precipitated into a solid that is affected by certain nutrients not being abundant in the feed solutions. In addition, pH adjustment could be a quick solution to improving the practicality of chemical precipitation since it is a fast and readily understood technique in water/wastewater treatment. In contrast, this would present potential roadblocks in FO and membrane performance. For example, lower rejection rates of perfluorohexanoic acid were observed at pH=3.3 (80%) versus at pH=10 (>90%) [140]. Electroneutrality between the feed and draw solutions is maintained by the passage of $H^+$ across the membrane[141] and may be a better approach to pH adjustment that needs to be investigated along with DS selection. Future research efforts should seek ways to provide necessary ratios without major pH adjustment to allow maximum precipitation.
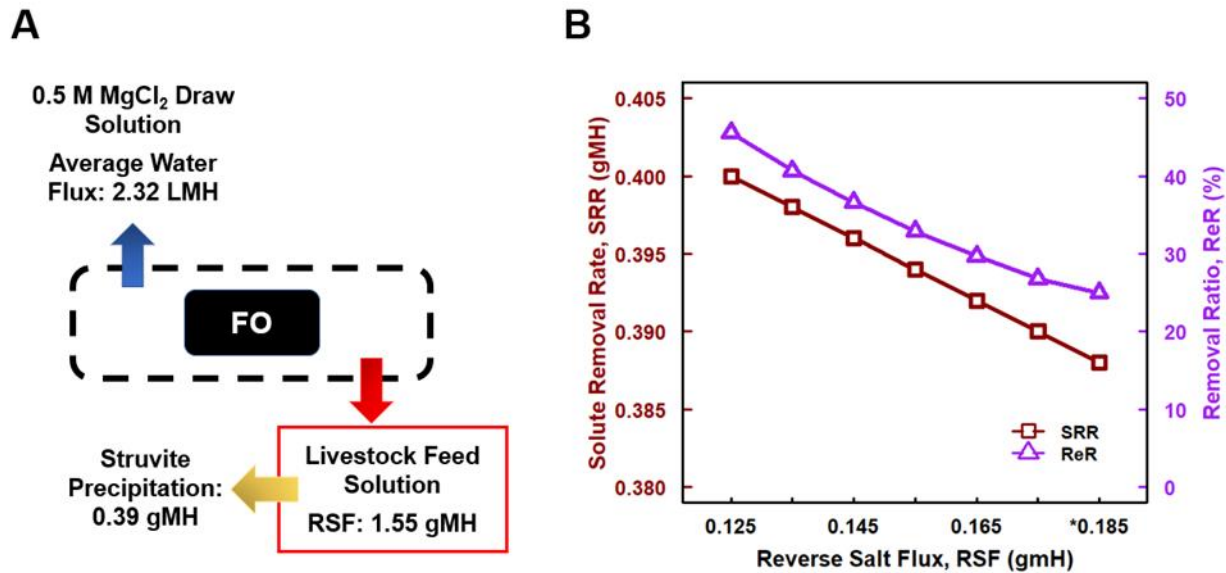
**Figure 2.4** A case study of chemical removal of accumulated solutes: (A) system balance with water flux, reverse salt flux, and removal rates being included to show SRR and ReR parameter's applicability to comparable FO-related studies; and (B) SRR and ReR values for different RSF if RSF mitigation is applied (data sourced from ref. [119]).

### 2.3.3 Biological removal

Biological removal of reverse – fluxed DS depends on the degradability of DS and assimilation of microorganisms. In the presence of microbial processes, either aerobic or anaerobic, an FO system can be converted to an OMBR [142]. A typical OMBR is capable of removing organic-based DS through biodegradation. For example, poly(acrylic acid) (PAA) polymers have been studied as DS that can be removed biologically with a degradation rate exceeding 40 mg $L^{-1}$ $d^{-1}$ and this degradation helped to maintain a higher water recovery, compared to NaCl DS [143]. Ammonia based DS have a particular affinity since nitrogen treatment is desired for many wastewater sources. For example, the nitritation-anammox process was integrated with a submerged FO to remove reverse-fluxed $NH_4HCO_3$ (Fig. 2.5A) [42]. During the initial phase, stable conditions were

obtained from the FO (water flux: ~2 LMH, RSF: ~1.2 gMH for N). The incorporation of nitritation has improved the FO performance with a water flux increasing to 3 LMH and decreasing the nitrogen chemical species with complete $NO_2^-$ removal in the annamox reactor. Successful combination of nitritation-anammox and FO processes not only renders a good effluent water quality (i.e., no accumulation of $NH_4^+$, $NO_3^-$, and $NO_2^-$; conductivity of 1.3 mS cm$^{-1}$) but also provides sufficient alkalinity and nutrients for the proliferation of anammox bacteria under long-term operation [121].

Biodegradation of reverse-fluxed DS may be limited to very few DS that are biodegradable. In addition, it could also create the DS influence on microbial activities and stimulate biofouling. Toxicity of reverse-fluxed DS to microbes in OMBRs was studied using *Escherichia coli (E. coli)* as a model organism. It was found that different DS have exhibited different effects on the growth of *E. coli*, for example NaCl stimulated the bacterial growth, $MgCl_2$ decreased it, and $NH_4HCO_3$ at a moderate concentration resulted in an optimal growth (Fig. 2.5B) [144]. As a side effect of biodegradation, biofouling resulted from microbial growth is expected to noticeably increase, leading to the decreased water flux. Biofouling can be a major performance inhibitor [145-147]. For example, a 60% decrease in the normalized water flux was experienced with a biofilm formed to be approximately 70-µm thick [148]. It is important to take into account that biodegrading the DS would result in the need to regenerate the draw solution with additional resources, which can become costly. There is insufficient knowledge about whether microbial activity would effectively degrade the reverse fluxed DS. These two concerns would attenuate the application of biological removal of DS. In general, there have not been a great number of studies on biological removal of DS and thus more remain to be explored in this area.
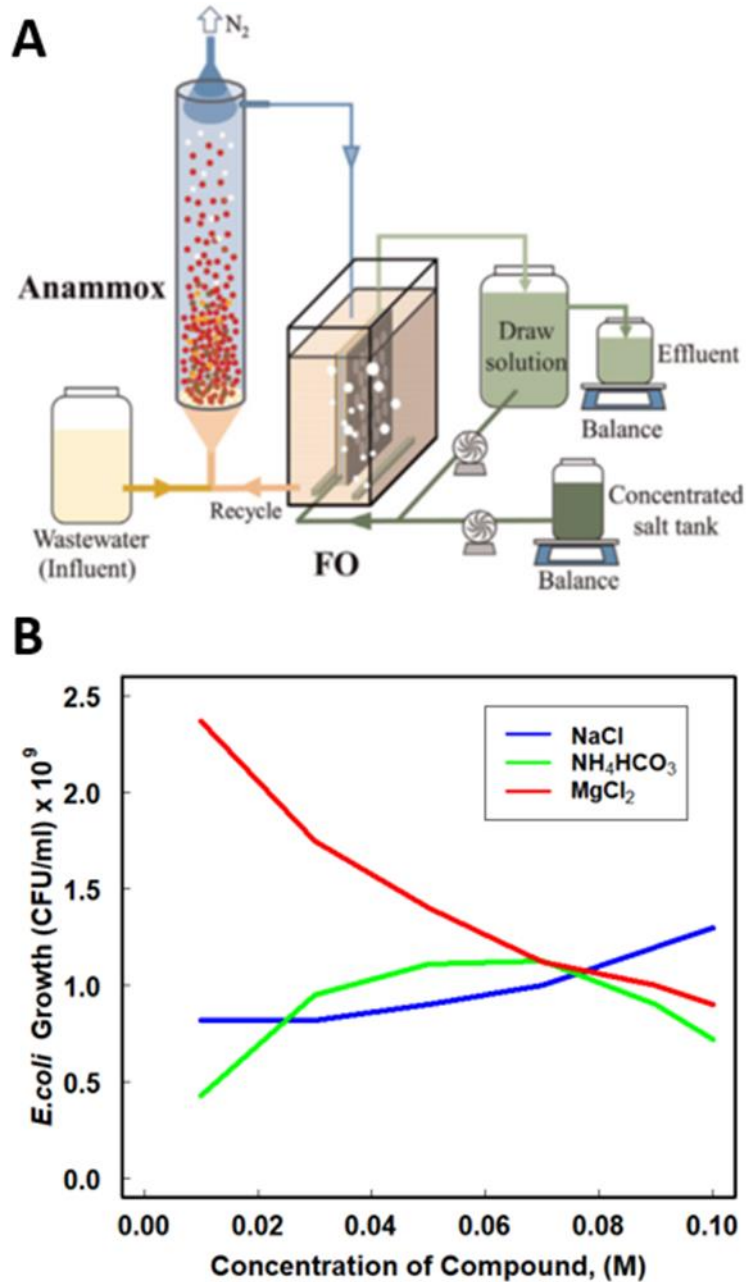
**Figure 2.5** Biological removal of accumulated solutes: (A) schematic of an FO-Anammox system (figure is adapted with permission from ref [42]); and (B) effects of the increased concentrations of DS ($NH_4HCO_3$, NaCl, and $MgCl_2$) on E. coli growth (modified after results in ref. [67]).

## 2.4    Recovery of reverse-fluxed solute

Solute recovery from the feed solution, instead of removal, provides a more attractive option to potentially reuse those "wasted DS". Because most DS are charged ions, they can be separated from the feed solution by electricity/electrical field, which can be generated by electrochemically-active microorganisms in a bioelectrochemical system (BES) or through direct exertion of voltage in an electrodialysis (ED). In this section, those two recovery approaches are introduced and discussed for their performance, advantages, and drawbacks.

Bioelectrochemical systems are based on interaction between microbes and solid electrode acceptors/donors. Representative examples of BES include microbial fuel cells (MFCs) and microbial electrolysis cells (MECs) [149]. In BES, movement of biologically produced electrons also drives the transport of ions across a separator (e.g., ion exchange membrane) [150], and such an ion transport has been employed to accomplish desalination in microbial desalination cells (MDCs) [8]. BES present an opportunity to maximize the sustainability if the ions – dissolved DS – can be recovered as opposed to wasted. This has been demonstrated in an OMBR study that employed BES to mitigate DS accumulation and then recover DS (Fig. 2.6A). It was found that bioelectricity generation (closed circuit) led to better salinity control as the conductivity stabilized around 9 mS cm$^{-1}$ compared to 24.1 mS cm$^{-1}$ under the open circuit (no electricity, Fig. 2.6B).

Such a difference in the feed conductivity resulted in a higher water flux of 5.5 LMH (closed circuit) than 0.7 LMH (open circuit) at the end of an operation cycle. The recovery of ammonium was significantly enhanced from 7.8-8.8 g N m$^{-3}$ h$^{-1}$ to 100.0–125.0 g N m$^{-3}$ h$^{-1}$ with the addition of $CO_2$ [151]. The benefit of using BES for recovering reverse-fluxed DS is the low energy

consumption of the recovery process, because electrons are produced from low-grade substrates via biological oxidation in the anode. The performance of such a recovery will be strongly related to two factors. First, a higher current generation would promote ion transport and thus DS recovery. How to increase current generation in BES has been well discussed before [152] and thus is not focused here. Second, reverse-fluxed DS need to be separated from the anolyte of BES. That is especially important to obtaining high purity/quality DS for reuse, because an anolyte contains a variety of compounds (to support microbial growth) and cannot be used as DS directly. In the abovementioned example, reverse-fluxed DS was separated from the anode (which was also a feed chamber) and then concentrated in the cathode. Such a separation would increase the requirement of system operation and reactor complexity.

To avoid the problems with BES-based recovery approach, ED can be used with an externally applied electrical force to separate ions from a feed solution. ED has been studied to separate target compounds such as amino acids [153], cupric [154], fluoride and nitrate [155], and toxic metals (e.g., lead) from waste streams [156]. Maximum efficacy of this process depends on multiple factors such as applied potential and configuration [157]. The size and charge of the ions, however, is a significant determinate in recovery. It was found that monovalent ions (e.g., $Na^+$) could be separated better than the divalent and trivalent ions [158]. A recent study has employed ED to recover a fertilizer (diammonium phosphate (($NH_4$)$_2$$HPO_4$, DAP)) DS from an FO (Fig. 2.7A) [159]. A high recovery percentage of 96.6% was obtained for the reverse-fluxed DAP on a daily basis under DI water feed conditions. The reported recovery using a wastewater treatment effluent reached approximately 5.9 g $L^{-1}$ and 6.2 g $L^{-1}$ for $NH_4^+$-N and $PO_4^{3-}$-P, respectively. The SRR for this study were 1.16 and 1.22 g $m^{-2}$ $h^{-1}$ for $NH_4^+$-N and $PO_4^{3-}$-P, respectively.

**Figure 2.6** Recovery of draw solute by using a bioelectrochemical system: (A) schematic of an OMBR-BES; and (B) comparison of anolyte conductivity (AC) and water flux (WF) between closed and open circuit. Figures are adapted with permission or modified from ref. [151].

A major concern for ED-based recovery method is high energy consumption. It was estimated that the energy consumption could be 1.49 kWh m$^{-3}$ of water with highly concentrated DS, which would be reduced to about half (0.72 kWh m$^{-3}$) with a less concentrated solution [159]. The major contributor to energy consumption in an ED-FO system is ED, which can consume about 90% of total energy input, while FO requiring about 10% energy (Fig. 2.7B). The external power supply is a key energy consumer being approximately 90% of the total ED energy required. Another challenge for ED based recovery is membrane fouling, which affects the electrochemical properties (i.e., potential dropped due to increased resistance from buildup on the membrane) [160]. This is particularly the case when wastewaters with high concentrations of acidic compounds are being treated [161]. ED is an ion/charge-based separation process and thus is essentially non-selective towards charged ions. Efforts have been invested to show that some ED systems can allow only singly or doubly charged cations across an exchange membrane, but the process requires specific conditions (e.g., pH and current density) to achieve optimal separation [162]. These conditions are understudied and expected to change based on the targeted ions. This shortfall would ultimately decrease the purity of the recovered DS and make it harder to regenerate for reuse in FO; however, the recovered DS may have other applications, for example being applied to agricultural land when fertilizer compounds are used as DS.

## 2.5    Conclusions

To establish a foundational understanding of methods to mitigate salinity buildup, this paper has presented and analyzed major approaches for removal and recovery of DS in FO-based systems. New parameters for solute reduction and recovery rates/ratios were proposed to better evaluate

and identify the most effective method that remove or recover reverse-fluxed DS. Operation

parameters (e.g., MF flux rate) should be optimized to have maximum recovery without much



**Figure 2.7** Recovery of draw solute by electrodialysis: (A) schematic of an ED-FO system; and

(B) energy consumption of ED-FO system with a 2.5 V applied. Figures are adapted with

permission from ref [84].

energy demand for physical separation. For chemical precipitation, operation parameters and understanding chemical composition of the feed solution will be the most critical variables in increasing SRR and ReR. Biological removal is still an underexplored area and may have application for some special DS that, when being reverse fluxed, can be a nutrient to stimulate biological growth. Recovery of reverse fluxed DS is of great interest but has not been well investigated in detail. The current recovery approach is based on ion separation driven by electricity, which is either generated *in situ* (e.g., BES) or applied externally (e.g., ED). To move forward for effective control of reverse fluxed DS, it is important to include information on the amount of solute caused by RSF and to explore approaches that can be integrated with FO for removing or recovering solutes.

# Chapter 3

# Effects of Draw Solutes on an Integrated Forward Osmosis—Microbial Fuel Cell System Treating a Synthetic Wastewater

**Abstract**

Microbial fuel cells (MFCs) and forward osmosis (FO) are both attractive and versatile wastewater treatment technologies that possess disadvantageous qualities that prevent their optimal performance. This study aimed to investigate how draw solute selection for FO treatment would affect MFC performance in a coupled FO-MFC system. Two types of draw solutes, $NH_4HCO_3$ and NaCl, were studied, and it was found that 1.0 M $NH_4HCO_3$ (FO-MFC-A) and 0.68 M NaCl (FO-MFCB) had similar water fluxes of 6.04 to 3.39 LMH and 6.25 to 3.54 LMH, respectively. The reverse salt flux from the draw decreased the feed solution resistance for both draw solutes, but the FO-MFC-A system (0.32 W $m^{-2}$) had a higher maximum power density than the FO-MFC-B system (0.26 W $m^{-2}$). The current density for the FO-MFC-B system increased due to continuous solution resistance decrease, whereas it remained constant for the FO-MFC-A. The difference in Coulombic efficiencies (32.8% vs. 25.6%) but similar Coulombic recoveries (10.2% vs. 11.4%) between the FO-MFC-A and FO-MFC-B systems suggested that the FO-MFC-A might have the inhibited microbial activity by high ammonium/ ammonia. The FO-MFC-A system had the lower energy consumption for nutrient removal (2.01 kWh $kg^{-1}$ $NH_4^+$-N) and recovery (8.87 kWh $kg^{-1}$ $NH_4^+$-N). These results have shown that $NH_4HCO_3$ as a draw solute can have advantages of higher

power density, higher Coulombic efficiency, and recoverability for draw regeneration, but its potential inhibition on microbial activity must also be considered.

**Keywords:** Forward osmosis, microbial fuel cell, coupled system, reverse solute flux, nutrient recovery

# 3.1   Introduction

Microbial fuel cells (MFCs) are a versatile technology that has been studied to treat various wastewaters [21]. In a typical MFC, microbes degrade organic substances in its anode chamber to release electrons, which flow to a cathode electrode and reduce electron acceptors such as oxygen [163]. The generated electricity drives the separation of ions through ion exchange membranes. For example, ammonium ions can migrate from the anode chamber into the cathode chamber across a cation exchange membrane (CEM) [18]. In the past two decades, MFC technology has been advanced through both fundamental studies and system development. Researchers have obtained in-depth understanding of microbial mediated electron transfer and functional microbiome involved in MFCs [164]. Fundamental insights also help scale up MFCs to treat real wastewaters with desirable organic removal and energy recovery performance. For example, a 200-L MFC system was deployed in a wastewater treatment plant to treat primary effluent, and the produced energy was revered and then reused to support the MFC operation [165]. Because of elimination or minimization of aeration, MFCs can be an energy efficient approach for wastewater treatment and their energy consumption is much lower than typical activated sludge processes [166]. More information about MFC can be found in several thorough review papers [167, 168].

Despite the progress, MFC technology still faces some major challenges, including high capital cost (mostly due to electrode/catalyst/membrane materials) and relatively low energy recovery from low-strength mainstream wastewaters. One potential approach to address some of those challenges is to concentrate mainstream wastewater before MFC treatment. Such a concentration process may benefit MFCs with a smaller wastewater volume (and thus a compact reactor size and a reduced capital investment) and higher ionic and organic concentrations to favor mass transfer and kinetics. For example, a concentrated wastewater yields a higher ionic conductivity to reduce the internal resistance of an MFC, as well as an elevated nutrient level to facilitate nutrient recovery (e.g., ammonium nitrogen) from low-strength wastewaters. This pre-concentration process can be achieved using membrane technologies such as nanofiltration (NF), reverse osmosis (RO), and forward osmosis (FO). NF and RO are pressure driven membrane processes that requires more energy input [169]. FO, on the other hand, utilizes an osmotic pressure gradient to recover water from a low (feed) to a high (draw) salinity solution separated by a semipermeable membrane [40]. It offers a good rejection to a wide range of compounds when concentrating various wastewater feeds [40, 170]. Still, an FO-based concentration process needs to carefully select the draw solutes to minimize reverse solute flux (RSF), a phenomenon that can introduce additional salinity into the feed wastewater [89, 171]. In general, regeneration-free draw solutes are preferable to avoid energy-intensive solute regeneration/separation. For example, fertilizer-based draw solutions (DS) have been studied to recover water from wastewater for non-potable water reuse [172, 173]. Systematic research has also been completed to understand how concentration polarization, dilution rate, membrane fouling, membrane type and orientation affect water flux and RSF [174-176].

To reap the benefits of FO-based concentration, previous efforts have been focused strategically on integrating FO membrane or modules with the MFC technology towards simultaneous wastewater treatment and resource recovery [177]. The first integrated system was to use FO membrane to replace ion exchange membrane, which creates an osmotic microbial fuel cell (OsMFC) [178]. This OsMFC could generate a significantly higher current density at 100 A $m^{-3}$ than a conventional MFC (55 A $m^{-3}$) because of its smaller membrane resistance (9.7 $\Omega$ vs. 14.3 $\Omega$) [179]. MFC and FO have also been combined to concurrently treat low strength synthetic wastewater in a membrane bioreactor equipped with membrane filtration. Operation of this novel system showed both a stable voltage (0.38-0.41 V) for 38 days and a higher power output compared to similar systems in part because of conductivity control in the mixed liquor of the bioreactor [180]. In addition, a three chamber configuration with the FO chamber in between the anode and cathode achieved high removal of COD and total dissolved solids from actual wastewater [181]. While FO has also been considered a favorable complement to bioelectrochemical systems [118, 182, 183], full integration of FO and MFC presents potential operational issues if implemented in the real world and suggests further investigation of separate units in a treatment process.

In this study, we proposed to employ an FO unit to concentrate a synthetic wastewater and then the concentrated feed solution was treated in an MFC. The FO unit was operated with two inorganic salts (NaCl and $NH_4HCO_3$) as draw solutes. Since the MFC treatment could recover some ammonium that migrated across the CEM, the two draw solutes will help determine the effects that draw solute selection has on the coupled FO-MFC system's performance. The specific objectives of this study include: (1) investigate how use of different draw solutes and RSF during FO operation alter the composition of medium strength wastewater, and (2) understand the effects that coupling FO and MFC have on energy consumption and nutrient recovery. Specific energy

consumption and contaminant removal rates were considered when comparing the systems to evaluate coupled system performance to better compare COD removal, $NH_4^+$ removal and $NH_4^+$ recovery for coupled FO-MFC treatment.

## 3.2 Materials and Methods

### 3.2.1 FO Setup and Operation

A two-chamber FO unit (11 cm x 9 cm x 3.5 cm) was constructed to have identical draw and feed compartments of 60 mL each, separated by a piece of CTA membrane with an effective area of 48 $cm^2$ (Fluid Technology Solutions, Albany, OR, USA). Each compartment was connected to a reservoir, which contained an initial volume of 350 mL of the draw/feed solution. The $NH_4HCO_3$ and NaCl DS were examined at three concentrations (0.5, 1.0, 1.5 M). Then, a 0.68 M NaCl DS was used to compare to 1.0 M $NH_4HCO_3$ DS for FO-MFC operation because they produced similar final feed volumes (Section 2.3.1). The feed solution was a synthetic wastewater containing (per liter of DI water): 0.15 g $NH_4Cl$, 0.5 g NaCl, 0.015 g $MgSO_4$, 0.02 g $CaCl_2$, 0.1 g $NaHCO_3$, 1.07 g $K_2HPO_4$, 0.53 g $KH_2PO_4$, and 1 mL of trace elements. In addition, 1.29 g sodium acetate (~1,000 mg COD $L^{-1}$) and 1.76 g $NH_4HCO_3$ (~ 400 mg $NH_4^+ - N\ L^{-1}$) were added to mimic the organic and ammonium concentrations in anaerobically digested livestock wastewater [184]. The feed and DSs were recirculated at a rate of 10 mL $min^{-1}$. Each FO treatment cycle had a 6-hour duration. The FO membrane was cleaned with 400 mL of DI water that was recirculated at a higher flow rate for at least 4 hours between each FO treatment cycle to minimize fouling effects. The draw and feed solutions were sampled before and after the FO treatment. All tests were performed under a room temperature (24 °C) and in triplicates.

### 3.2.2 MFC Setup and Operation

The MFC had an anode chamber and a cathode chamber (450 mL/each) that were separated by a cation exchange membrane (CEM, CMI-7000, Membrane International Inc., Glen Rock, NJ, USA) with an effective area of 130 $cm^2$. The anode electrode was a carbon brush pretreated by acetone. The anode chamber was inoculated with the sludge from a wastewater treatment plant (St. Louis, MO, USA) and operated at decreasing external resistance until a consistent electricity generation was established. The MFC was operated under a batch mode and at a room temperature. The cathode electrode (100 $cm^2$) was a stainless steel mesh wrapping carbon cloth secured by titanium wire. The carbon cloth (Zoltek Companies, Inc., MO, USA) was coated with powdered activated carbon (4 mg $cm^{-2}$), which served as an oxygen reduction catalyst. The catholyte (cathode solution) contained (per liter of DI water) 0.54 g $K_2HPO_4$ and 0.27 g $KH_2PO_4$ to maintain a pH of ~7.0. Dissolved oxygen was supplied to the cathode using an air diffuser. Both the anolyte and catholyte were circulated at a rate of 30 mL $min^{-1}$. The anode and cathode electrodes were connected through a 10-$\Omega$ external resistance to generate a high current for driving migration of ammonium ions from the anode into the cathode. Anolyte, catholyte and sulfuric acid absorption solution samples were collected during each anolyte replacement. In the FO-MFC system, the synthetic wastewater was first concentrated by the FO before pumped into the MFC. In the FO-MFC system, the FO was operated for 6 hours and MFC was operated for the subsequent 18 hours, resulting in a total treatment time of 24 hours (Fig. 3.1).

### 3.2.3  Measurement and Analysis

The voltage of the MFC was recorded every two minutes by a digital voltage meter (2700, Keithley Instruments Inc., Cleveland, OH, USA). The polarization curves were generated from data collected from a potentiostat (600+, Gamry, Warminster, PA, USA) operating at a $0.5 \text{ mV s}^{-1}$ scan rate. Chemical oxygen demand (COD) was measured using colorimetric methods (HACH Co., Ltd., USA). The ion concentrations were measured using ion chromatography (Thermo Fisher



**Figure 3.1** Schematic of the coupled FO-MFC system with 6-hour FO operation and 18-hour MFC operation. Ammonia recovery was conducted via air stripping using a 1 M absorption solution.

Scientific Dionex Integrion HPIC, Madison, WI, USA). The electrical conductivity was measured using a conductivity meter (Mettler-Toledo, Columbus, OH, USA). The pH was measured using a bench pH meter (Oakton Instruments, Vernon Hills, IL, USA). To monitor the change in water volume during the FO operation, the mass of the feed solution was measured by a digital balance

(Scout Pro, Ohaus, Columbia, MD, USA) and recorded onto LoggerPro data collection software. Water flux ($J_w$, L m$^{-2}$ h$^{-1}$ or LMH) was calculated according to Eq. (1):

$$J_w = \frac{\Delta m}{A \times \Delta t} \tag{1}$$

where $\Delta m$ (g) is the change in mass of the feed solution that is converted to liters, $A$ is the effective membrane area (m$^{-2}$) used for water permeation, and $\Delta t$ is the change in time (h$^{-1}$).

The osmotic pressures ($\pi$, atm) of the DSs were based on a previous study [185] and the osmotic pressure of the feed was estimated based on Eq. (2):

$$\pi = iMRT \tag{2}$$

where $i$ is van't Hoff's factor, $M$ (mol L$^{-1}$) is the molar concentration of the solute, $R$ (L atm mol$^{-1}$ K$^{-1}$) is the ideal gas constant, and $T$ (K) is the temperature of the solution. The osmotic pressure gradient then was calculated using the difference of the draw and feed solution osmotic pressures ($\pi_{draw} - \pi_{feed}$).

The RSF ($J_S$, g m$^{-2}$ h$^{-1}$) is determined based on the change in the amount of the draw solute in the feed solution at the beginning and end of the FO cycle. The RSF was calculated using Eq. (3):

$$J_S = \frac{C_f V_f - C_i V_i}{A \times \Delta t} \tag{3}$$

where $C_f$ and $C_i$ (g L$^{-1}$) represent the final and initial concentration of the draw solute, respectively. The $V_f$ and $V_i$ (L) variables represent the final and initial volumes of the feed solution.

The specific reverse solute flux (SRSF, g L$^{-1}$) is a ratio between the RSF and the water flux and can be expressed as Eq. (4).

$$SRSF = \frac{J_S}{J_w} \tag{4}$$

The current density was calculated by finding the quotient of the recorded date from the voltage digital meter and the area of the cathode electrode. The energy production and consumption ($E_{production}$ and $E_{consumption}$, kWh) were estimated using Eq. (5) and Eq. (6), respectively, according to a previous study [22].

$$E_{production} = (\sum I^2 R)\Delta t_{MFC} \tag{5}$$

$$E_{consumption} = (P_{FO,recirc})\Delta t_{FO} + (P_{MFC,recirc})\Delta t_{MFC} \tag{6}$$

where $I$ (mA) represents the current, $R$ ($\Omega$) represents the resistance, $\Delta t_{FO}$ and $\Delta t_{FO}$ represent the operation time of the FO cell and MFC, respectively, and $P_{FO,recirc}$ and $P_{FO,recirc}$ represent the power estimated for recirculation of the solutions in the FO cell and MFC, respectively.

The normalized energy consumption (NEC, kWh kg$^{-1}$) [22] was calculated to understand the energy consumption used for COD removal, $NH_4^+$ removal and $NH_4^+$ recovery and is expressed in Eq. (7).

$$NEC = \frac{E_{consumption} - E_{production}}{\Delta COD_{rem.}} \ or \ \frac{E_{consumption} - E_{production}}{\Delta NH_4^+{}_{rem.or\ rec.}} \tag{7}$$

where $\Delta COD_{rem}$ represents the removed COD and $\Delta NH_4^+{}_{rem.or\ rec.}$ represents the removed and recovered $NH_4^+ - N$ during MFC operation.

The Coulombic efficiency (CE) and Coulombic recovery (CR) were calculated as outlined by previous studies [186].

## 3.3   Results and Discussion

### 3.3.1   FO Performance using different DSs

The $NH_4HCO_3$ and NaCl DSs had different osmotic pressure gradients between the feed and the draw that produced different FO concentrated feed solutions. The initial to final osmotic pressure gradient for the 0.5, 1, and 1.5 M $NH_4HCO_3$ DSs were $20.0 \pm 0.1$ to $13.3 \pm 0.6$ atm, $38.2 \pm 0.6$ to $24.0 \pm 0.1$ atm, and $52.7 \pm 1.0$ to $32.9 \pm 0.7$ atm, respectively (Fig. 3.2A). This decreasing osmotic pressure is because of the dilution from water recovered from the feed solution. The decreased DS ionic strength also resulted in a lower water flux for the 0.5 M (4.32 to 2.29 LMH), 1.0 M (6.08 to 3.33 LMH), and 1.5 M (6.56 to 4.32 LMH) $NH_4HCO_3$ DSs.

The same trend is evident for the 0.5, 1.0, and 1.5 M NaCl DS as the osmotic pressure gradients decreased from $21.3 \pm 0.1$ to $15.9 \pm 0.2$ atm, $45.1 \pm 0.3$ to $30.7 \pm 0.4$ atm, and $66.7 \pm 0.4$ to $41.8 \pm 0.7$ atm, respectively. The NaCl DSs achieved a higher water flux at the same molarity compared to $NH_4HCO_3$. In conjunction with the decreased strength of the DSs, the feed solution's osmotic pressure increases due to RSF (Fig. 3.2B). The concentration changes of $NH_4^+$ for the $NH_4HCO_3$ DSs and $Na^+$ and $Cl^-$ for the NaCl DSs suggest that there is ion migration across the membrane during FO treatment. The average RSF of $NH_4^+$ (2.31, 3.43, and 3.67 g $m^{-2}$ $h^{-1}$), $Na^+$ (1.91, 2.89, and 4.01 g $m^{-2}$ $h^{-1}$), and $Cl^-$ (2.64, 4.89, and 6.90 g $m^{-2}$ $h^{-1}$) of each ion increased for each increase in DS molarity. Interestingly, RSF of the sodium cations was less than the chloride anions for each experiment iteration. As observed by previous studies, it is most likely due to the different diffusion rates in conjunction with the negatively charged CTA membrane that repels anions such as chloride [187]. Ammonium also has a faster diffusion rate than sodium, as evidenced by a higher RSF for the 0.5 and 1.0 M $NH_4HCO_3$ FO operations. This is likely due to
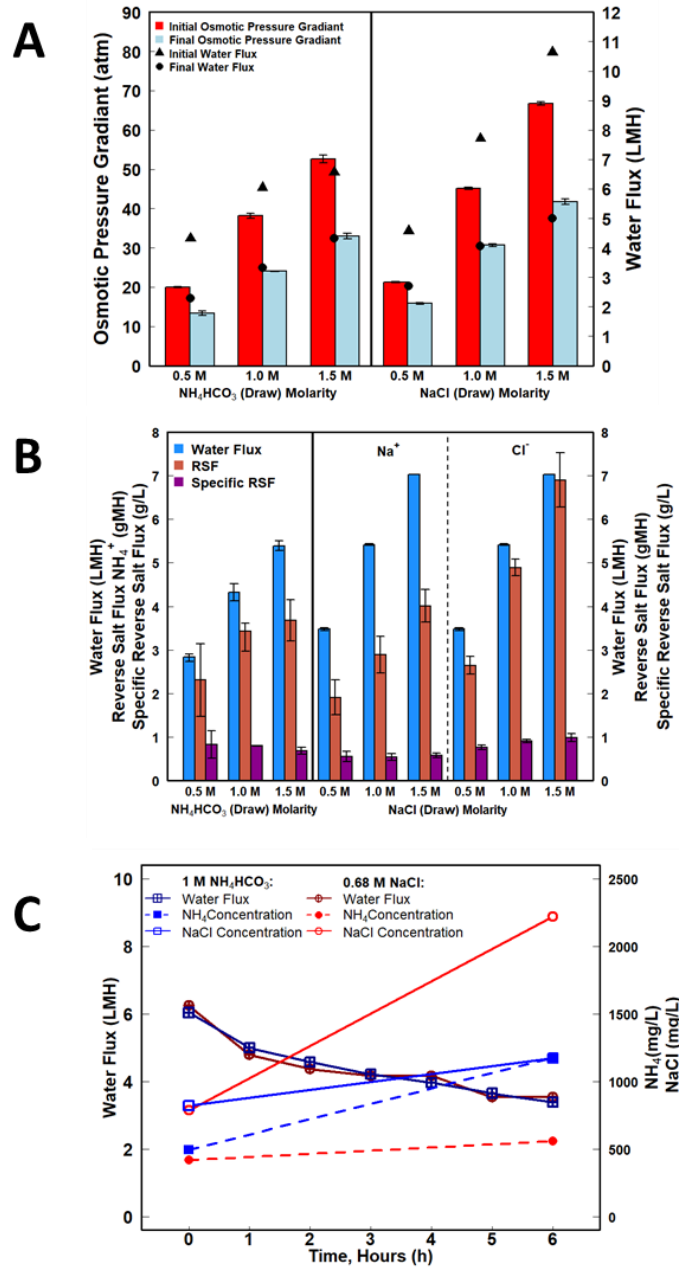
**Figure 3.2** The effects of using different draw solutes for FO treatment. (A) Osmotic pressure gradient between the feed and draw (NH₄HCO₃ and NaCl) solutions before and after FO treatment with the initial and final water fluxes. (B) Water flux, reverse salt flux, and specific salt flux for individual ions. (C) Water flux and salt concentration changes for 1.0 M NH₄HCO₃ and 0.68 M NaCl DSs.

ammonium's smaller hydrated rates compared to sodium [188], which makes it easier to move through the pores of membrane. Forward solute flux of $NH_4^+$ due to the concentrating effect may have played a role in the lower averaged RSF for the 1.5 M $NH_4HCO_3$ DS. Despite the increases in water flux and RSF for each iteration of the FO tests, the average SRSF remained in a close range for $NH_4^+$ -N (0.68 – 0.82 g $L^{-1}$), $Na^+$ (0.53 – 0.57 g $L^{-1}$), and $Cl^-$ (0.76 – 0.98 g $L^{-1}$). This is likely due to the balanced exchange of water molecules and ions in order to achieve electrical neutrality between the draw and feed solution during FO treatment. Additionally, while the RSF was higher when $NH_4HCO_3$ was used as a DS, $NH_4^+$ enriches the feed with nutrients unlike the NaCl DS. Fig. S1 shows electrical conductivity and pH changes in the feed solution. An observation made of the latter is that when $NH_4HCO_3$ was the draw solute, the pH increased higher $(8.26 \pm 0.08$ vs. $7.97 \pm 0.16$, $8.24 \pm 0.18$ vs. $8.01 \pm 0.04$, $8.25 \pm 0.08$ vs. $8.19 \pm 0.06)$ than when NaCl was the draw solute due to the buffer capacity of $HCO_3^-$ ions.

To effectively compare the FO-MFC systems with different DSs, the $NH_4HCO_3$ and NaCl based DSs would need to produce as the same final feed volume to use as an anolyte for the MFC. The 1.0 M $NH_4HCO_3$ DS was selected for the next phase of investigation because it produced a feed volume that would replace half of the anolyte for every MFC batch operation. A linear regression was used to select a 0.68 M NaCl DS to achieve a comparable final feed volume (~36% recovered) as the 1.0 M $NH_4HCO_3$ DS (Fig. 3.2C). The water flux decreased at similar rates for the $NH_4HCO_3$ (6.04 to 3.39 LMH) and NaCl (6.25 to 3.54 LMH) DSs. Even though the initial osmotic pressure gradients between the two DSs ($NH_4HCO_3$: $38.16 \pm 0.60$ atm; NaCl: $30.40 \pm 0.38$ atm) were different but yielded relatively close final osmotic pressure gradients ($NH_4HCO_3$: $24.02 \pm 0.08$ atm; NaCl: $21.52.02 \pm 0.29$ atm). The greater osmotic pressure gradient when using 1.0 M $NH_4HCO_3$ presumably would achieve a higher water flux than the 0.68 M NaCl DS. This

expectation is likely not observed because the higher RSF when $NH_4HCO_3$ is used causes a faster draw dilution and feed concentration than the slower RSF for the NaCl draw solute. The overall FO water recovery was statistically insignificant ($p > 0.05$) between the two different DSs. Every other DS resulted in significantly different ($p < 0.05$) results except for 1.5 M $NH_4HCO_3$ vs. 1.0 M NaCl ($p = 0.73$) (Table B.1). The averages for the produced solution characteristics from the feed solution not treated with FO, $NH_4HCO_3$ draw solute FO pretreatment, and NaCl draw solute FO pretreatment are shown in Table 3.1.

**Table 3.1** Synthetic wastewater composition before FO treatment and composition of anolyte fed in the FO-MFC-A and FO-MFC-B systems.

| Water Parameter (unit) | Synthetic Wastewater | FO-MFC-A | FO-MFC-B |
|---|---|---|---|
| COD (mg/L) | $1002 \pm 87$ | $1348 \pm 85$ | $1443 \pm 67$ |
| Electrical Conductivity (mS/cm) | $7.32 \pm 0.10$ | $12.79 \pm 0.79$ | $11.67 \pm 0.12$ |
| pH | $7.52 \pm 0.06$ | $8.24 \pm 0.18$ | $8.11 \pm 0.21$ |
| $NH_4^+ - N$ (mg/L) | $439.04 \pm 38.94$ | $1191.14 \pm 38.34$ | $558.52 \pm 5.99$ |
| $Na^+$ (mg/L) | $692.06 \pm 48.11$ | $1100.88 \pm 42.25$ | $1415.13 \pm 92.90$ |
| $Cl^-$ (mg/L) | $482.92 \pm 35.58$ | $743.19 \pm 39.79$ | $1343.89 \pm 96.24$ |
| $PO_4^{3-}$ (mg/L) | $323.12 \pm 16.26$ | $492.02 \pm 19.76$ | $488.64 \pm 24.70$ |

### 3.3.2 Electricity generation in the MFC using FO concentrated anolyte

Polarization curves showed that partitioning characteristics of the reverse fluxed draw solutes affected the maximum power density and internal resistance of the MFC. The two systems investigated for energy and nutrient recovery were an FO coupled MFC fed with anolyte FO concentrated using 1.0 M $NH_4HCO_3$ DS ("FO-MFC-A") and an FO coupled MFC fed with anolyte FO concentrated using 0.68 NaCl DS ("FO-MFC-B"). The FO-MFC-A had a higher maximum power density of 0.32 W m$^{-2}$ compared to the FO-MFC-B maximum power densities of 0.26 W m$^{-2}$ (Fig. 3.3). There could be several reasons why the power densities were different for the FO concentrated systems. First, the FO-MFC-A (30.6 $\Omega$) and the FO-MFC-B (30.2 $\Omega$) systems had lower internal resistance likely due to electrolyte concentration (conductivity) increase because of
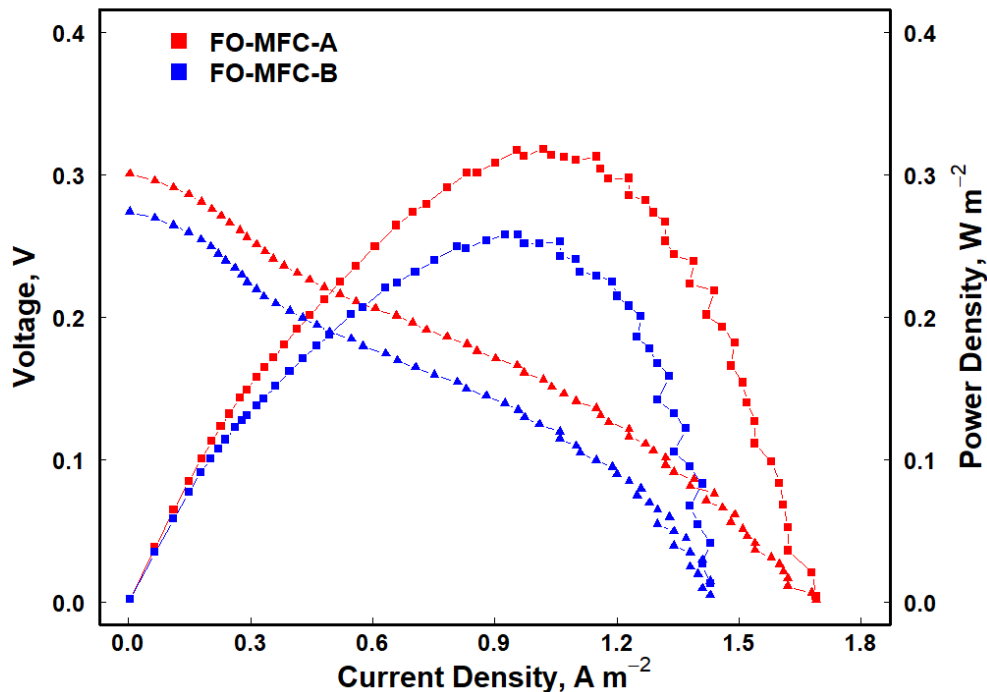


**Figure 3.3** Polarization Curves for FO-MFC-A and FO-MFC-B systems after 7 batch operation.

RSF from the FO pretreatment. Second, the increased organic loading from traditional 24-h MFC operation could have promoted microbial performance in the anode. This has been observed in other MFC studies when the electrolyte and organic loading increased [189]. In particular to the FO-MFC-A having the highest power density, the higher availability of nitrogen as ammonium possibly improved microbial growth. The average current densities observed during the 7-batch test was higher for the FO-MFC-B system ($0.82\pm 0.07$ A m$^{-2}$) than the FO-MFC-A system ($0.73 \pm 0.03$ A m$^{-2}$) (Fig. 3.4A). The electrical conductivity of the anolyte and catholyte also reflect in the current density for each system with the FO-MFC-B being mostly lower than the FO-MFC-A at the end of the batch tests (Fig. 3.4B). In addition, the catholyte electrical conductivity of the FO-MFC-B increased from 7.35 to 11.17 mS cm$^{-1}$, while the FO-MFC-A system had less change (8.47 to 9.64 mS cm$^{-1}$). No major pH fluctuations were observed for any system (Fig. B.3). This is indicative of Na$^+$ ions concentrating after passing through the CEM and NH$_4^+$ leaving the catholyte as NH$_3$ gas. This increase appears beneficial at first but likely had adverse effects due to solute accumulation in the anolyte towards the end of the batch experiments. The removal and recovery of ammonium was then compared to coulombic efficiency and energy consumption to determine the nutrient-based benefits.

### 3.3.3  Contaminant removal by the MFC

Comparing the COD removal, Coulombic efficiencies, and Coulombic recoveries of each system revealed that the microbial composition can be a major factor to consider when selecting a draw solute for FO pretreatment. The average COD removal for the FO-MFC-A and FO-MFC-B systems was $24.8 \pm 2$ % and $35.9 \pm 4$ %, respectively (Fig. 3.5).
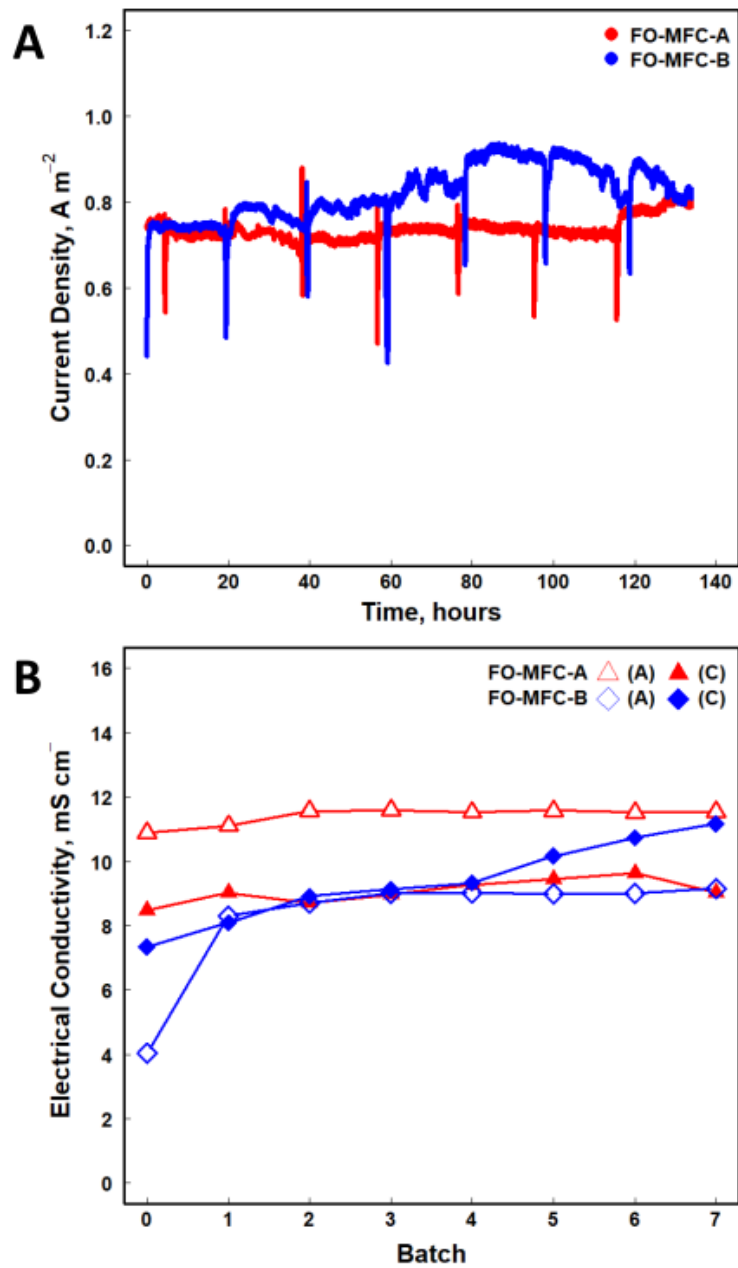
**Figure 3.4** (A) Current Density for FO-MFC-A and FO-MFC-B systems after 7 batch operation

and (B) Electrical Conductivity of the anolyte ("(A)") and catholyte ("(C)") after each batch.
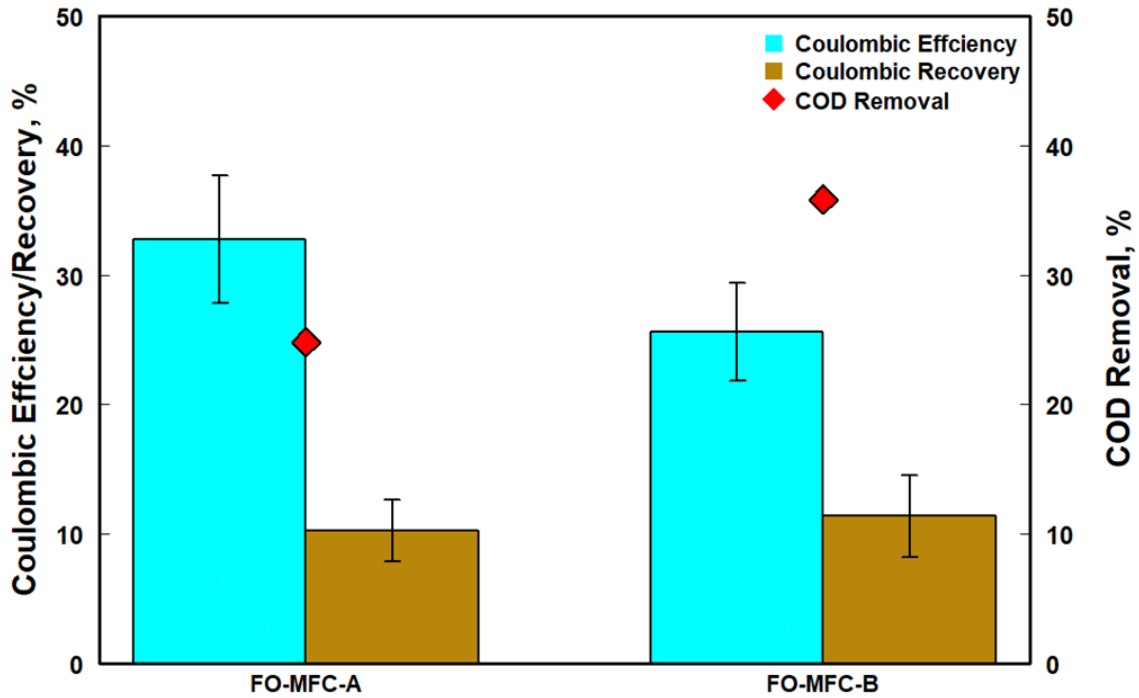
**Figure 3.5** Coulombic efficiency, Coulombic recovery, and chemical oxygen demand (COD) removal for the FO-MFC-A and FO-MFC-B systems.

The coulombic efficiency of the FO-MFC-A system ($32.8 \pm 5\%$) was higher than the FO-MFC-B system ($25.6 \pm 4\%$) despite it having a higher COD removal than the FO-MFC-A system. A previous study found that methanogenic bacteria are less inhibited by higher $Na^+$ concentrations than higher $NH_4^+$ concentrations [190]. This would suggest that while methanogens would also consume organics, they would not contribute to energy generation like the electrogenic bacteria. The Coulombic recoveries of $10.2 \pm 2$ % and $11.4 \pm 3$ % for FO-MFC-A and FO-MFC-B , respectively, were similar. The CE being higher than the CR is intrinsic due to the inputs of the equations. FO-MFC-A having a higher CE with a similar CR further suggest microbial inhibition as pointed out by other researchers [186].

The average $NH_4^+$ removal for the FO-MFC-A and FO-MFC-B systems were 47.4 ± 1 %, and 43.3 ± 2 %, respectively (Fig. 3.6). The absolute removal is presented in Figure B.4. The lower removal in the FO-MFC-B system is probably due to the higher concentration of $Na^+$ crossing the CEM to achieve electroneutrality compared to $NH_4^+$ being the primary cation for the FO-MFC-A system.
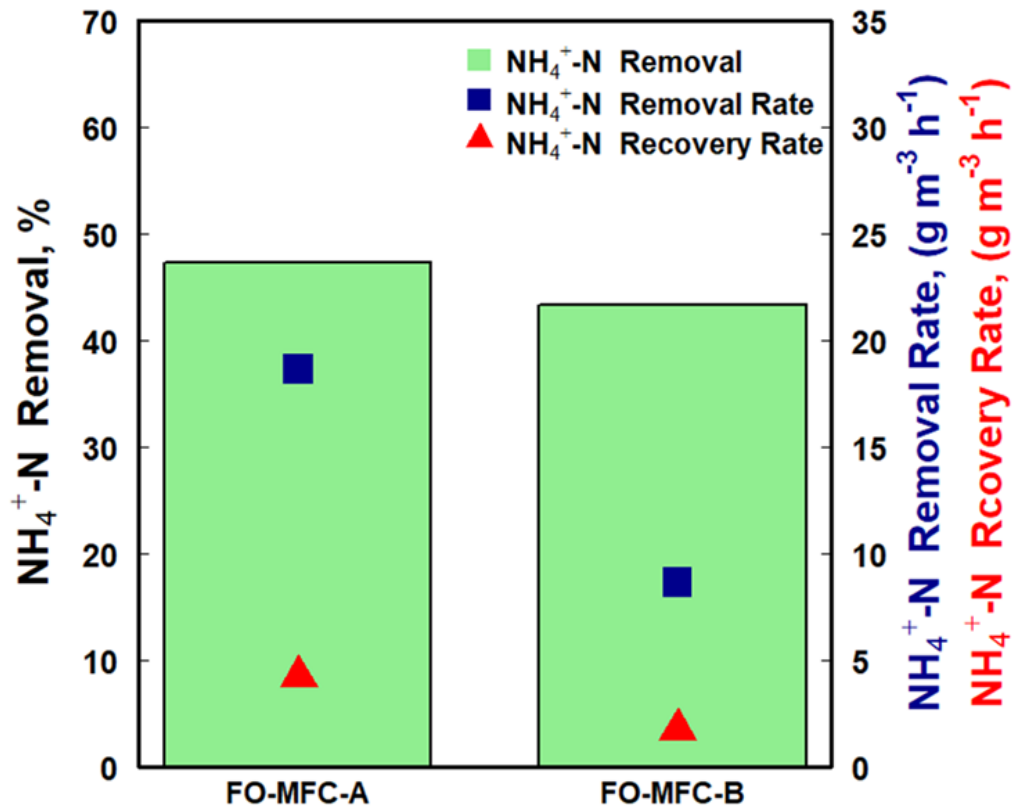


**Figure 3.6** Ammonium removal, ammonium removal rate, and ammonium recovery rate for the FO-MFC-A and FO-MFC-B systems.

The FO-MFC-A system had the highest $NH_4^+$ removal (18.6 g $NH_4^+$-N m$^{-3}$ h$^{-1}$) and recovery (4.2 g $NH_4^+$-N m$^{-3}$ h$^{-1}$) rate compared to the FO-MFC-B system (removal rate: 8.6 g $NH_4^+$-N m$^{-3}$ h$^{-1}$;

recovery rate: 1.7 g $NH_4^+$-N $m^{-3}$ $h^{-1}$). This high removal may be likely due to both the concentration of $NH_4^+$ and the balance of solution charges during MFC operation. This also shows the sustainability of ammonium based draw solutes which can be reused to generate DSs like similar studies [191] that is not observed for NaCl.

The total energy consumption, COD NEC, and $NH_4^+$ NEC of the FO-MFC-A and FO-MFC-B system had divergent results. It is very evident that aeration is the largest energy consumer in MFC treatment, which has been reflected in previous studies [192]. The recirculation energy consumption was always lower for the coupled systems as well because of FO operating at a lower recirculation rate. The coupled systems saw a decrease in energy consumption normalized to the removed COD at 2.47 kWh kg $COD^{-1}$ and 1.73 kWh kg $COD^{-1}$ for the FO-MFC-A and FO-MFC-B systems, respectively (Fig. 3.7A). In particular for the FO-MFC-B system, the decreased specific energy consumption for COD removal may be because of the microbiome makeup as mentioned previously when discussing CE and CR. The $NH_4^+$ removed and recovered NEC data showed lower consumption during the FO-MFC-A operation at 2.01 kWh $kg^{-1}$ $NH_4^+$-N compared to the energy consumptions of the FO-MFC-B system (4.33 kWh $kg^{-1}$ $NH_4^+$-N) (Fig. 3.7B). The lowest NEC for ammonium was 8.87 kWh $kg^{-1}$ $NH_4^+$-N for the FO-MFC-A system and FO-MFC-B (21.5 kWh $kg^{-1}$ $NH_4^+$-N) with a significantly higher NEC. This can be attributed to the increased concentration of $NH_4^+$ and migration across the CEM during MFC operation. Higher $NH_4^+$ removal also allowed for greater $NH_4^+$ recovery from the high pH catholyte.
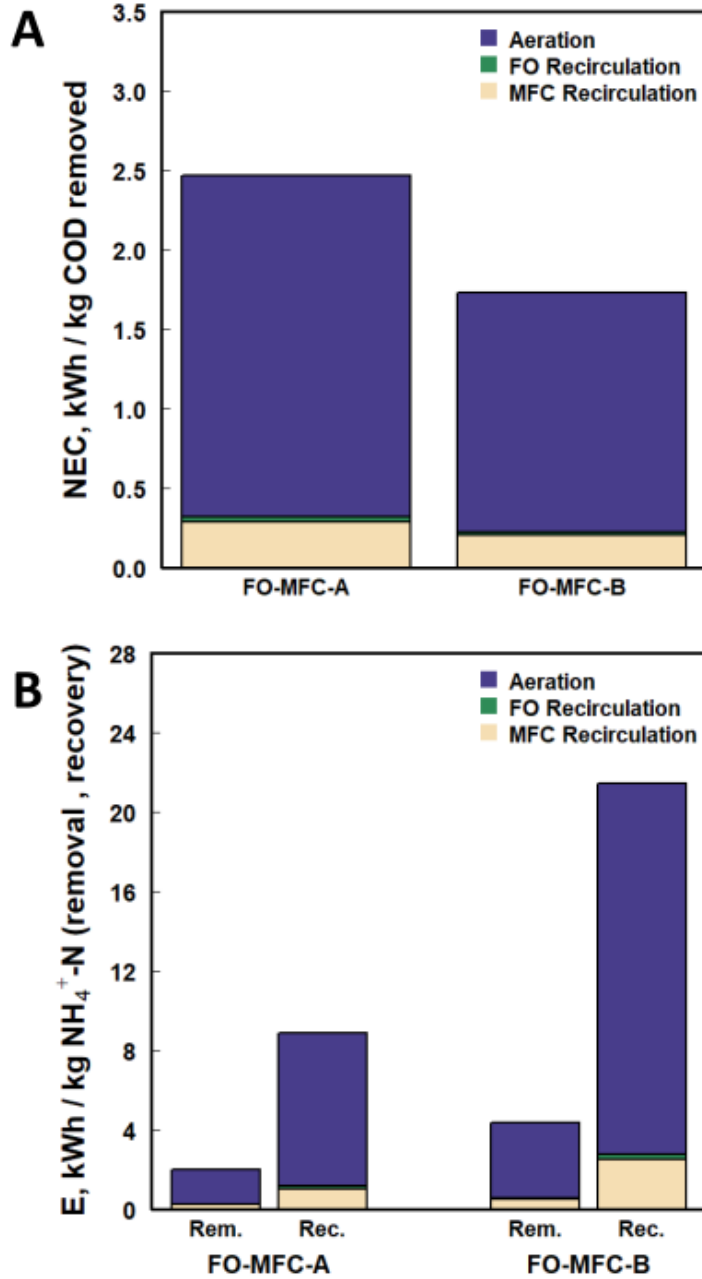
**Figure 3.7** Normalized energy consumption for aeration, FO recirculation, and MFC recirculation based on: (A) chemical oxygen demand (COD) removal; and (B) ammonium removal and recovery for FO-MFC-A and FO-MFC-B systems.

### 3.3.4 Holistic comparison between two coupled systems

A pentagon radar chart was generated in order to holistically determine the best performing system based on net energy consumption, COD removal rate, $NH_4^+$ removal rate, $NH_4^+$ recovery rate and water recovery (Fig. 3.8). Coverage of the chart is being used to show how well the systems are to the maximum values or highest performance variable outlined in the figure. The FO-MFC-A and FO-MFC-B systems covered 60.4% and 42.5%, respectively, of the total area.
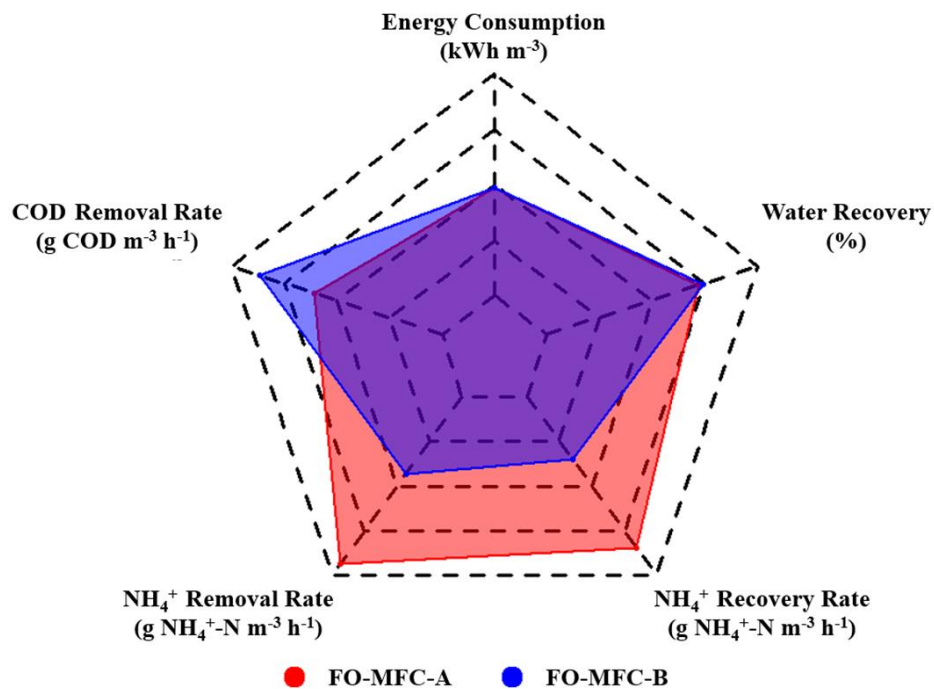


**Figure 3.8** A pentagon radar chart for FO-MFC-A and FO-MFC-B systems for energy consumption (kWh m$^{-3}$, min.: 0; max.: 10), COD removal rate (g COD m$^{-3}$ h$^{-1}$, min.: 0; max.: 25), ammonium removal rate (g $NH_4^+ - N$ m$^{-3}$ h$^{-1}$, min.: 0; max.: 20), ammonium recovery rate (g $NH_4^+ - N$ m$^{-3}$ h$^{-1}$, min.: 0; max.: 5), and FO water recovery percentages (%, min.: 0; max.: 50).

Energy consumption was relatively the same for FO-MFC-B (4.53 kWh m$^{-3}$) than FO-MFC-A (4.57 kWh m$^{-3}$). The highest COD removal rate of 21.6 g COD m$^{-3}$ h$^{-1}$ was observed

during the FO-MFC-B operation due most likely to inhibition in the FO-MFC-A system. Water recovery at 36% and 37% for the FO-MFC-A and with FO-MFC-B, respectively, are unique only for the coupled systems. This is doubly beneficial compared to a standalone MFC as less wastewater would need to be treated and recovered water could be recycled for other purposes which would decrease water consumption. Despite the FO-MFC-A system covering more area of the pentagon chart, further consideration is necessary when reviewing both the highlights and challenges so balance between coupled system performance and sustainability to elucidated. For example, the FO-MFC-B system was able to achieve higher current density because NaCl is a tolerable draw solute for microbes but cannot be regenerated for reuse in FO treatment like $NH_4HCO_3$. This is important especially in determining solute mitigation strategies to avoid solute accumulation [193]. To address this problem, future research should focus on optimizing hydraulic connection between FO and MFC since the concentration and draw solute enrichment affect the performance. This includes investigating different strength wastewaters and sustainable draw solutes. Additionally, the CE and CR data of the two systems revealed a need to perform microbial analysis under various operation times may further elucidate when draw solutes are most effective for use in FO-MFC coupled systems.

## 3.4 Conclusions

This work has explored the performance of FO-MFC coupled systems for two different draw solutes and their advantages when treating medium strength wastewater. As the DS molarity increases, the water recovered from the feed solution and reverse salt flux will increase. Using FO pretreatment will increase the concentration of electrolytes in the anolyte due to the concentrating

effect and RSF, and it will increase in the catholyte if an ion exchange membrane is used to allow ion migration. The decrease in solution resistance and increase in current density are due to the FO-MFC-B system having increased electrical conducted because $Na^+$ remained in solution while $NH_4^+$ was recovered via air stripping from the cathode. The microbiome was also affected by the different anolyte compositions and resulted in COD removal that did not directly correlate to the Coulombic efficiency and recovery. The FO-MFC-A system also showed beneficial performance in lower volumetric energy consumption, ammonium removal and recovery rates, and water recovery during FO operation. These results have shown that MFC performance can be enhanced when using FO pretreatment with nonrecoverable and recoverable draw solutes and that further systematic studies should be completed to find synergy between different technologies to improve resource recovery.

## Acknowledgements

# Chapter 4

# Recovery of both Volatile Fatty Acids and Ammonium from Simulated Wastewater: Performance of Membrane Contactor and Understanding the Effects of Osmotic Distillation

**Abstract**

Membrane Contractor (MC) is a separation method that has had growing interest because of its recovery performance and comparably lower energy consumption. Herein, a two-stage recovery MC system was investigated to recover volatile fatty acids (VFAs) and ammonium from simulated wastewater. The MC achieved the total VFA recovery of 77% ± 3%, 82% ± 5%, and 74% ± 8%, with 0.1, 0.3, and 0.5 M NaOH permeate solutions, respectively. The 0-M NaOH permeate recovered only 38% ± 2% of the VFAs due to the osmotic distillation occurring in the opposite direction (permeate to feed) of the VFA transport. Despite the initial pH of the feed solution, osmotic distillation was similar when the permeate was maintained at 0.5 M NaOH. The vapor pressure changes at each sampling period showed high correlation with the water transported ($R^2$=0.958). Ammonium recovery was not significantly different when the pH was maintained while increasing the molarity of the $H_2SO_4$ permeate, likely due to the high vapor pressure of ammonia gas. Multi-criteria decision analysis was used to determine the optimal operation conditions for MC operation. The results of this study would encourage further exploration of MC technologies for efficient recovery of VFA and ammonium from wastewater.

**Keywords:** Membrane contractor; volatile fatty acid; ammonium; anaerobic digestate, wastewater treatment

## 4.1 Introduction

Anaerobic digestion (AD) is a waste treatment technology capable of recovering energy in the form of biogas. Factors that determine the efficacy of the AD process include waste feed source, digester temperature, and microbial community composition [194, 195]. Among the key compounds of interest in digestate, both volatile fatty acids (VFAs) and ammonia can be separated and then recovered with reuse value in the agricultural, textiles and food industries [196, 197]. They abundantly co-exist in environments where anaerobic process or fermentation is occurring. Ammonia (pKa~9.23) is a reduced nitrogen species of weak base and commonly found in wastewater and sludge [198]. VFAs (e.g., acetic (pKa~4.76), propionic (pKa~4.88), and butyric (pKa~4.82) acid) are weak acids that are produced during acidogenesis from biological degradation of carbohydrates [199]. Despite the robustness of AD, there are many toxins that negatively affect the treatment process [200]. For example, a high ammonium concentration can significantly alter the carbon-nitrogen ratio which inhabits microbial degradation of long-chained carbon molecules to simple carbon structures [201, 202]. This can result in the accumulation of VFAs in the digestate and low biogas production because microorganisms cannot properly carry out acetogenesis and methanogenesis reactions [203]. However, it also presents an opportunity for the digestate to have increased amounts of VFAs and ammonium for subsequent recovery, for example using membrane technologies.

Membrane based technologies such as membrane distillation (MD), electrodialysis (ED) and reverse osmosis (RO) have been employed to recover useful resources from wastewater, and

factors such as energy consumption, recovery efficiency and efficacy, and technology durability are used to assess a technology's applicability [204]. MD operation requires a temperature gradient between a feed solution and a permeate solution which promotes water vapor transport from the hot to the cold source [205]. It was reported that nutrients such as ammonia can have a higher flux at a higher temperature of 60°C ($0.82 \pm 0.02$ g m$^{-2}$ h$^{-1}$) compared to that at a lower temperature of 20°C ($0.26 \pm 0.03$ g m$^{-2}$ h$^{-1}$) during the MD treatment [206]. Typical ED treatment takes advantage of an applied voltage to increase the migration of anions and cations across ion exchange member towards different compartments, resulting in the concentrated solutions of cations or anions [155]. Previous ED studies have reported ammonia recovery efficiency of 95.8-100% [207] and 95% recovery for acetic acid [208]. The main challenges that arise with ED and MD approaches are the increased inputs of electrical and thermal energy to drive resource recovery. Although RO is typically used as a desalination technology, it has also shown potential for ammonia recovery via concentration or gas permeation depending on the feed pH [209]. For example, 95% of ammonium was concentrated when the solution pH < 9 but 63% of ammonia gas was able to pass the RO membrane when pH > 9 [5]. The demand for a high pressure that causes acute fouling however would let RO to be less considered for resource recovery compared to other technologies.

Evolved from MD, membrane contactor (MC) has received a growing interest for resource recovery because of its low energy consumption and comparably good recovery efficiency [210]. MC has been studied to remove carbon dioxide from air sources [45, 46], and other compounds such as sulfur dioxide [211], alcohols [212], ammonia [213] and VFAs [214] as its applicability has become broader. Specifically for ammonia and VFAs, MC works if a pH gradient exists so that the gaseous form is released from the feed solution and then absorbed in the aqueous form in the permeate solution. For example, the mass flux rate of acetic acid decreased from ~11.03 to

~2.45 g m$^{-2}$ h$^{-1}$ when the solution pH was adjusted from 3 to 5.45, suggesting the immobility of acetic acid in its ionic form at the higher pH level, and the increased acetic acid recovery was observed for the increased NaOH absorption solution normality [215]. One factor that has been overlooked in many MC studies is water vapor transport via osmotic distillation because of vapor pressure difference between the feed and permeate solutions [216]. Recent studies have begun to report water flux [217, 218], but the further understanding of the implications that osmotic distillation may have on VFA and ammonia recovery is still necessary. Modeling ammonia recovery using MC has been pursued in a few studies [219-222], but many of these models lack the consideration of how water vapor transport affects recovery of volatile compounds as well as economic feasibility of using MC.

In this study, the effects of permeate composition and pH adjustment on osmotic distillation and resource recovery via MC were investigated. We proposed a two-step recovery process using a hollow fiber membrane module where switching pH would allow VFAs recovery in a NaOH absorption solution and then ammonium recovery in a H$_2$SO$_4$ absorption solution. The operation mode used in this study was direct contact, liquid-liquid MC with no temperature gradient between the feed and permeate solution, thereby minimizing the temperature influenced water vapor transport. The specific objectives of this study included: (1) demonstrating the feasibility of two-step recovery of VFAs and ammonia; (2) optimizing operation conditions for maximum VFA and ammonium recovery; (3) developing a model to predict VFA recovery, ammonium recovery, and water movement based on operation conditions; and (4) conducting initial evaluation of economic feasibility of recovering VFAs and ammonium using MC.

## 4.2  Materials and Methods

### 4.2.1  Membrane Contractor Set Up & Operation

A hollow fiber membrane module (St. Louis, USA) was used for the membrane contactor experiment. The initial volumes of the feed and permeate solutions were equal at 400 mL before pH adjustments. The detailed operation conditions are shown in Table 1 that outlines the initial pH and solute molarity for the feed and permeate solutions.

**Table 4.1** Operation Conditions for MC experiments. The VFA Recovery experiments varied permeate molarity (A) and initial feed solution pH (B). The $NH_4^+$ Recovery experiments varied initial feed solution pH (A) and varied permeate molarity (B).

| | Condition | pH (Feed) | Permeate Solution (NaOH) | | Condition | pH (Feed) | Permeate Solution ($H_2SO_4$) |
|---|---|---|---|---|---|---|---|
| VFA Recovery (A) | (i) | 3 | 0.5 M | $NH_4^+$ Recovery (A) | (i) | 9 | 0.5 M |
| | (ii) | 3 | 0.3 M | | (ii) | 10 | 0.5 M |
| | (iii) | 3 | 0.1 M | | (iii) | 11 | 0.5 M |
| | (iv) | 3 | 0 M | | (iv) | 12 | 0.5 M |
| VFA Recovery (B) | (i) | 3 | 0.5 M | $NH_4^+$ Recovery (B) | (i) | 12 | 0.5 M |
| | (ii) | 4 | 0.5 M | | (ii) | 12 | 0.3 M |
| | (iii) | 5 | 0.5 M | | (iii) | 12 | 0.1 M |
| | (iv) | 6 | 0.5 M | | | | |

The feed solution composed of 2000 mg $L^{-1}$ acetic acid, 750 mg $L^{-1}$ propionic acid, 750 mg $L^{-1}$ butyric acid, and 3.68 g $L^{-1}$ $(NH_4)_2HPO_4$, and other elements (per liter of DI water): 0.15 g $NH_4Cl$, 0.5 g NaCl, 0.015 g $MgSO_4$, 0.02 g $CaCl_2$, 0.1 g $NaHCO_3$. The pH adjustments were made with $H_2SO_4$ and/or NaOH. The feed and permeate solutions were recirculated through the

membrane module at 20 mL min$^{-1}$. The VFA recovery tests were operated in a batch mode of 24 hours with sample collection at 0, 3, 6, 12, and 24 h. The ammonium recovery tests were operated in a batch mode of 6 hours with samples taken at 0, 1, 2, 3, and 6 h. The membrane was cleaned by (i) backwash with DI water, (ii) backwards flushing with acid/ base, (iii) acid/base soak, and (iv) forward flushing with DI water. Before VFA separation, an acid solution was used on the feed side of the membrane and a base solution was used on the permeate side for membrane cleaning step (ii) and (iii). Before ammonium separation, a base solution was used on the feed side of the membrane and an acid solution was used on the permeate side for membrane cleaning step (ii) and (iii). All tests were performed in triplicate under room temperature (~24 ℃). Schematic of set-up is presented in Figure 4.1.
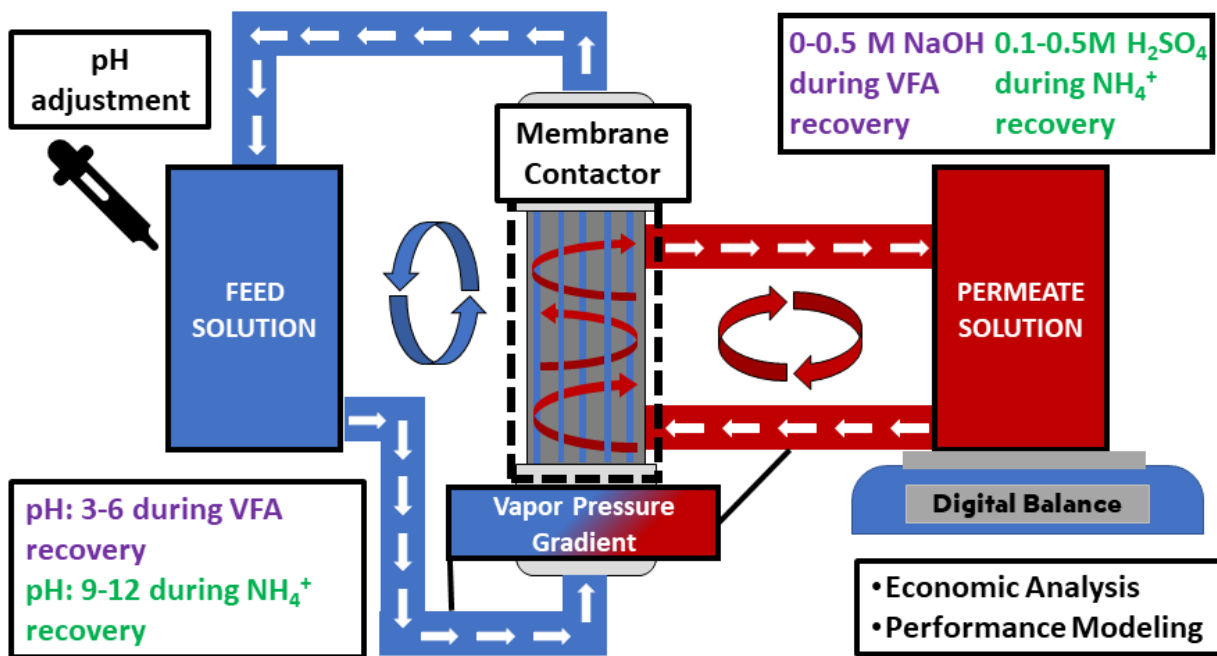


**Figure 4.1** Schematic and experimental description for membrane contactor setup.

## 4.2.2 Measurement and Analysis

A digital balance (Scort Pro, Ohous, Columbia, MD, USA) was used to measure the permeate solution mass. LoggerPro data collection software was used to record mass of the permeate at 2-minute intervals. Water flux ($J_w$, L h$^{-1}$) was calculated according to Eq. (1):

$$J_w = \frac{\Delta m}{\Delta t} \tag{1}$$

where $\Delta m$ (g) is the change in mass of the feed solution that is converted to liters and $\Delta t$ is the change in time (h$^{-1}$).

The VFA and NH$_4^+$ transport and recovery were calculated using Eq. (2-3):

$$J_S = \frac{C_f V_f - C_i V_i}{\Delta t} \tag{2}$$

$$\% = \frac{C_f V_f - C_i V_i}{C_i V_i} \tag{3}$$

where $C_f$ and $C_i$ (mmol L$^{-1}$ and mg L$^{-1}$) represent the final and initial concentration, respectively, of VFA and NH$_4^+$. The $V_f$ and $V_i$ (L) variables represent the final and initial volumes of the feed solution, respectively.

Specific flux (g L$^{-1}$) was calculated according to Eq. (4):

$$\text{Specific flux} = J_S/J_w \tag{4}$$

VFAs were analyzed using gas chromatography equipped with a flame ionization detector (Focus GC, Thermo Scientific; GC-FID). The ammonium concentration was analyzed using cation chromatography equipped with IonPac CS12A (Dionex Easion, Madison, WI, USA). Electrical Conductivity (Mettler-Toledo, Columbus, OH, USA) and pH (Oakton Instruments, Vernon Hills, IL, USA) were measured using benchtop conductivity and pH meters.

## 4.2.3 Modeling

To understand water permeation during the MC treatment, the vapor pressures of the feed and permeate solutions were calculated. Raoult's Law was used to calculate the theoretical vapor pressure ($P_{solution}$) of each solution according to Eq. (5-8):

$$P_{solution} = P_{water} - \sum_{1}^{n} \chi_{solvent} P^o_{solvent} + \sum_{1}^{n} \chi_{solvent} P^o_{solvent} \tag{5}$$

$$\chi_A = \frac{n_A}{n_A + n_B} \tag{6}$$

$$K_a = \frac{[H^+][VFA^-]}{[VFA]} \tag{7}$$

$$K_b = \frac{[NH_4^+][OH^-]}{[NH_3]} \tag{8}$$

where $P_{water}$ (mmHg) is the vapor pressure of pure water (23.8 mmHg), $\chi_A$ is the mole fraction of the solvent, $P^o_{solvent}$ (mmHg) is the initial vapor pressure of the solvent, $n_A$ and $n_B$ represent the moles of the solvents and solutes, $K_a$ represents the disassociation constant of the acids to determine the state of VFAs based on pH and $K_b$ represents the disassociation constant of the base to determine the state of ammonium based on pH in the solution.

The vapor pressure gradient between the feed and permeate solution was calculated according to Eq. 9:

$$\Delta(P_{feed} - P_{permeate}) = \frac{(P_{feed} - P_{permeate})_f - (P_{feed} - P_{permeate})_i}{2} \tag{9}$$

where $P_{feed}$ and $P_{permeate}$ (mmHg) are the vapor pressure of the feed and permeate solutions, respectively, and the $P_f$ and $P_i$ are the vapor pressure gradients of the final and initial samples, respectively.

## 4.3  Results and Discussion

### 4.3.1 VFAs recovery dependence on NaOH and pH

VFAs were successfully recovered using the MC with NaOH in the permeate solution. In details, the recovery of acetic acid was less affected by NaOH and exhibited similar efficiency of $76 \pm 3\%$, $79 \pm 6\%$, and $70 \pm 9\%$ with the 0.1 M, 0.3 M, and 0.5 M of NaOH, respectively (Fig. 4.2A). The MC achieved more recovery of propionic acid ($80 \pm 3\%$, $86 \pm 2\%$, and $80 \pm 8\%$) and butyric acid ($86 \pm 8\%$, $92 \pm 2\%$, and $89 \pm 5\%$) with three tested NaOH solutions.
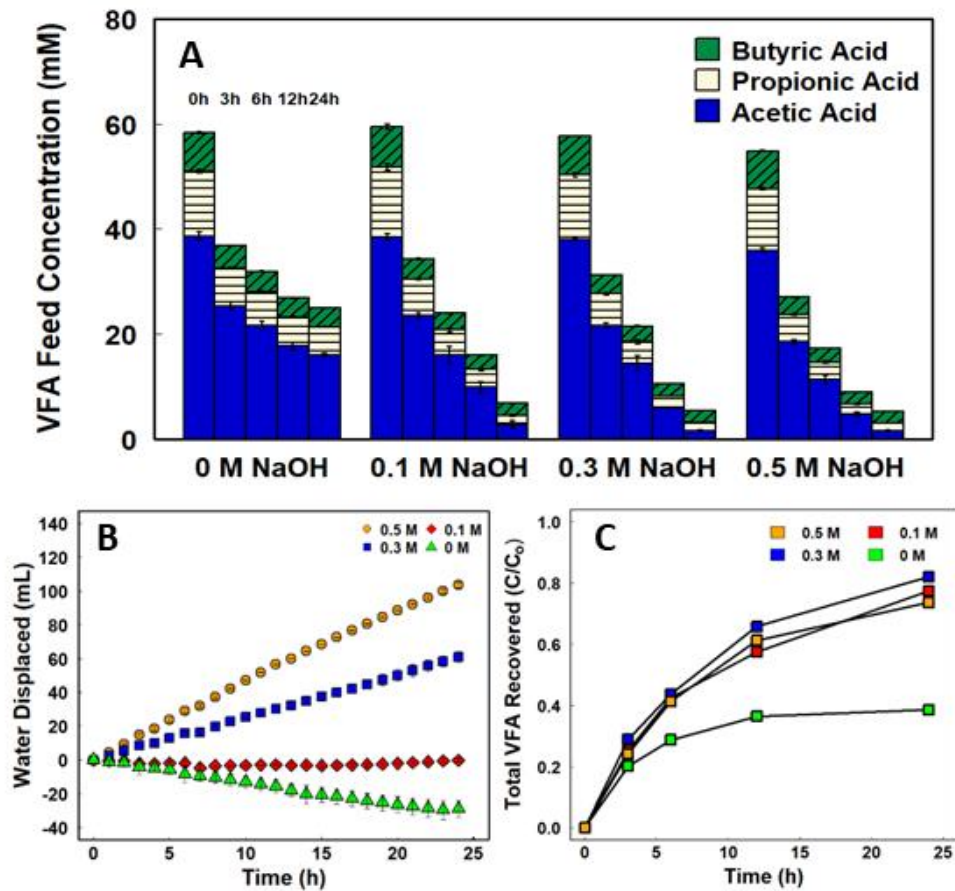


**Figure 4.2** VFA separation using various NaOH molarities as the permeate while maintaining feed pH=3: (A) Feed VFA distribution at each sampling time, (B) water displacement, and (C) total VFA recovery.

68

The phenomenon that higher recovery of higher-chained VFAs was also reported in the previous studies that utilized gas permeable membranes for VFAs separation and recovery [214]. In the absence of NaOH in the permeate solution (0 M), the MC recovered $36 \pm 2\%$, $39 \pm 2\%$, and $45 \pm 2\%$ of three different types of VFAs, with a total VFAs recovery efficiency of $38 \pm 2\%$ in a period of 24 hours. Despite a lack of alkaline solution in the permeate, the highly acidic feed (pH=3) should have resulted in some VFAs being able to cross the gas permeable membrane. The previous finding that increasing the molarity permeate solutions yield greater recovery across gas permeable membrane [215] was not clearly observed in the present study.

Because of water osmosis, the 0.5 M and 0.3 M NaOH adsorption solutions extracted $100\pm5$ mL and $60\pm8$ mL of water from the feed solution, respectively (Fig. 4.2B). That is, some water was moving in the same direction as VFAs from the feed to the permeate solution. On the contrary, when the adsorption solution did not contain NaOH, $30\pm9$ mL of water transported in a reverse direction from the permeate to the feed, because the pure water permeate (0 M NaOH) had a higher vapor pressure due to the lack of solutes than the feed solution. This reversal water movement in the opposite direction of VFAs migration might have created some resistance to VFAs migration and contributed to the significantly lower VFAs recovery ($38 \pm 2\%$) ($p<0.05$) than that with the 0.1, 0.3, and 0.5 M NaOH ($77 \pm 3\%$, $82 \pm 5\%$, and $74 \pm 8\%$) (Fig. 4.2C).

To further understand the effects of osmotic distillation, the permeate solution containing 0.5 M NaOH was maintained while the pH of the feed solution was adjusted from 3 to 6. After the MC treatment, the total VFAs concentration in the feed was 5.30 mM, 15.36 mM, 40.91 mM, and 53.14 mM, at the pH of 3, 4, 5, and 6, respectively (Fig. 4.3A). A higher VFAs concentration at a higher feed pH was because of VFAs being more ionized at the higher pH level and thus rejected by the gas permeable membrane. Interestingly, these results occurred under relatively high water

transport compared to the tests where the pH was maintained and the permeate solution molarity was adjusted. The water displaced increased from $91.5 \pm 2.9$ mL (pH=6) to $101.8 \pm 0.9$ mL (pH=5), $103.5 \pm 1.7$ mL (pH=3), or $110.8 \pm 9.8$ mL (pH=4) (Fig. 4.3B). The total VFAs recovered was significantly lower at pH=5 ($28 \pm 4\%$) or pH=6 ($16 \pm 2\%$) because of the solution pH exceeding the $pK_a$ for each VFA (Fig. 3C). The pH and EC of the feed and permeate solutions had little effect on the VFA recovery (Fig. C.2 and C.3).
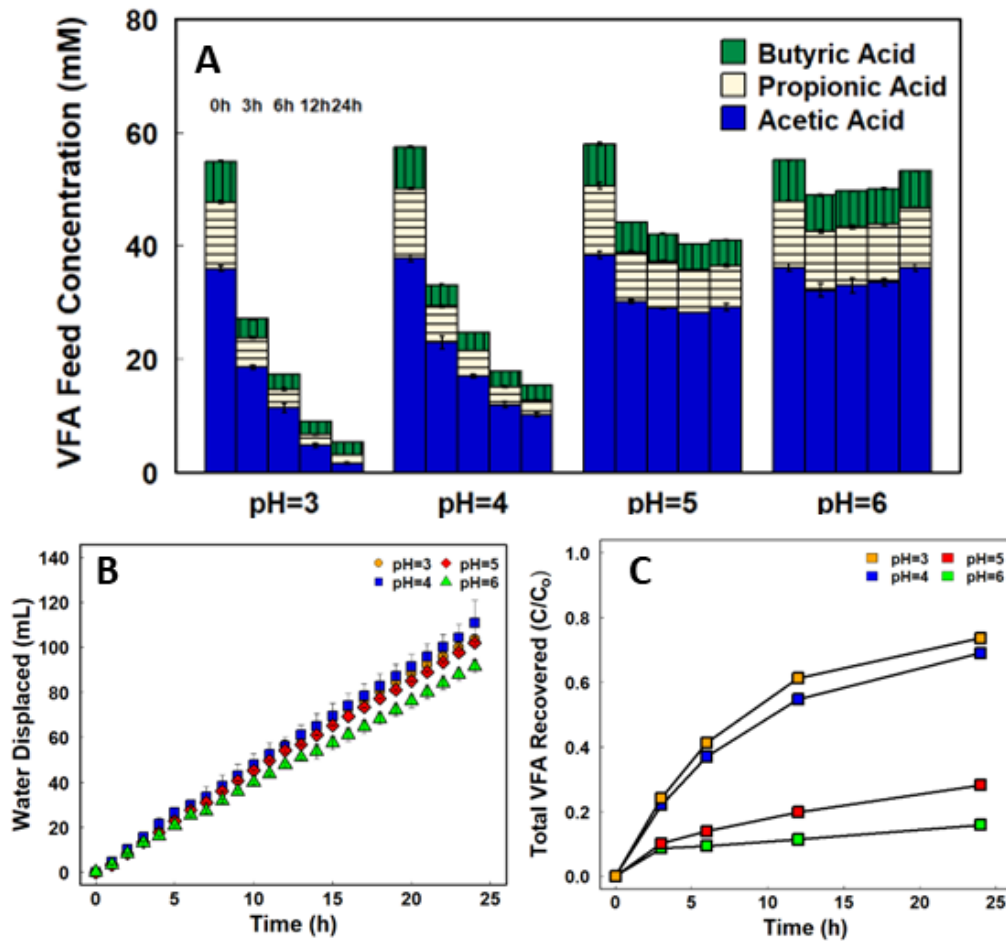


**Figure 4.3** VFA separation using various initial feed pH levels while maintaining 0.5 M NaOH permeate: (A) Feed VFA distribution at each sampling time, (B) water displacement, and (C) total VFA recovery.

Specific VFAs flux corroborated the observation that VFAs transport is a separate phenomenon from osmotic distillation. When the permeate solution was maintained at 0.5 M NaOH, the water flux decreased from 5.26 mL h$^{-1}$ at 3 h to 3.65 mL h$^{-1}$ after 24 h of the MC treatment (Fig. 4.4). The test under the condition of 0.1 M NaOH and pH=3 showed that VFAs
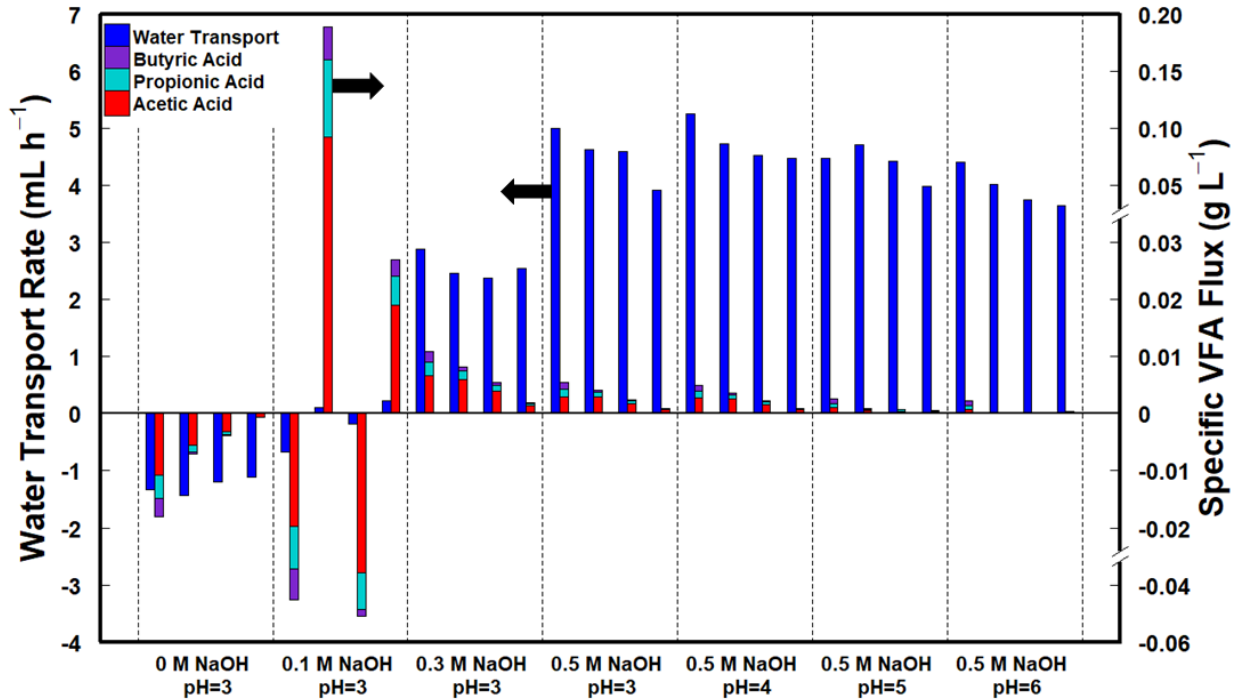


**Figure 4.4** Water transport and specific VFA flux for MC operation modes.

could transport across the membrane despite water movement. The vapor pressure difference due to different compositions of the feed and permeate solutions was more likely the driving force for water transport. In the presence of individual VFAs, the water transport showed high correlation (R$^2$=0.958) to the vapor pressure gradient (Fig. 4.5). As the theoretically calculated vapor pressure increased, more water moved from the feed to the permeate. Reverse water transport was observed when the vapor pressure of the permeate was higher than that of the feed (pH=3, pure water permeate). A small range (0.126-0.173 mmHg) of vapor pressure gradient difference with an

average of $0.154 \pm 0.015$ mmHg was determined for the operation modes using 0.5 M NaOH as a permeate, because the amount of VFAs in the gaseous state did not alter the solutions vapor pressure compared to the amount of base that did significantly decrease the permeates vapor pressure.
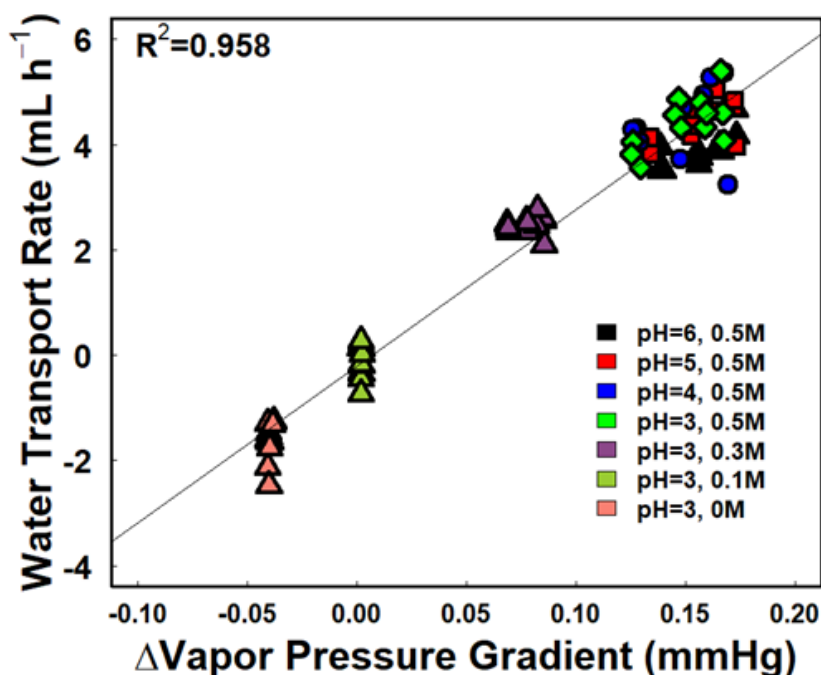


**Figure 4.5** Water transport during each sampling period for each iteration of the MC separation of VFAs.

### 4.3.2 Ammonium recovery dependence on $H_2SO_4$ and pH

Ammonium recovery was mainly dependent on the initial pH of the feed solution instead of the $H_2SO_4$ molarity of the permeate (adsorption solution). The water displaced also had direct correlation to the permeate solution. As the $H_2SO_4$ molarity in the permeate increased from 0.1 to 0.5 M, the water displaced from the feed to the permeate increased from $19.1 \pm 6.4$ to $54.2 \pm 8.1$

mL (Fig. 4.6A). Similar to the VFA recovery, the displaced water was due to osmotic distillation based on the vapor pressure gradient between the feed and the permeate. Ammonium recovery efficiencies of $63.9 \pm 6$ % (0.1 M of $H_2SO_4$), $69.7 \pm 1$ % (0.3 M), and $73.3 \pm 18$ % (0.5 M) were obtained in the first hour of MC separation (Fig. 4.6B), benefited from the high vapor pressure of $NH_3$ gas when the pH of the feed solution was adjusted to 12 using NaOH.

After 6 hours of the MC operation, the recovered ammonium using 0.1 M, 0.3 M and 0.5 M $H_2SO_4$ permeate solutions was $71.1 \pm 6$ %, $74.9 \pm 2$ %, and $81.0 \pm 7$ %, respectively. The difference of recovery efficiency between 1-hour and 6-hour operation suggested that most of recovery occurred in a relatively short period of time and thus the extended MC operation might not be necessary (which would help decrease the operation related expense). Indeed, less than 10% of the recovered ammonium was obtained in the last 5 hours of the treatment time. Changes in pH for feed pH=9-10 explain the decrease in recovery (Fig. C.4). Additionally, less water was displaced with the lower molarity permeate solutions, suggesting that the vapor pressure gradient was lower than the higher molarity permeate solution tests. Water displacement increased as the feed pH was adjusted from 9 to 12 due to the increased vapor pressure gradient. Only $25.4 \pm 1.9$ mL of the feed water transported into the permeate at the feed pH of 9, much lower than $54.6 \pm 7.5$ mL at the pH=12, related to the $NH_4^+/NH_3$ ratio (Fig. 4.7A): the solution having more $NH_4^+$ present at lower pH levels would lower the vapor pressure and thus result in less water transport; in contrast, higher pH levels mean more $NH_3$ is present which increases the vapor pressure resulting in a greater vapor pressure gradient and more water transport. The pH and EC of the feed and permeate also adjusted as ammonium moved across the membrane (Fig. C.5). Ammonium recovery obtained after 6 hours of operation was $29.7 \pm 7$%,
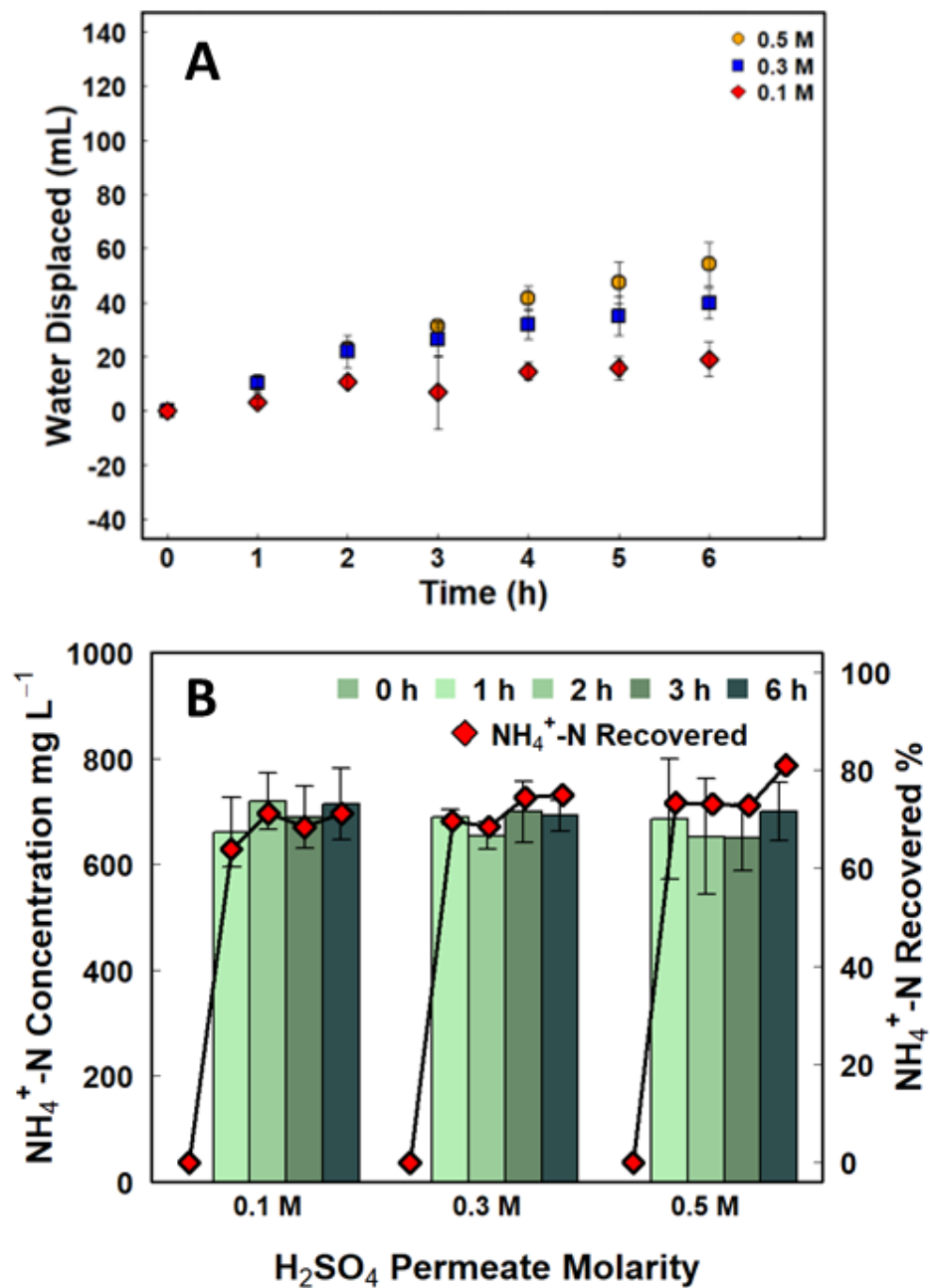
**Figure 4.6** Ammonium separation using different $H_2SO_4$ solutions as the permeate while maintaining initial feed pH=12: (A) water displacement and (B) $NH_4^+$ concentration and recovered amount in the permeate.

63.1 ± 4%, 70.2 ± 3%, and 81.0 ± 7 %, at pH=9, 10, 11 and 12, respectively. Clearly, a higher

permeate pH could drive more $NH_3$ to transport across the gas permeable membrane. Compared

to the $H_2SO_4$ permeate solution tests, ammonium recovered went from 16.6 ± 4 % to 29.7 ± 7 %
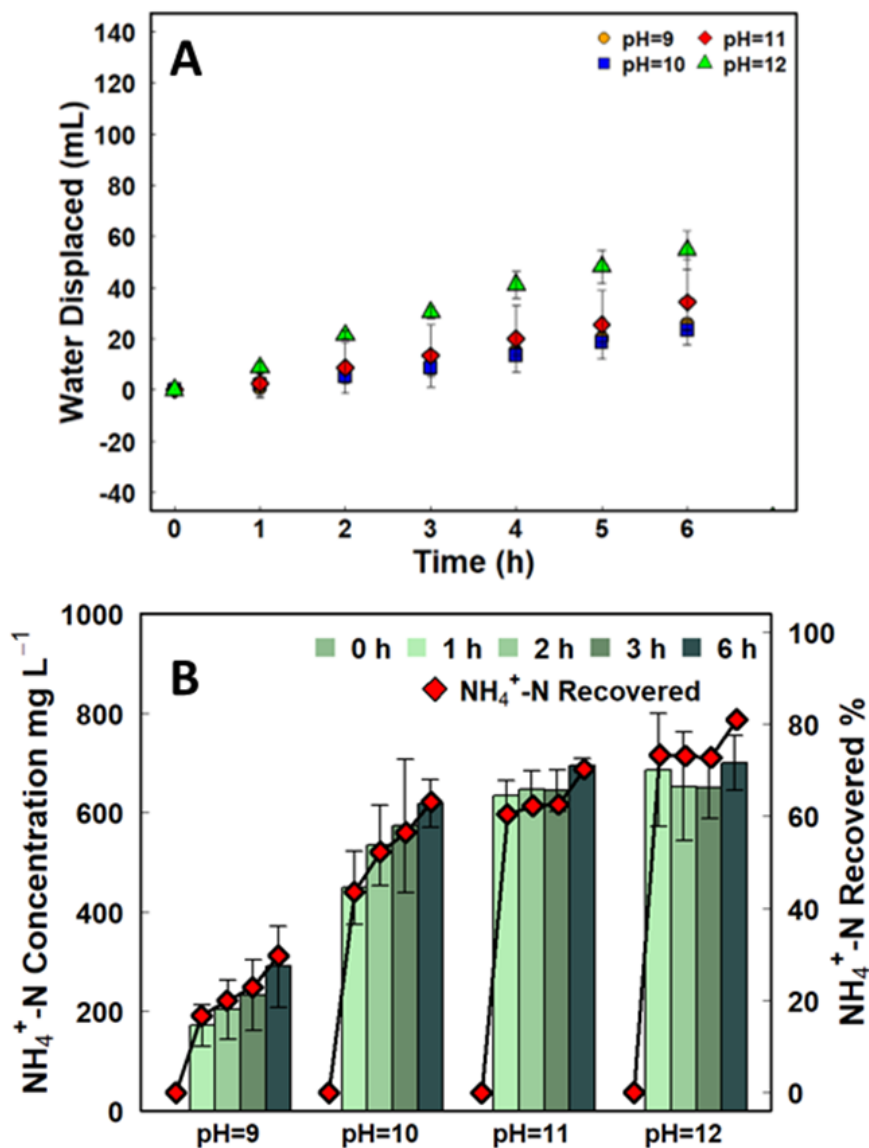


**Figure 4.7** Ammonium separation using different initial feed pH levels while maintaining 0.5 M

$H_2SO_4$ permeates: (A) water displacement and (B) $NH_4^+$ concentration and recovered amount in

the permeate.

(pH=9) and 43.6 ± 7 % to 63.1 ± 4 % (pH=10) from the first to last hour, respectively. Higher recovery was observed initially for pH=11 and pH=12, indicating that less time is necessary for ammonium recovery at higher pH levels despite the molarity of the permeate solution. Additional benefits of less acid usage and less energy demand could be beneficial to the overall MC recovery process.

The specific flux of ammonium between the tests where the permeate solution was maintained (0.5 M $H_2SO_4$) decreased from 59.9 g $NH_4^+$-N $L^{-1}$ at pH=11 to 16.4 g $NH_4^+$-N $L^{-1}$ at pH=9. When the pH of the feed was maintained at pH=12, the specific flux of ammonium trended downward with an increase in permeate solution molarity. The highest specific ammonium fluxes
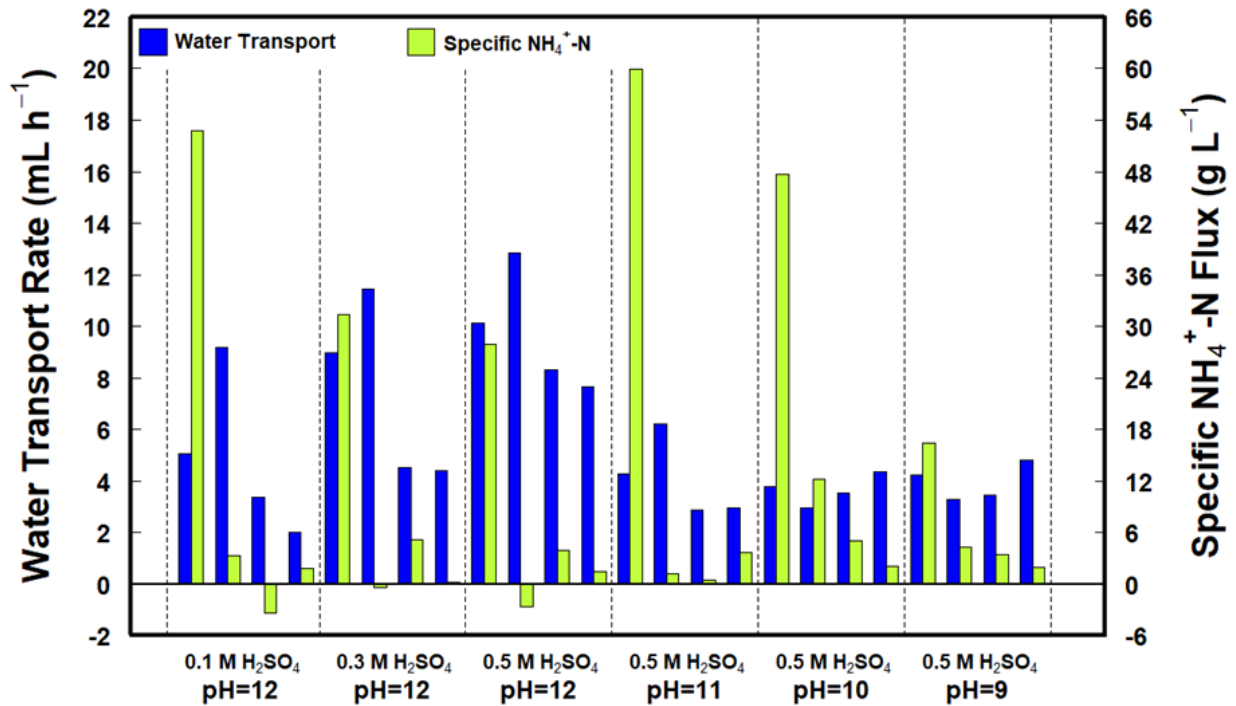


**Figure 4.8** Water transport and specific $NH_4^+$ flux for MC operation modes.

were 59.9 g $NH_4^+$-N $L^{-1}$ (0.5 M $H_2SO_4$ and feed pH=11), 52.7 g $NH_4^+$-N $L^{-1}$ (permeate: 0.1 M $H_2SO_4$ and feed pH=12), and 47.7 g $NH_4^+$-N $L^{-1}$ (permeate: 0.5 M $H_2SO_4$ and feed pH=10) (Fig. 4.8).

An evident trend was not observed based on pH or molarity. A point to highlight however is that similar recovery at the different starting feed pH levels may suggest that adjusting to the highest pH or generating a higher molarity permeate might not be necessary. This would decrease the need for dilution of the permeate and cost for operation. In addition, the water transport rate for the conditions when the feed pH=12 for the 0.1 M, 0.3, and 0.5 M permeate solutions increased from $5.07 \pm 3.4$ to $6.30 \pm 3.6$ mL $h^{-1}$, $8.97 \pm 3.2$ to $13.00 \pm 3.5$ mL $h^{-1}$, and $10.13 \pm 3.4$ to $12.83 \pm 1.5$ mL $h^{-1}$, respectively, from the first hour to the second hour of the MC operation. This is likely due to the decrease of the permeate vapor pressure after the rapid recovery of ammonium. A similar transport rate trend ($4.27 \pm 3.9$ mL $h^{-1}$ to $6.23 \pm 4.8$ mL $h^{-1}$) was observed when the permeate was 0.5 M $H_2SO_4$ and the pH=11 in the feed. In the case where the ammonium recovery happened more slowly due to a lower $NH_4^+/NH_3$ ratio (pH=9 and 10) at pH levels closer to $pK_a$=9.23, lower water transport was observed. However, higher water recovery occurred when the feed pH=10 compared to feed pH=9 that did not yield greater ammonium transport, suggesting that the pH of the solution had a greater effect than osmotic distillation. This ultimately means that each operating conditions optimal recovery requires less time because of $NH_3$ having a high vapor pressure at higher pH levels.

### 4.3.3 Economic Factors and Decision Analysis

Economic feasibility of the proposed two-stage recovery system should be considered when determining optimal operating conditions. The cost of each operation condition is related to

the amount of acid ($H_2SO_4$) and base (NaOH) necessary to adjust the pH of both feed sand permeate solutions (Table C.1). The cost increased as the feed pH decreased in the VFA recovery mode or the feed pH increased in the $NH_4^+$ recovery mode, as well as for increasing molarity permeate solutions. The cost of each combination of VFA and $NH_4^+$ recovery was then compared to the recovery percentages observed during the MC experiments (Fig. 4.9). The recovery of ammonium had the lowest Quartile range (66.5%-78.0%) for variables that would determine operation conditions. The VFA recovery ranged from the 1st Quartile to the 2nd Quartile is 35.9% to 74.8%, respectively, suggesting that operational decisions are more important to the MC efficacy separation for VFA recovery compared to ammonium recovery. The use of acid and base for pH change and permeate generation also showed a wide range from $0.27 to $1.19 for the various configuration of VFA and ammonium recovery that were possible based on combining operation modes. The balance between VFA recovery, ammonium recovery, and cost are not well explained by the variability to understand which operation modes would be most favorable. Additional analysis is warranted to identify optimal conditions based on economic feasibility and resource recovery efficacy.

Multi-criteria decision analysis was used to determine the optimal operating conditions based on VFA recovery, ammonium recovery and cost of operation. The 42 number of possible combinations were evaluated using 4 variables ($v_1$=Cost, $v_2$=VFA recovery, $v_3$=$NH_4^+$ recovery $v_4$=VFA/$NH_4^+$ ratio) for 4 situations ($S_1$- equal variable weight, $S_2$- cost variable heavily considered $S_3$- cost variable mildly considered , $S_4$- cost variable lowly considered). The different situations were able to evaluate the cases where recovery performance and cost were of equal importance, as well as a range of importance of either variable. After compiling the operation
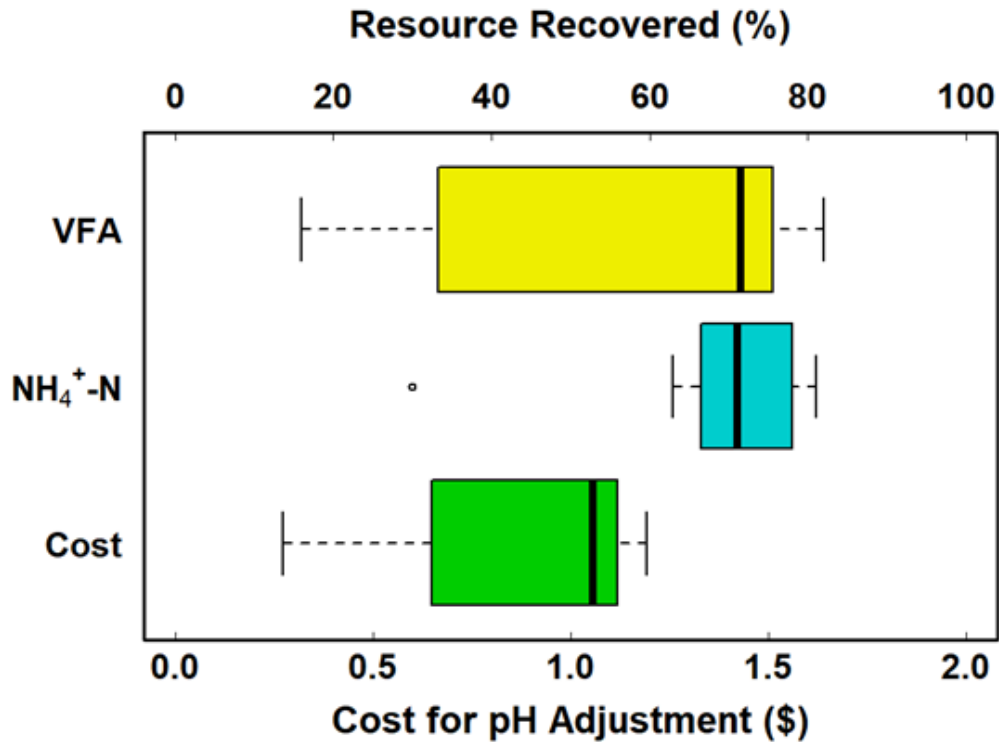
**Figure 4.9** VFA and NH$_4^+$ recovered for every experiment iteration and cost based to generate either the NaOH or H$_2$SO$_4$ and adjust the feed pH.

combinations, multiple combinations were favorable in more than 1 situation due to high rankings after applying variable weights (Table 4.2). The only combination recovery steps that made it into the top of the analysis of the 4 situations was NH$_4^+$ (pH=12, 0.1 M H$_2$SO$_4$; pH=3, 0.1 M NaOH). This is due mainly to the low cost necessary to generate the permeate solutions in both VFA and NH$_4^+$ recovery modes. Situation 2 is the only situation where a different operation mode was favored because of a lack of a NaOH permeate solution. Overly considering cost however may not be a strong evaluation due to such low consideration of performance. While not considered in the multi-criteria decision analysis, limiting the dilution of the permeate due to osmotic distillation

**Table 4.2** Multiple Criteria Decision Analysis for 4 Situations (S) with 4 decision variables (v) normalized between 0 and 1. $S_1$- Equal variable weight, $S_2$- Cost variable heavily considered $S_3$- Cost variable mildly considered , $S_4$- Cost variable lowly considered. $v_1$=Cost, $v_2$=VFA recovery, $v_3$=$NH_4^+$ recovery $v_4$=VFA/ $NH_4^+$ ratio

| | $S_1$ ($v_1$=0.25, $v_2$=0.25, $v_3$=0.25, $v_4$=0.25) | $S_2$ ($v_1$=0.70, $v_2$=0.10, $v_3$=0.10, $v_4$=0.10) | $S_3$ ($v_1$=0.40, $v_2$=0.20, $v_3$=0.20, $v_4$=0.20) | $S_4$ ($v_1$=0.10, $v_2$=0.30, $v_3$=0.30, $v_4$=0.30) |
|---|---|---|---|---|
| 1 | [A]$NH_4^+$:pH=12,0.1M VFA: pH=3,0.1M | [E]$NH_4^+$:pH=12,0.1M VFA: pH=3,0M | [A]$NH_4^+$:pH=12,0.1M VFA: pH=3,0.1M | [C]$NH_4^+$:pH=12,0.5M VFA: pH=3,0.1M |
| 2 | [B]$NH_4^+$:pH=12,0.3M VFA: pH=3,0.1M | [A]$NH_4^+$:pH=12,0.1M VFA: pH=3,0.1M | [B]$NH_4^+$:pH=12,0.3M VFA: pH=3,0.1M | $NH_4^+$:pH=12,0.5M VFA: pH=3,0.3 M |
| 3 | [C]$NH_4^+$:pH=12,0.5M VFA: pH=3,0.1M | $NH_4^+$:pH=12,0.3M VFA: pH=3,0 M | [E]$NH_4^+$:pH=12,0.1M VFA: pH=3,0M | $NH_4^+$:pH=12,0.5M VFA: pH=3,0.3 M |
| 4 | [D]$NH_4^+$:pH=11,0.5M VFA: pH=3,0.1M | $NH_4^+$:pH=10,0M VFA: pH=3,0 M | [C]$NH_4^+$:pH=12,0.5M VFA: pH=3,0.1M | [B]$NH_4^+$:pH=12,0.3M VFA: pH=3,0.1M |
| 5 | $NH_4^+$:pH=12,0.1M VFA: pH=3,0.3M | $NH_4^+$:pH=11,0.5M VFA: pH=3,0 M | [D]$NH_4^+$:pH=11,0.5M VFA: pH=3,0.1M | [A]$NH_4^+$:pH=12,0.1M VFA: pH=3,0.1M |

would allow for a more concentrated source of each resource. To determine if there are any advantages of recovering VFA or $NH_4^+$ first, additional MC separation tests were completed.

The recovery of acetic acid (1st: 71 ± 4% vs. 2nd: 70 ± 4%), propionic acid (1st: 77 ± 4% vs. 2nd: 76 ± 3%) and butyric acid (1st: 81 ± 3% vs. 2nd: 81 ± 3%) was the similar regardless of the recovery order and minimal loss (Fig. 4.10). The $NH_4^+$ recovered was higher at 81 ± 7 % as the second step compared to 73 ± 3% as the first step based on the amount of ammonium available. However, the absolute amount revealed that $NH_4^+$ lost was lower when it was recovered first. This suggests that the 1-hour recovery of A should take place initially before the 24-hour VFA recovery.
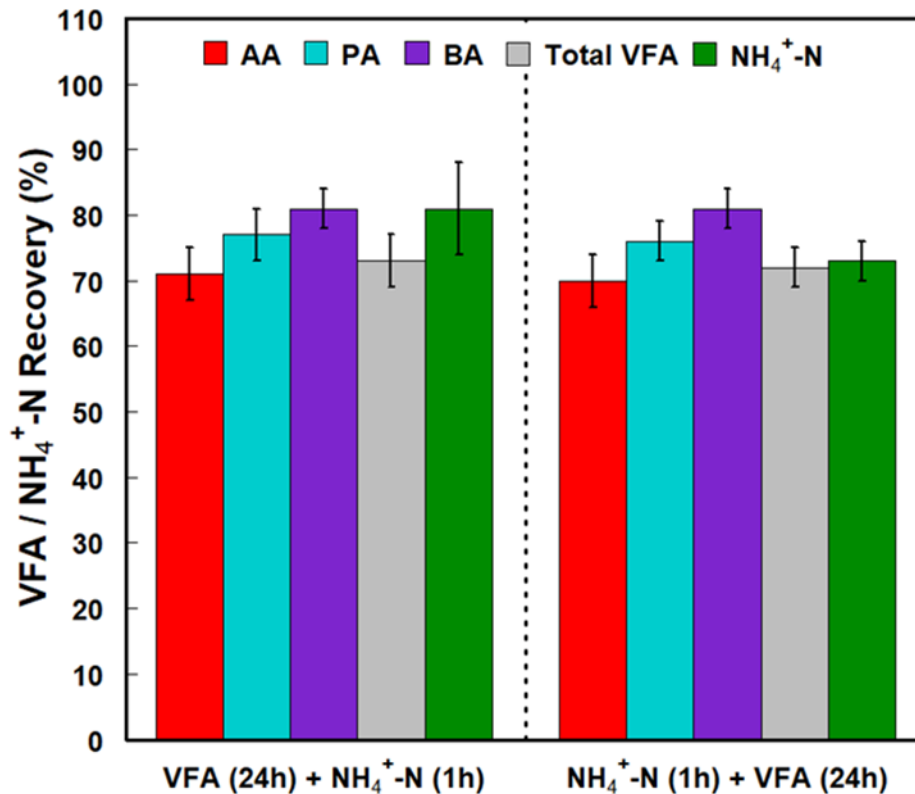
**Figure 4.10** VFA and $NH_4^+$ recovered in two phases for both altering which compound was recovered first.

### 4.3.4 Perspectives

Utilizing MC for recovery of volatile fatty acids and ammonium is potentially a promising method because of the decreased energy demand compared to MD. Challenges around recovery time, operational cost, and performance decline due to fouling would need to be addressed to improve the technologies implementation. First, VFAs in their gaseous state have a much lower vapor pressure than ammonia which results in a long recovery time that is over 24 times slower. This could be solved through design where MC retention time for VFA recovery is greater than that for ammonia. Absorption of VFAs utilizing amine-functional groups has shown to have recovery times less than 280 minutes [223] and could potentially be applied in membrane fabrication to

increase recovery rate during MC operation. Second, the use of acids and bases can increase the cost of the operation for both VFA and ammonium recovery. Addressing this issue is highly necessary to increase the economic feasibility of MC separation. Producing acid and based using electrolysis has shown to be an effective approach for recovery of many resources from wastewater [224] but would increase the energy intensiveness. Using renewable energy such as solar energy that is becoming more popular in wastewater treatment plants may help address the energy need by electrolysis that provides onsite acid/base production. Third, membrane fouling is an inevitable issue. Because the two-stage recovery MC process requires acidification and alkalization of the wastewater, the effects of membrane fouling might be decreased during operation changes [225]. Understanding long term effects of VFA and ammonium recovery could help increase the financial feasibility inclusive of membrane requirements. For instance, using less acid and base to achieve recovery with less osmotic distillation could increase the chances of biological fouling in membrane pores [226]. This could be averted using different membrane fabrication and modification techniques that has been explored in membrane fouling literature.

## 4.4 Conclusions

This study has demonstrated a two-stage MC system for effective recovery of both VFAs and ammonium. The VFAs were recovered from the feed solution most effectively when the pH was less than the pKas of the VFAs. Recovery of VFAs was hindered in cases when the vapor pressure of the permeate solution was higher than the feed solution. A correlation was observed between the vapor pressure difference and water transport across the hollow fiber membrane. Ammonium recovery occurred much faster than VFA recovery due to its higher vapor pressure. Multi-criteria decision analysis also identified the most optimal operating conditions when considering the cost

and recovery performance of each operating condition. Future research should seek to address the challenges about VFA/$NH_4^+$ recovery coordination, operation costs, performance prediction, and membrane fouling due to long term operation.

# Chapter 5

# Integrating Membrane Contactor into Microbial Fuel Cell Treatment for Energy Reduced Ammonium Recovery and Optimized System Performance

**Abstract**

Microbial fuel cell (MFC) technology is an innovative technology capable of recovering energy and nutrients from wastewater. However, aeration necessary for MFC treatment is energy demanding. This study seeks to understand how the incorporation of membrane contactor (MC) into a MFC can lower energy requirements and increase recovery of ammonium from the catholyte stream. Three phases were used to determine the optimal operation condition based on system configuration, aeration supplied, and strength of the absorption solution. The maximum power density for the first three system configurations was found to be 0.192 W $m^{-2}$ (MFC), 0.172 W $m^{-2}$ (MFC+MC$_C$), and 0.163 W $m^{-2}$ (MFC+MC$_U$). The decrease in power density and concurrent increase in internal resistance is likely due to the increased ammonium removal. Both MFC+MC systems recovered 1.4x and 2.4x more ammonium than the sole MFC (air stripping only) with MC being responsible for 96% of the ammonium recovered. Decreasing the aeration resulted in lower electrical performance of the MFC. The highest aeration operation mode also had the highest ammonium removal rate (9.50 ± 0.3 kg $m^{-3}$ $h^{-1}$). Low aeration resulted in lower ammonium removal (6.27 ± 1.5 kg $m^{-3}$ $h^{-1}$) and accumulation of ammonium in the anode that likely caused decreased MFC energy generation. Overall energy consumption, normalized energy consumption

(NEC) ratio with COD removal, and NEC ratio in ratio with ammonium removed/recovered was used to evaluate the systems between the three phases of experiments. These results have shown that MC is an efficient non energy intensive approach to recovery ammonium and decrease energy consumed by a coupled MFC.

**Keywords:** Microbial fuel cell, membrane contactor, ammonium recovery, coupled system, wastewater treatment

## 5.1   Introduction

Bioelectrochemical systems (BES) have been explored as robust technologies to treat various types of wastewater [227]. One of the most common and sustainable configurations of BES are microbial fuel cells (MFC). MFCs function when electrogenic bacteria oxidize organic matter to carbon dioxide at the anode electrode [228, 229]. Electrons are then released and flow to the cathode electrode and reduce dissolved oxygen to water. MFCs can operate as single chamber or multi-chamber systems [230, 231]. In dual chamber systems, MFC chamber can be separated by a cation exchange membrane (CEM) for the added separation of cations (e.g., ammonium) [18, 232]. Removal of ammonium is pivotal for decreasing environmental impacts of algae blooms and eutrophication that occur due to nutrient overloading [233]. Focusing on ammonium recovery could also help reduce various industries' nitrogen footprint.

A major limitation in MFC technology is the high energy demand necessary to aerate the cathode chamber [234, 235]. Previous studies have shown that greater than 50% of the energy consumed during BES treatment is due to aeration [192]. Intermittent aeration has also been

considered to reduce energy consumption [236, 237]. The disadvantage of aeration can also be advantageous for ammonium recovery since ammonia can be air stripped if the pH is greater than 9.23 to convert ammonium to gaseous ammonia [238]. Air stripping (AS) is a common approach to removal of ammonium from the cathode of BES [239-241]. Other approaches for ammonium removal have been applied to MFC technology as well. Techniques including biological nitrogen removal have achieved 151 g $NH_4^+$-N $m^{-3}$ $day^{-1}$ during MFC-MEC treatment [242]. Chemical precipitation to struvite has been shown to be effective at ammonium removal when treating urine [243]. These techniques however require system specificity that may not be achievable based on a variety of conditions. Overall, decreasing the energy required to recover ammonium from wastewater needs to be considered to make MFC treatment more sustainable.

Membrane contactor (MC) is a membrane approach to removal of gases (e.g., $NH_3$, $N_2$, $CO_2$, CO, and $O_2$) from both liquid and gas waste streams [244]. A gas permeable membrane is used to separate the feed and permeate solution, which allows free flow of gas compounds with rejecting liquids and solids from transporting. MC technology was originally developed for $CO_2$ removal [45, 46]. One study achieved 7.68 mol $m^{-2}$ $s^{-1}$ absorption flux of $CO_2$ using polyvinylidene fluoride (PVDF) membrane [245]. This separation approach has recently been developed for removal of other compounds such as alcohols, sulfur dioxide, volatile fatty acids, and ammonia [246, 247]. Weak acids and bases are good candidates for MC separation due to disassociation characteristics. In particular, ammonium has a relatively low disassociation constant ($K_b$ =1.8 x $10^{-5}$) and can convert to a gas in alkaline environments. Ammonia also has a high vapor pressure that allows its transfer from aqueous environments to occur faster than other gases. Gaseous ammonia can then be converted to ammonium after being extracted from wastewater.

In this study, we aim to evaluate MC are a more energy efficient method of ammonium recovery from an MFC. AS and MC will be compared as ammonium recovery methods. The specific objectives of this study are (1) explore the benefits of system configuration incorporating MC, (2) determine the effects of aeration on MFC performance and ammonium distribution in the coupled system, and (3) elucidate the effects of the absorption solution on recovering ammonium. The comparison analysis will consider electrical performance, energy consumption, ammonium removal and recovery rates of the various system configurations. This study will provide insight on ways to optimize ammonium removal and recovery while decreasing energy demand of the coupled MFC-MC system.

## 5.2  Materials and Methods

### 5.2.1  Microbial Fuel Cell Setup and Operation

A flat plate design was used to construct the MFC used in this study. The MFC anode chamber and a cathode chamber (450 mL/each) were separated by a cation exchange membrane (CEM, CMI-7000, Membrane International Inc., Glen Rock, NJ, USA) with an effective area of 130 cm$^2$. A carbon brush was used as the anode electrode. It was pretreated with acetone and then put into 450°C oven for 60 minutes. The anode chamber was inoculated with the sludge from a wastewater treatment plant (St. Louis, MO, USA). A solution made up of 2 g of sodium acetate was fed into the anode until stable performance was observed by the MFC. The cathode electrode (100 cm$^2$) was a stainless steel mesh wrapping carbon cloth secured by titanium wire. The carbon cloth (Zoltek Companies, Inc., MO, USA) was coated with the powder activated carbon (4 mg cm$^{-2}$). The activated carbon served as the catalyst for reduction of the dissolved oxygen. The catholyte

(cathode solution) was a phosphate buffer solution (PBS) contained (per liter of DI water) 0.54 g

$K_2HPO_4$ and 0.27 g $KH_2PO_4$ to maintain a pH of ~7.0. An air diffuser was used to supply oxygen

to the cathode chamber. The anolyte and the catholyte were circulated at a rate of 30 mL min$^{-1}$.

The anode and cathode electrodes were connected through a 10-$\Omega$ external resistance to generate

a high current for driving migration of ammonium ions from the anode into the cathode. Daily

samples were collected from the MFC chamber solutions and the sulfuric acid solution. Half of

the anolyte was replaced daily (HRT=2 days).

## 5.2.2  Membrane Contactor Set Up and Coupled System Operation

A two-chamber MC cell (9 cm x 8 cm x 3 cm) was constructed for ammonium recovery from the

catholyte of the MFC. The feed and permeate chamber had the capacity to hold 50 mL of solution.

The MC cell utilized gas permeable membrane (GE Healthcare Hybond™ PVDF flat sheet

membranes, Chicago, IL, USA) with a pore size of 0.45 μm in direct contact mode. The MC cell

had an effective membrane area of 30 cm$^2$ (6 cm x 5 cm). The MC solutions were recirculated in

tandem with the MFC at 30 mL min$^{-1}$.

This study was completed in three phases. Phase I explored 3 configurations: (1) sole MFC

treatment with AS as the only ammonia recovery method, (2) MFC coupled with MC with MC

separated/air stripped ammonium collected in the same solution (MFC+MC$_C$), and (3) MFC

coupled with MC with MC separated ammonium and air stripped ammonium collected in separate

absorption solutions (MFC+MC$_U$). The effluent of the MFC cathode chamber was connected to

the MC cell when MC was employed. AS was employed at the cathode reservoir. A 1.0 M $H_2SO_4$

solution was used to capture the ammonia as $(NH_4)_2SO_4$. Phase II explored the effect of aeration

on the removal and recovery of ammonia using configuration (3) from Phase I. The MFC was

operated with low (1.5 L min$^{-1}$), medium (3 L min$^{-1}$), and high (4.5 L min$^{-1}$) rates of aeration supplied to the cathode chamber. Phase III explored the effect of absorption solution molarity on the removal and recovery of ammonia using configuration (3) from Phase I. A 0 M, 0.1 M, and 1 M $H_2SO_4$ were used to absorb ammonium via MC separation and AS. The feed solution fed into the MFC contained (per liter of DI water): 0.15 g $NH_4Cl$, 0.5 g $NaCl$, 0.015 g $MgSO_4$, 0.02 g $CaCl_2$, 0.1 g $NaHCO_3$, 1.07 g $K_2HPO_4$, 0.53 g $KH_2PO_4$, and 1 mL of trace elements. In addition, 1.29 g sodium acetate (~1,000 mg COD L$^{-1}$) and 1.76 g $NH_4HCO_3$ (~ 400 mg $NH_4^+$-N L$^{-1}$). The MC gas permeable membrane was replaced between each iteration of the experiment stages. All tests were performed at room temperature (~24ºC) and in batch mode.

### 5.2.3 Measurement and Analysis

The voltage of the MFC was recorded every thirty seconds by a digital voltage meter (2700, Keithley Instruments Inc., Cleveland, OH, USA). The polarization curves were generated from data collected by a potentiostat (600+, Gamry, Warminster, PA, USA) operating at a 0.5 mV s$^{-1}$ scan rate. The ion concentrations were measured using ion chromatography (Thermo Fisher Scientific Dionex Integrion HPIC, Madison, WI, USA). Chemical oxygen demand (COD) was measured using colorimetric methods (HACH Co., Ltd., USA). The pH was measured using a bench pH meter (Oakton Instruments, Vernon Hills, IL, USA). The electrical conductivity was measured using a bench top conductivity meter (Mettler-Toledo, Columbus, OH, USA).

The current density was calculated by finding the quotient of the recorded date from the voltage digital meter and the area of the cathode electrode. The energy production and consumption ($E_{production}$ and $E_{consumption}$, kWh) were estimated using Eq. (1) and Eq. (2), respectively, according to a previous study [22].

$$E_{production} = (\sum I^2 R)\Delta t_{MFC} \tag{1}$$

$$E_{consumption} = (P_{MC,recirc})\Delta t_{MC} + (P_{MFC,recirc})\Delta t_{MFC} + P_{Aeration} \tag{2}$$

where $I$ (mA) represents the current, $R$ ($\Omega$) represents the resistance, $\Delta t_{MFC}$ represents the operation time for the MFC, $P_{aeration}$ represents the power estimation for aeration and $P_{MFC}$ represent the power estimated for recirculation of the solutions in the MFC, respectively. The $P_{recirculation}$ and $P_{aeration}$ were calculated using Eq. (3) and (4), respectively:

$$P_{recirculation} = \frac{Q_S \gamma H}{1000} \tag{3}$$

$$P_{aeration} = \frac{X_1 \lambda T}{982800 \times \varsigma \times (\lambda-1) \times \rho_0} \times \left( \left( \frac{X_2}{X_1} \right)^{1-\left( \frac{1}{\lambda} \right)} - 1 \right) \tag{4}$$

Where $Q_S$ (m$^3$ s$^{-1}$) represents the solution flow rate; $\gamma$ is the specific weight of water (9800 N m$^{-3}$); H (m) represents the hydraulic pressure head; and $X_1$ and $X_2$ represent the standard atmospheric pressure (101,325 Pa) and blower inlet pressure (Pa), respectively; T is air temperature (294 K); $\varsigma$ is blower efficiency (0.8); $\lambda$ is aerator constant (1.4); and $\rho_0$ is air density in standard conditions (1.29 kg m$^{-3}$).

The energy consumption was calculated as a ratio of the total power and flow rate. The normalized energy consumption (NEC, kWh kg$^{-1}$) [22] was calculated to understand the energy consumption used for COD removal, $NH_4^+$ removal and $NH_4^+$ recovery and is expressed in Eq. (5).

$$NEC = \frac{E_{consumption} - E_{production}}{\Delta COD_{rem.}} \quad or \quad \frac{E_{consumption} - E_{production}}{\Delta NH_4^+{}_{rem.\ or\ rec.}} \tag{5}$$

Where $\Delta COD_{rem}$ represents the removed COD and $\Delta NH_4^+{}_{rem/rec}$ represents the removed and recovered ammonium.

## 5.3 Results and Discussion

### 5.3.1 Effects of incorporating membrane contactor into microbial fuel cell treatment

Electrical performance was affected by the configuration of the MFC and MC. Since the membrane used for MC separation is gas permeable, it is expected that oxygen loss across the membrane could have some adverse effects on MFC performance and ammonium recovery. The MFC was able to achieve a maximum power density of 0.192 W m$^{-2}$ after reaching stable performance (Fig. 5.1). The MFC+MC$_C$ and MFC+MC$_U$ had slightly lower maximum power densities of 0.172 W m$^{-2}$ and 0.163 W m$^{-2}$, respectively. The internal resistance also increased between the MFC, MFC+MC$_C$, and MFC+MC$_U$ set ups and reached 39.7 $\Omega$, 42.5 $\Omega$, and 52.0 $\Omega$, respectively, in the systems. In addition to the loss of oxygen as an electron acceptor, decreases of ammonium as an electrolyte likely caused an increase in the resistance [248]. This is plausible considering the coupled systems achieved greater ammonium recovery than the MFC without MC separation (Fig. 5.1A). The highest recovery of 437.5 mg L$^{-1}$ in the absorption solution was achieved by the MFC+MC$_U$ system. The MFC+MC$_C$ 311.2 mg L$^{-1}$ had lower recovery likely due to adverse effects of aeration in the absorption solution from air stripped ammonium. The sole MFC 129.6 mg L$^{-1}$ had lower recovery due to inefficiency from AS. Interestingly, the MFC was able to achieve only 61 $\pm$ 8 % ammonium removal from the anode chamber while the MFC+MC$_C$ and MFC+MC$_U$ achieved 78 $\pm$ 9 %  and 74 $\pm$ 10%, respectively (Fig. 5.2B). When the AS and MC ammonium were analyzed, it was shown that MC recovered 96% of the total ammonium. This highly shows that MC is the favorable method for ammonium recovery compared to AS.
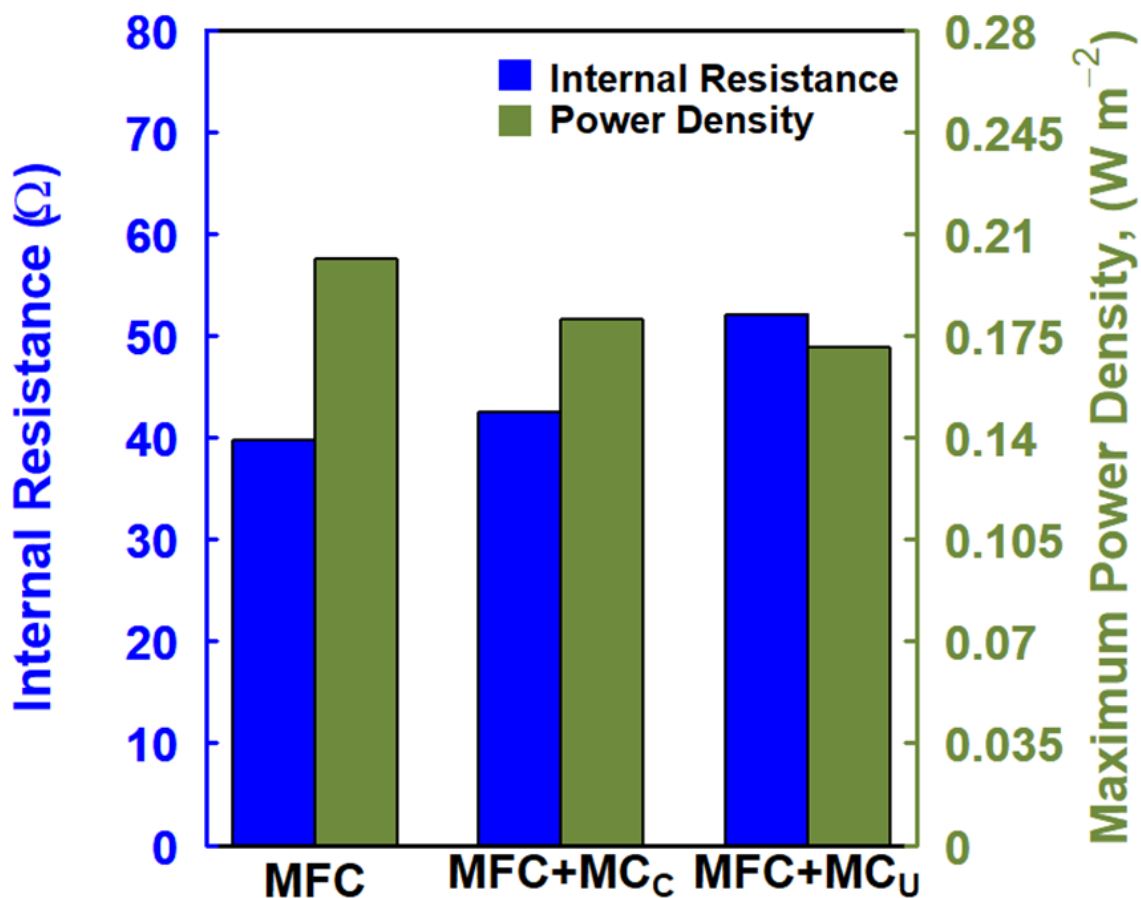
**Figure 5.1** Internal resistance and maximum power density of MFC, MFC-MC$_U$ and MFC-MC$_C$ systems.

### 5.3.2 Effects of aeration on ammonium recovery

The catholyte is typically saturated with dissolved oxygen. In order to determine the effects of aeration on MC separation, different aeration rates were investigated for MFC+MC coupled system performance. As the rates were decreased from 4.5 to 3 to 1.5 L min$^{-1}$ the maximum current
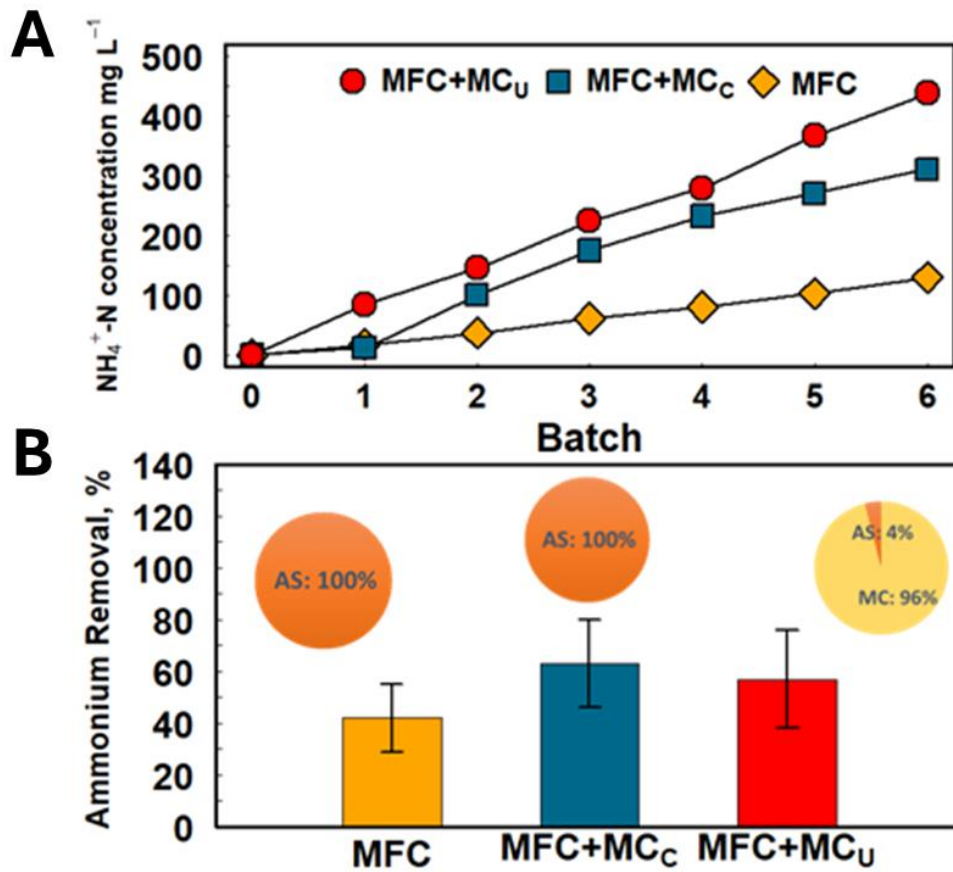
**Figure 5.2.** (A) Total recovered ammonium and (B) ammonium removed from the anode chamber with recovery method percentages (AS: air stripping; MC: membrane contactor ) for MFC, MFC-MC$_U$ and MFC-MC$_C$ systems.

density decreased from $520.6 \pm 34.7$ to $507.4 \pm 26.9$ to $448.0 \pm 39.3$ mA m$^{-2}$ , respectively (Fig. 5.3A). This decrease is likely a result of oxygen available for reduction at the cathode [249]. The

effect this had on the distribution of ammonium throughout the MFC+MC$_U$ system were considered and compared to the ammonium removed from the anode chamber. Ammonium collected were in the absorption solution were not significantly different (p>0.05), but the medium

aeration mode recovered the greater amount of ammonium (840.2 mg $L^{-1}$) (Fig. 5.3B). The amount of ammonium that was recovered via AS also decreased which is likely due to less stripping ability due to low aeration. The removal rate from the anode decreased ($9.50 \pm 0.29$ kg $m^{-3}$ $h^{-1}$ to $6.27 \pm 1.54$ kg $m^{-3}$ $h^{-1}$) as the aeration was decreased. The amount of ammonium that is transported across the CEM is directly connected to the decrease in electrical performance [191]. Concurrently, the ammonium accumulated  in the anode likely had adverse effects on electroactive microbes [250].

### 5.3.3  Effects of MC absorption solution on ammonium recovery

The absorption solution strength was considered to observe whether higher concentrations promote more ammonium removal and recovery. The current density increased to $585.2 \pm 21$ mA $m^{-2}$ when the 0.1 M $H_2SO_4$ was used compared to the 1.0 M $H_2SO_4$ ($520.6 \pm 34.7$ mA $m^{-2}$) absorption solution (Fig.5.4A). This increase could likely be due to optimized condition between the MFC and MC for ammonia removal from the anode chamber and not removed from the catholyte. However, the system performance decreased when 0 M $H_2SO_4$ ($486.4 \pm 73.3$ mA $m^{-2}$) was used. The decrease in electrical performance is most likely due to ammonium accumulation in the anode. This was reflected in analysis of ammonium distribution through the system. The 1 M $H_2SO_4$ absorption test resulted in a 731.2 mg $L^{-1}$ of ammonium solution (Fig. 5.4B). The 0.1 M $H_2SO_4$ and 0 M $H_2SO_4$ ended with lower concentrations of ammonium at 629.5 and 315 mg $L^{-1}$, respectively. Initially, it was suspected that higher molarity absorption solutions do extract more ammonia from the feed. However, the 0 M $H_2SO_4$ MC absorption solution reached maximum capacity at the fourth day of operation ~235 mg $L^{-1}$ (Fig. 5.4C).
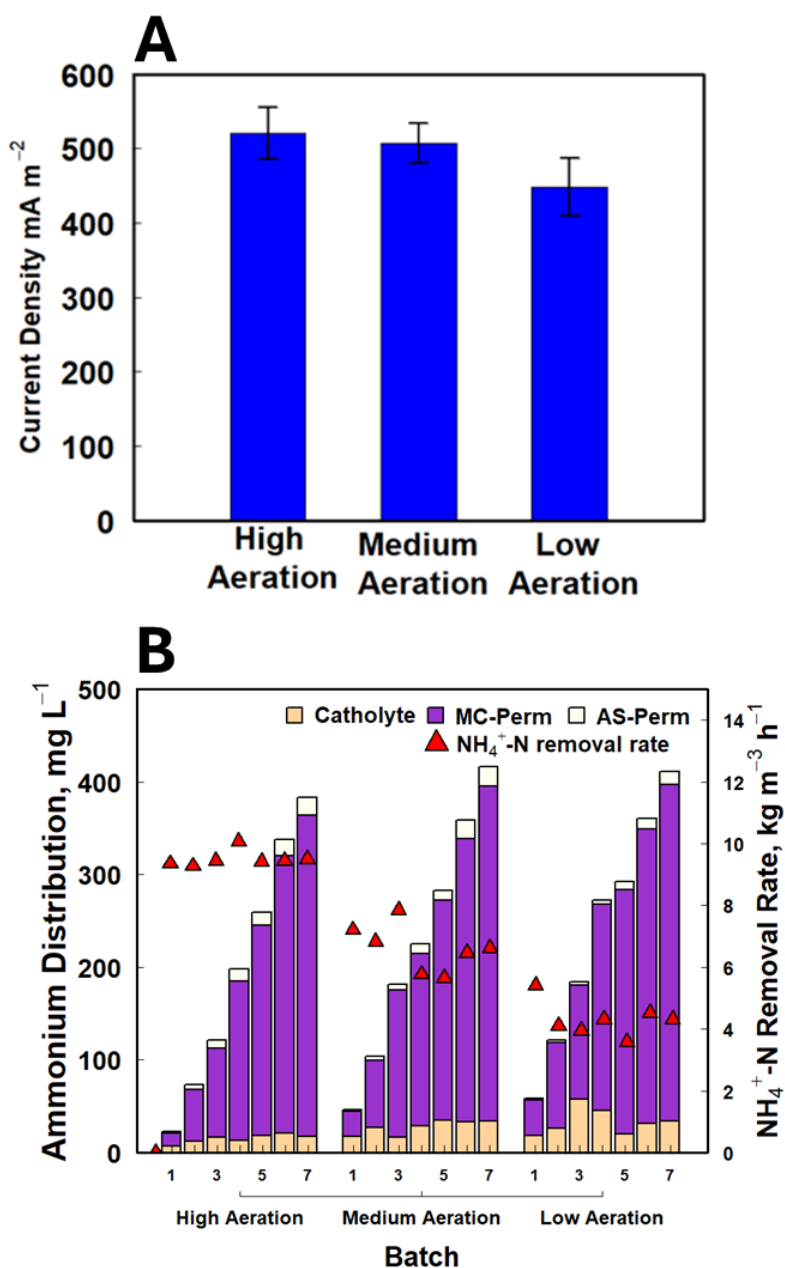
**Figure 5.3** (A) Current density and (B) ammonium distribution for cathode chamber and absorption solution for high (4.5 L min$^{-1}$), medium (3.0 L min$^{-1}$), and low (1.5 L min$^{-1}$) aeration operation modes; and ammonium removal rates.
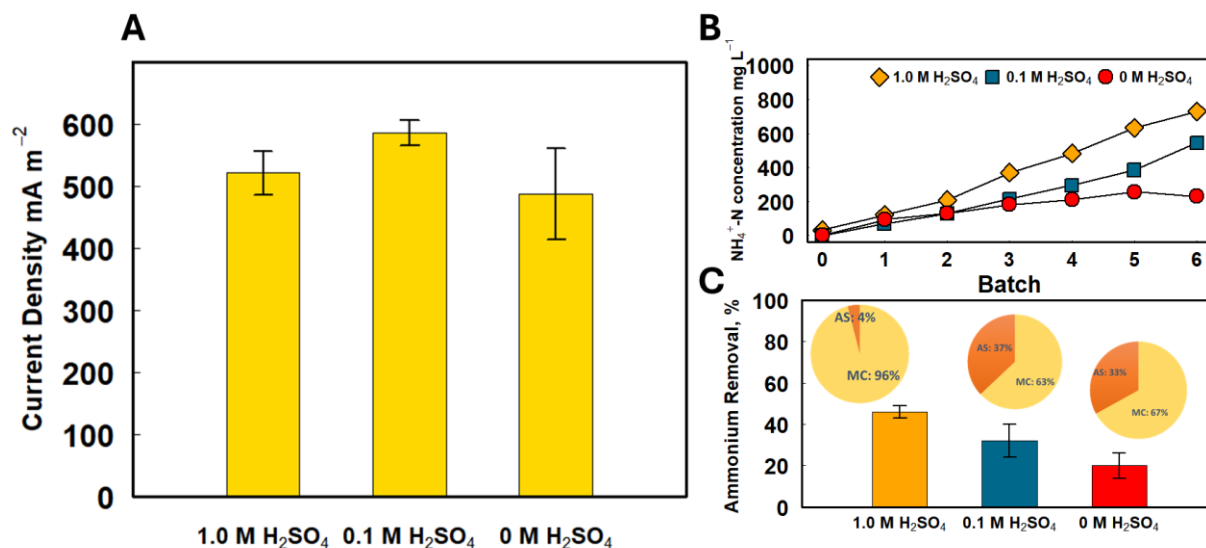
**Figure 5.4**. (A) Current density, (B) total recovered ammonium, and (C) ammonium removed from the anode chamber with recovery method percentages (AS: air stripping; MC: membrane contactor ) for 0, 0.1, and 1.0 M $H_2SO_4$ absorption solutions.

These results suggest that vapor pressure likely affected ammonium recovery. Despite ammonia having a high vapor pressure, the solution vapor pressure can restrict transport of other gases across the membrane. This phenomenon is commonly seen in membrane distillation studies [251]. In this case, the PBS as the catholyte had a lower vapor pressure than the permeate 0.1 and 0 M $H_2SO_4$ absorption solution. Additionally, the ammonium removal rate from the anode decreased from $9.50 \pm 0.29$ kg m$^{-3}$ h$^{-1}$ to $4.32 \pm 0.63$ kg m$^{-3}$ h$^{-1}$ between the 0 M $H_2SO_4$ and 0 M $H_2SO_4$ absorption solutions, respectively. Interestingly, the amount of ammonium collected via AS increased to 37% and 33% for the 0.1 M and 0 M $H_2SO_4$ absorption solutions, respectively. This reinforces the idea that the vapor pressure difference due to the molarity of the absorption is an important factor for MFC+MC treatment.

### 5.3.4  Energy Consumption

The overall energy consumption, normalized energy consumption ratio with COD removal, and NEC ratio in ratio with ammonium removed/recovered had varying results between the different parameters investigated. The energy consumption in Phase I was generally the same (Fig. 5.5A). The slight increase for the coupled systems (6.52 kWh) was due to the energy necessary for recirculation of the MC permeate. For Phase II, the high, medium, and low resulted in an expected energy consumption decrease of 6.42, 4.62, and 2.83 kWh, respectively. Aeration is the highest consumer of energy in biological wastewater treatment. These results combined with the ammonium recovery results suggest that aeration techniques need to continue to be optimized. The NEC for COD removal was higher in the aeration (2.62-4.37 kWh) and absorption solution (3.65-4.76 kWh) experiments compared to Phase I (Fig. 5.5B). Lower COD removal was the main variable that affected energy consumption for Phase II and III. Further investigation on COD removal needs to be considered. Generally, the NEC for ammonia removed was lowest in Phase I (Fig. 5.5C). Increases during Phase II (4.09-5.86 kWh) occurred due to decreases in ammonium removal due to lower current generation for lower aeration conditions. For Phase III, the low removal was due to ineffective ammonium recovery from the cathode. Phases II and III had much lower NEC for recovered ammonia showing the effectiveness of MC separation to AS (Fig. 5.5D). The lowest energy consumption was observed during Phase II (7.64-7.93 kWh). The increase during Phase III was attributed to the distribution of ammonia due to ineffective MC separation which was previously discussed.
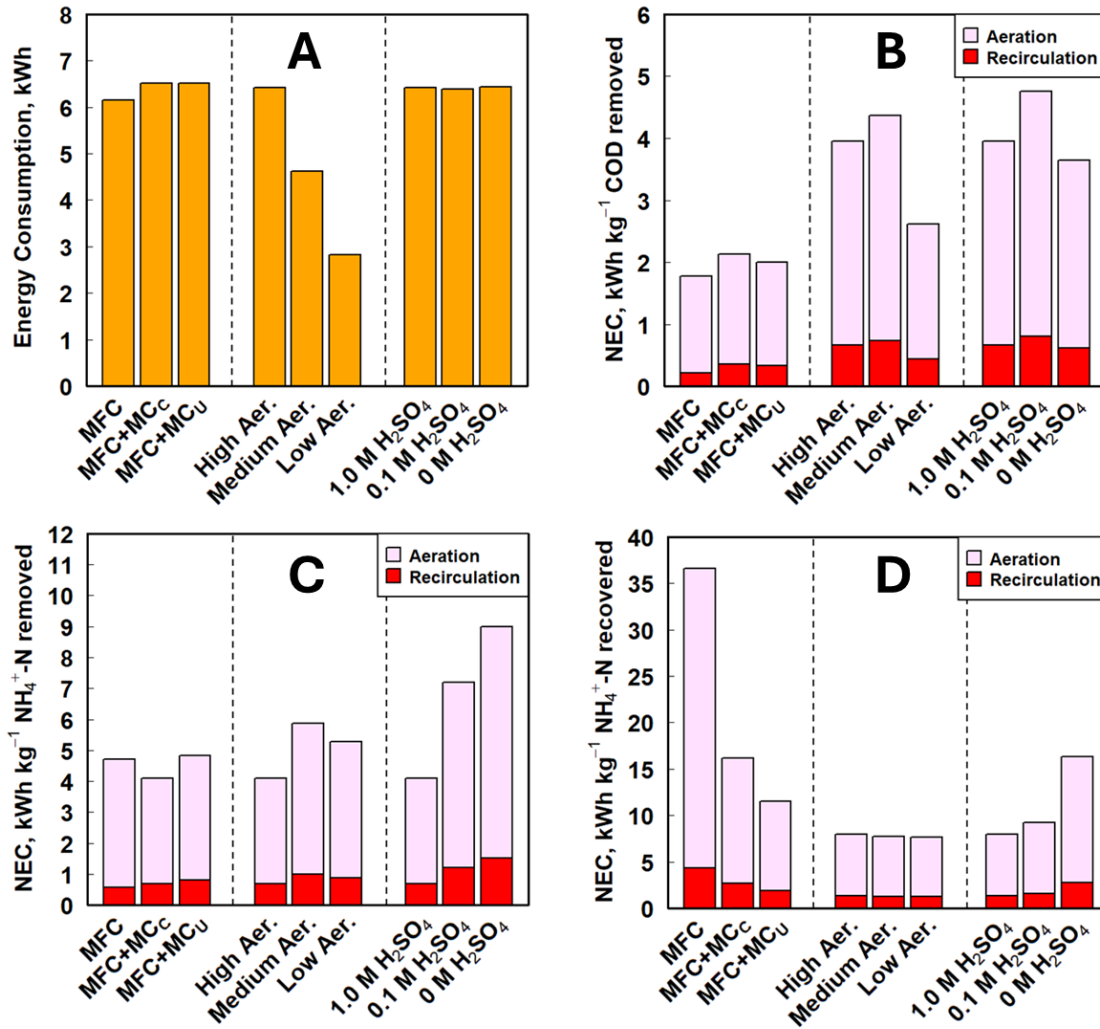
**Figure 5.5** (A) Energy consumption, (B) Normalized energy consumption for COD removal (C) ammonium removal and (D) ammonium recovery for aeration and MFC recirculation for Phase I, II, and III.

## 5.4    Conclusion

This study has shown that integrating MC into the catholyte effluent stream can be an effective, non-intensive approach to recovering ammonium from wastewater. MC collected >90% of the

ammonium while AS. MC and AS being collected in separate vessels resulted in higher ammonia recovery. Lower aeration had decreased electrical performance ($448.0 \pm 39.3$ mA m$^{-2}$) and ammonium removal rate ($4.32 \pm 0.63$ kg m$^{-3}$ h$^{-1}$) from the anode chamber compared to high aeration conditions. MC was observed to be ineffective if the absorption solution has a higher vapor pressure than the catholyte. The energy consumption for low aeration during Phase II was 2.83 kWh and was due to the decrease in aeration. NEC data for COD removal, ammonium removal and ammonium recovery revealed that aeration is the most important factor to optimize for ammonium recovery in MFC+MC coupled system. This study shows that MC should be employed into MFC systems with further investigation on the role aeration plays in wastewater treatment and ammonium recovery.

# Chapter 6

# Optimizing Thermoelectric Generator Powered Microbial Electrolysis Cell Performance Treating Synthetic Brewery Wastewater

**Abstract**

Microbial electrolysis cells (MEC) are a versatile technology that generate electricity and $H_2$ while treating wastewater. A major concern is the need for an external power source to achieve $H_2$ production. Herein, we utilized thermoelectric generators (TEG) to convert waste heat into electrical energy to sustainably power a MEC. Open circuit voltages from 0.296 V to 1.496 V were achieved as we varied the temperature gradient ($\Delta T=10°C – 30°C$) and recirculation rate (12 mL $min^{-1}$ – 140.7 mL $min^{-1}$). Hydrogen gas production was not observed until $\Delta T=20°C$ because the voltage supplied was sufficient to overcome the overpotential of the hydrogen evolution reaction. The anolyte pH decreased to 6.79, 6.11, and 5.01 for temperature gradients of 10°C, 20°C, and 30°C, respectively. The addition of $HCO_3^-$ raised the pH towards neutral and restored hydrogen gas production. Coulombic efficiency ($3.2 \pm 0.0$ %, $27.2 \pm 14.5$ %, $48.3 \pm 11.4$ %) and recovery ($7.2 \pm 0.8$ %, $9.0 \pm 4.2$ %, $18.8 \pm 3.7$ %) increased as the temperature gradient was increased. Volatile fatty acids were used to closely mimic brewery wastewater and analyzed to see how organic matter composition changed after MEC treatment. The results show that TEGs can serve as an alternative power source to improve MEC technology sustainability.

## 6.1  Introduction

Microbial electrolysis cells (MEC) are a sustainable technology that have the ability to generate hydrogen gas while treating wastewater [252, 253]. This is particularly important since global population increases will also yield higher wastewater production. Domestic [254], hydrothermal liquid [255], and agricultural [256] wastewaters have been used to feed MECs in previous studies revealing their robustness. In MECs, microbes oxidize organic matter in the anode chamber and release electrons that flow to the cathode chamber where protons are reduced. An additional power source is also required to achieve the hydrogen evolution reaction (HER). Other hydrogen gas generation methods including steam methane reformation [257] and water electrolysis [258] depend mainly on eternal power sources. Since MECs can generate electricity, the offset of energy demand makes them more favorable compared to other approaches. This makes MEC technology an appealing approach to generate hydrogen gas.

There are many technical and operational challenges associated with MECs that diminish their potential for implementation. Microbiome specification [259, 260], system configuration [261, 262], and wastewater source [58] have been investigated to optimize MEC performance. In addition, use of expensive electrode catalyst material (e.g., Platinum) and decreased efficiency for large scale systems [263, 264] have been long standing problems. The overarching disadvantage of MEC treatment is the requirement of a power source. This is because the HER is not thermodynamically favorable when coupled with the oxidation of organics [265]. Previous studies have suggested that alternative catalysts could help offset energy demand. For example, a

polyaniline-graphene electrode produced 0.65 $m^3$ $H_2$ $m^{-3}$ $day^{-1}$ compared to 0.85 $m^3$ $H_2$ $m^{-3}$ $day^{-1}$ when a Pt electrode was utilized [266]. Another study showed uncoated recycled fibers could also achieve good hydrogen generation [267]. Even with these modifications, there is still an opportunity to make MEC technology more sustainable.

Thermoelectric generators (TEGs) are composite materials that can convert heat into electrical energy [268]. TEGs have been developed as a sustainable energy source for medical [269], aerospace [270, 271], industrial [272], and automotive [273, 274] applications. These composites are typical made of n-type and p-type semiconductors that promote electron movement when a temperature gradient exists between the two interfaces of the TEG [275]. This phenomenon is known as the Seebeck Effect. The material used to fabricate the TEG affects the electrical performance. For example, 308 $\mu W$ $m^{-1}$ $K^{-2}$ and 258 $\mu W$ $m^{-1}$ $K^{-2}$ power factors were achieved with a 150 K temperature gradient in one study that used an organic polymer TEG [276]. While another study achieved 1.5 mW m $K^{-2}$ using a $Bi_2Te_3$ at a lower temperature gradient. One challenge associated with TEGs is their susceptibility to conduction. This transfer of heat from the heat source to the heat sink reduces the performance of the TEG due to a lower temperature gradient [277]. Thermal interface materials are used to decrease this occurrence but can sometimes be ineffective due to their lack of wide applicability and ability to short circuit the TEG [278, 279].

Recently, TEG powered MEC systems have been explored for their applicability in environmental systems [73, 280-282]. However, the treatment of complex, organic rich anolyte solutions has not yet been considered. Therefore, we explored a coupled TEG-MEC system treating synthetic brewery wastewater to evaluate hydrogen generation with TEG power source. The specific aims of this study are (i) understand how temperature and system configuration affect TEGs as a power source, (ii) how MEC performance is affected when using wastewater mimicking

brewery wastewater, and (iii) the energy demand required to operate the system comparing a power supply (PS) to TEG. The coupled technology system will be evaluated based on hydrogen production, current generation and VFA composition.

## 6.2 Materials and Methods

### 6.2.1 TEG Setup and Operation

The TEG cells were constructed using PVC piping. The TEG composites (Model TEG2−126LDT, $Bi_2Te_3$, TECTEG MFR, Ontario Canada) had interface areas of 40 mm x 40 mm with a 1.5 mm thickness. The TEGs were sealed within the PVC pipe using adhesive and then sealed to restrict water transport from the heat source chamber to the heat sink chamber. Each chamber held 80 mL of solution. The TEGs were characterized using 2 interface configurations (air (cool)-liquid (hot) and liquid (cool)-liquid (hot)), at five recirculation rates (12, 42.5, 73.9, 105.9, and 140.7 mL min$^{-1}$) and three temperature gradients between the heat source and sink ($\Delta T$=10°C, 20°C, and 30°C). To determine any effects of multiple TEG usage, the characterization tests were repeated with two and three TEGs connected in series. Data collected from the characterization tests were then used to determine correlation between the variables previously outlined.

### 6.2.2 TEG-MEC and PS-MEC set up and operation

The MEC had an anode chamber (800 mL) and a cathode chamber (300 mL) that were separated by a cation exchange membrane (AEM, AMI-7000, Membrane International Inc., Ringwood, NJ, USA) with an effective area of ~100 cm$^2$. The anode electrode was a carbon brush pretreated by acetone for 24 hours. Then, the carbon brush was air dried. The anode chamber was inoculated with the sludge from a wastewater treatment plant (St. Louis, MO, USA). Initially, the MEC was

operated in microbial fuel cell mode. Dissolved oxygen was supplied to the cathode chamber using an air diffuser to promote microbe growth. Then, the oxygen was disconnected, and the cell was operated in MEC mode at 0.4 V using a PS (3644 A, Circuit Specialists, Inc., Mesa, AZ, USA). The MEC was operated in a batch mode and at a room temperature (~23°C). The cathode electrode (88 cm$^2$) was a stainless-steel mesh wrapping carbon cloth secured by titanium wire. The carbon cloth (Zoltek Companies, Inc., MO, USA) was coated with the 0.5 mg cm$^{-2}$ Pt/C (Millipore Sigma, St. Louis, MO, USA) to serve as a catalyst for hydrogen reduction to hydrogen gas. The catholyte (cathode solution) contained 50 mL of phosphorus buffer solution (PBS) containing $K_2HPO_4$ and $KH_2PO_4$. Both the anolyte and the catholyte were circulated at a rate of 30 mL min$^{-1}$. The anode and cathode electrodes were connected through a 10-$\Omega$ external resistance. Anolyte and catholyte samples were collected during each anolyte replacement (24 hours). The catholyte was completely replaced with fresh catholyte and 200 mL of anolyte was replaced with fresh anolyte every 24 hours. After stable performance, the MEC was switched from the power supply to three TEGs.

In stage I: the anolyte was used as the heat sink and water warmed by a water bath was used as the heat source. The TEGs powered the MEC using 10°C, 20°C, and 30°C temperature gradients. The MEC was fed with a synthetic solution containing (per liter): 2.5 g sodium acetate, 0.15 g NH$_4$Cl, 0.5 g NaCl, 0.015 g MgSO$_4$, 0.02 g CaCl$_2$, 0.1 g NaHCO$_3$, 1.07 g K$_2$HPO$_4$, 0.53 g KH$_2$PO$_4$, and 1 mL of trace elements. Preliminary experiments revealed that an additional 4.4 g NaHCO$_3$ needed to be supplied to maintain alkalinity and neutral pH levels in the anolyte. In stage II: the organic source was switched to (per liter of DI water): 1.56 mL of acetic acid, 0.44 mL of propionic acid, and 0.67 mL of butyric acid. The other parameters were kept the same from stage I. In stage III: the TEGs were replaced with the power supply. The output of the PS mimicked the

output of the TEGs at the three temperature gradient conditions. This resulted in the PS-MEC being operated at 0.330 V ($\Delta$T=10°C), 0.625 V ($\Delta$T=20°C), and 0.933 V ($\Delta$T=30°C).

### 6.2.3 Measurement and Analysis

The voltage of the MFC was recorded every two minutes by a digital voltage meter (2700, Keithley Instruments Inc., Cleveland, OH, USA). The polarization curves were generated from data collected by a potentiostat (600+, Gamry, Warminster, PA, USA) operating at a $0.5 \text{ mV s}^{-1}$ scan rate. Chemical oxygen demand (COD) was measured using colorimetric methods (HACH Co., Ltd., USA). Gas concentrations were analyzed using gas chromatography equipped with a flame ionization detector (Focus GC, Thermo Scientific; GC-FID). The ion concentrations were measured using ion chromatography (Thermo Fisher Scientific Dionex Integrion HPIC, Madison, WI, USA). The electrical conductivity was measured using a conductivity meter (Mettler-Toledo, Columbus, OH, USA). The pH was measured using a bench pH meter (Oakton Instruments, Vernon Hills, IL, USA). The current density was calculated by finding the quotient of the recorded date from the voltage digital meter and the area of the cathode electrode. The energy production and consumption ($E_{production}$ and $E_{consumption}$, kWh) were estimated using Eq. (1) and Eq. (2), respectively, according to a previous study [22].

$$E_{production} = (\sum I^2 R)\Delta t_{MEC} \tag{1}$$

$$E_{consumption} = (P_{MEC,recirc}) + (P_{power\,supply}) \tag{2}$$

where $I$ (mA) represents the current, $R$ ($\Omega$) represents the resistance, $\Delta t_{MEC}$ represents the operation time of MEC, respectively, $P_{MFC,recirc}$ represents the power estimated for recirculation of the anolyte and catholyte, and $P_{power\,supply}$ represents the power estimated for the power supply. The $P_{MFC,recirc}$ and $P_{power\,supply}$ were calculated using Eq. (3) and (4), respectively:

$$P_{MEC,recirculation} = \frac{Q_S \gamma H}{1000} \tag{3}$$

$$P_{power\ supply} = \int_{t=0}^{t} IU dt \tag{4}$$

Where $Q_S$ (m³ s⁻¹) represents the solution flow rate; $\gamma$ is the specific weight of water (9800 N m⁻³); H (m) represents the hydraulic pressure head; and U (V) represents the external voltage.

The normalized energy consumption (NEC, kWh $L_{H_2}$) was calculated to understand the energy consumption used for hydrogen gas production and is expressed in Eq. (5).

$$NEC = \frac{E_{consumption} - E_{production}}{L_{H_2}} \tag{5}$$

where $L_{H_2}$ represents the H₂ produced in liters.

The Coulombic efficiency (CE) and Coulombic recovery (CR) were calculated as outlined by the previous studies based on acetate removal.

## 6.3   Results and Discussion

### 6.3.1   Temperature gradient and recirculation rate affect TEG voltage output

The TEGs were characterized by changing the recirculation rate, temperature gradient and heat source/heat sink. Overall, the voltage output increased as the temperature gradient increased from 10°C to 30°C (Table 6.1). The air-liquid modes had lower output voltage for all operation modes compared to the liquid-liquid modes. This is likely due to the low heat capacity of air (1.01 J g⁻¹ K⁻¹) compared to water (4.18 J g⁻¹ K⁻¹). The air-liquid mode only had a 47.0% increase in voltage output compared to a 91.5% increase in the liquid-liquid mode from 12 mL min⁻¹ to 140.7 mL min⁻¹ when 3 TEGs were investigated at ΔT=10°C. This trend was also observed at the ΔT=20°C (air-liquid: 66.7%; liquid-liquid: 84.8%) and ΔT=30°C (air-liquid: 57.5%; liquid-liquid: 95.7%) operation conditions. None of the conditions examined using air-liquid interface reached 0.4 V

required for hydrogen generation in the MEC. Higher air temperatures (i.e., flue gas at a power station) would be necessary to achieve the required voltage. The number of TEGs connected also affected the output. The increase in voltage at each flowrate had a linear relationship which means the three TEGs were operating similarly. Moving forward, three TEGs using a liquid-liquid operating mode was considered.

**Table 6.1** Voltage output of TEGs based on temperature gradient, solution flow rate, and Red filled squares represent TEG voltages below 0.4 V (applied voltage needed to overcome overpotential in MEC for hydrogen generation). Yellow to Green represent voltage range 0.4-1.5V.

| Temperature Gradient (°C) | Flow (mL/min) | Air (cool) Liquid (hot) 3 TEGs | Liquid (cool) Liquid (hot) 1TEG | 2TEGs | 3TEGs |
|---|---|---|---|---|---|
| 10.0 | 12.0 | 0.0808 | 0.1358 | 0.2079 | 0.2955 |
|  | 42.5 | 0.1010 | 0.1719 | 0.2666 | 0.4106 |
|  | 73.9 | 0.1100 | 0.1844 | 0.3039 | 0.5035 |
|  | 105.9 | 0.1163 | 0.1982 | 0.3284 | 0.5415 |
|  | 140.7 | 0.1188 | 0.2121 | 0.3409 | 0.5660 |
|  | Flow (mL/min) | 3 TEGs | 1TEG | 2TEGs | 3TEGs |
| 20.0 | 12.0 | 0.1385 | 0.2648 | 0.4045 | 0.5701 |
|  | 42.5 | 0.1944 | 0.3363 | 0.5510 | 0.9080 |
|  | 73.9 | 0.2025 | 0.3455 | 0.5923 | 0.9693 |
|  | 105.9 | 0.2245 | 0.4043 | 0.6472 | 1.0121 |
|  | 140.7 | 0.2309 | 0.4141 | 0.6644 | 1.0537 |
|  | Flow (mL/min) | 3 TEGs | 1TEG | 2TEGs | 3TEGs |
| 30.0 | 12.0 | 0.2113 | 0.3578 | 0.5432 | 0.7641 |
|  | 42.5 | 0.2744 | 0.4744 | 0.7627 | 1.1655 |
|  | 73.9 | 0.2886 | 0.4737 | 0.7891 | 1.3063 |
|  | 105.9 | 0.3345 | 0.5524 | 0.9021 | 1.4481 |
|  | 140.7 | 0.3329 | 0.5669 | 0.9201 | 1.4955 |

The data collected for the 3-TEG configuration had a logarithmic regression when increasing the flowrate (Fig. 6.1). Similar trends also existed for the other configurations. This occurs because TEGs are most efficient when temperature is maintained at the TEG surface. Slower recirculation rates allow conduction to occur which will decrease the temperature gradient and voltage supplied by the TEGs. The highest voltage increases were 38.9% ($\Delta T=10°C$), 59.3% ($\Delta T=20°C$), and 52.5% ($\Delta T=30°C$), respectively, when the flowrate was adjusted from 12.0 mL min$^{-1}$ to 42.5 mL min$^{-1}$ (Fig. 6.1 inset). Compared to a 22.6% ($\Delta T=10°C$), 6.8% ($\Delta T=20°C$), 12.1% ($\Delta T=30°C$) increase when the flowrate was adjusted from 42.5 mL min$^{-1}$ to 73.9 mL min$^{-1}$, a trade off in increasing the flowrate exists as higher recirculation rates would consume more energy without equal return in the voltage output.
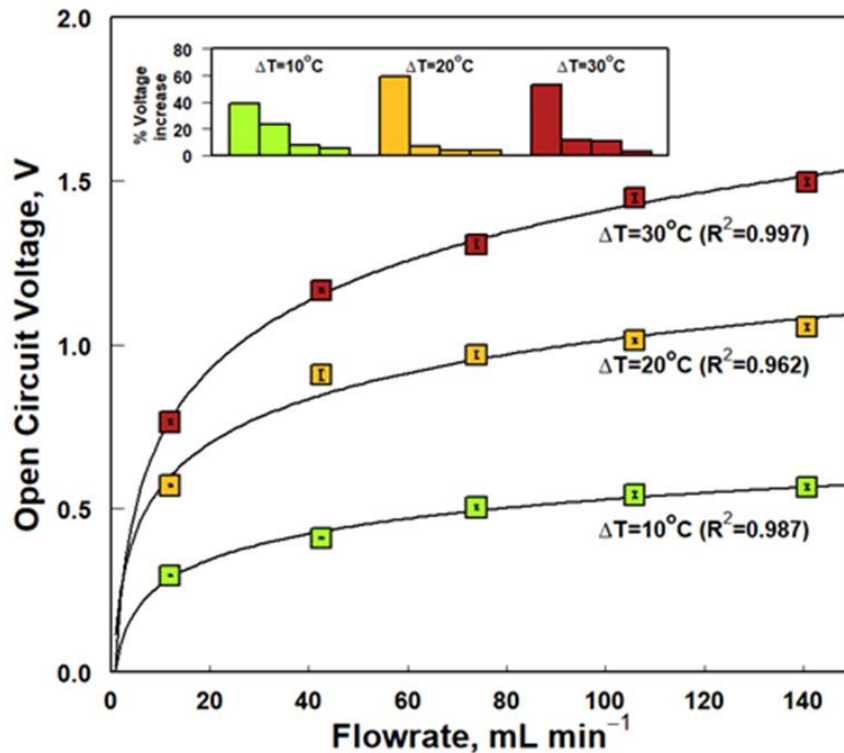


**Figure 6.1** Open circuit voltage for 3 TEGs operating in liquid-liquid mode at 10°C, 20°C, and 30°C temperature gradients.

### 6.3.2 MEC performance with brewery wastewater feed source

Low alkalinity levels in the synthetic brewery wastewater caused performance issues in the TEG powered MEC. At $\Delta T=10°C$, no hydrogen gas was generated since the voltage output was less than 0.4 V [283]. This allowed the anolyte pH to remain in neutral ranges (7.0-7.5) (Fig. 6.2A). When the temperature gradient was increased to 20°C, the pH trended toward acidic levels. This also caused decreases in the hydrogen being produced. This was further observed at $\Delta T=30°C$ when the pH reached 5.0 in the anolyte chamber. Analysis of the anolyte $HCO_3^-$ concentration showed were operated at $\Delta T=10\ °C$ ,20 °C ,30°C and the anolyte was an acetate based synthetic wastewater that $HCO_3^-$ was being completed consumed during MEC treatment (Fig. 6.2B). Previous studies showed that these conditions likely inhibited microbes from consuming organic matter [284]. This concurrently resulted in the decrease of hydrogen gas generation. Moving forward, $NaHCO_3$ was added to the synthetic brewery wastewater to maintain performance of the MEC.

This caused the anolyte pH to increase and restabilize at neutral levels. As the temperature gradient increased from $\Delta T=10°C$ to 30°C, the maximum current density was 0.12 mA cm$^{-2}$, 0.13 mA cm$^{-2}$, 0.19 mA cm$^{-2}$ for $\Delta T=10°C$, 20°C and 30°C, respectively (Fig 6.2C). A decrease in electrical performance was observed during MEC treatment during each temperature gradient investigated. This is most likely attributed to conduction from the hot source to the hot sink.

### 6.3.3 Comparison analysis between PS and TEG

The MEC performance decreased when the acetate based anolyte was replaced with a mixture of volatile fatty acids to closely mimic brewery wastewater (Fig. 6.3A). The $\Delta T=10°C$, 20°C and
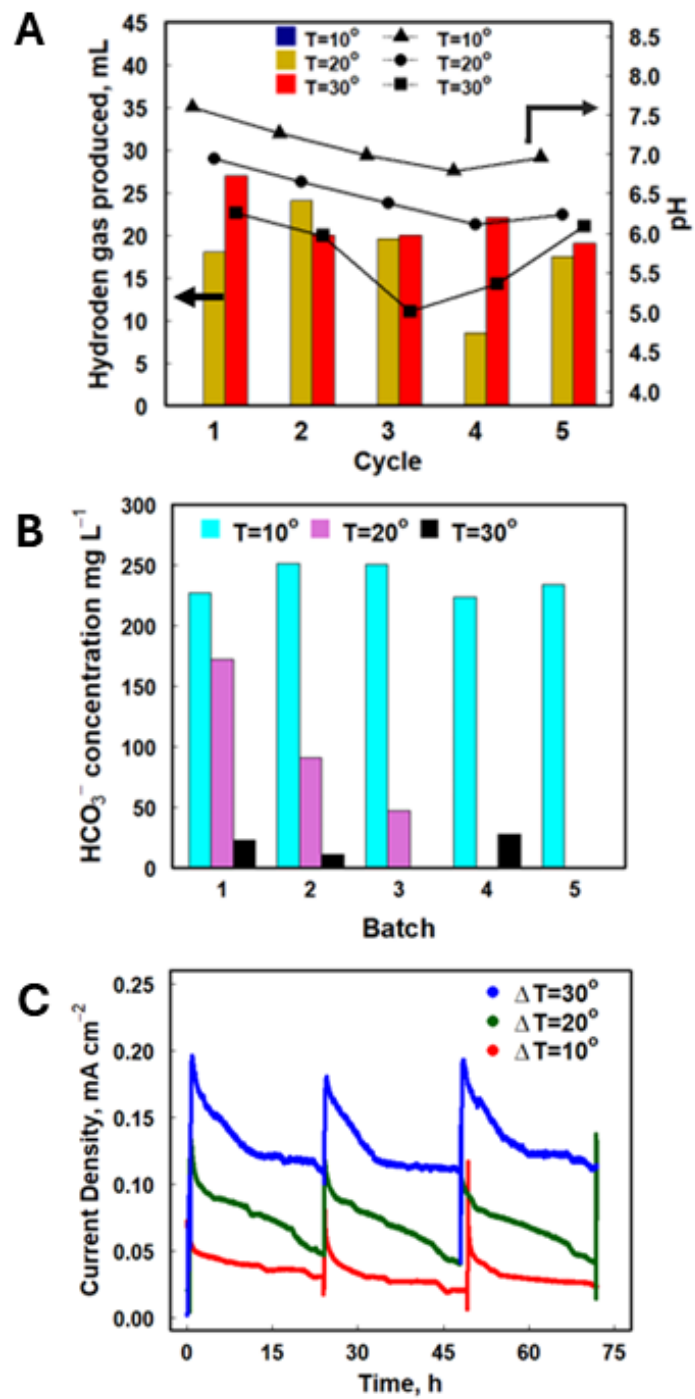
**Figure 6.2** (A) Hydrogen gas produced and pH levels in the anolyte, (B) anolyte bicarbonate

concentrations, and (C) current density during TEG-MEC operation.
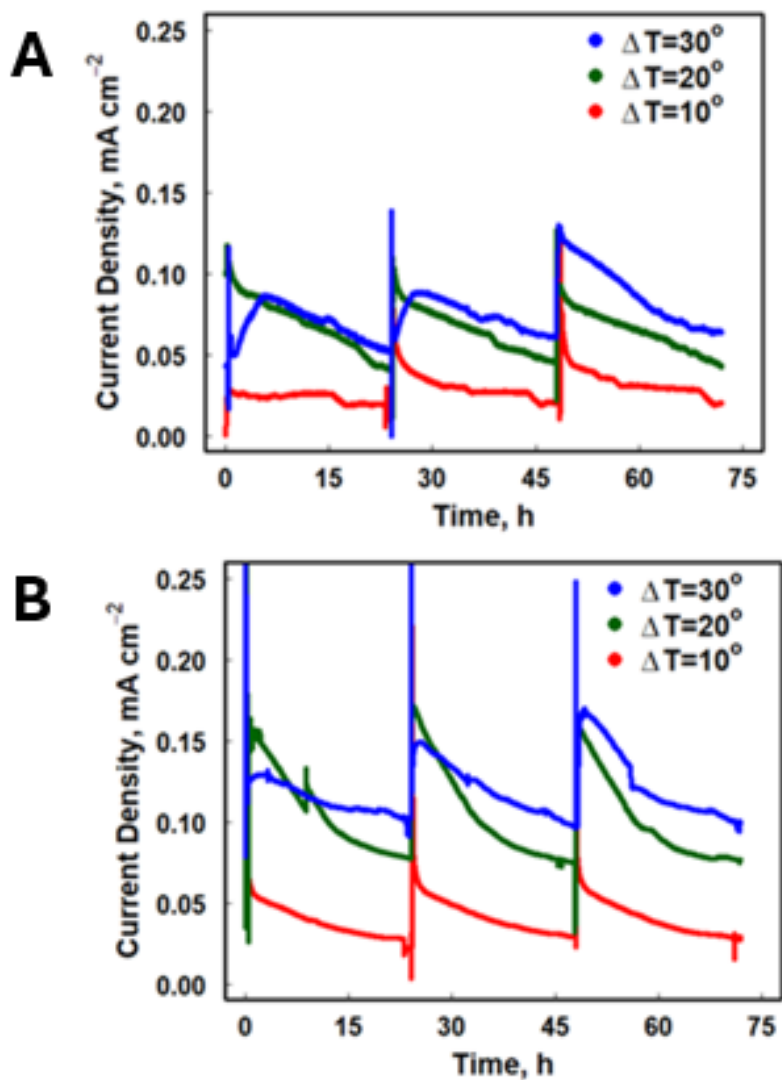
**Figure 6.3** Current density of MEC when the anolyte was an VFA based synthetic solution for (A) TEG powered MEC and (B) PS powered MEC.

30°C yielded current densities that were generally lower than presented in Fig 2C. This may be due to the inhibitory nature of complex organics. Geobacter are not able to consume higher chained organic matter directly [285]. This suggests that the acetate rich solution was a better feed source. To ensure that the TEGs were working properly, a traditional power supply was used to power the

MEC using the voltage produced at 10°C (0.330 V), 20°C (0.625 V) and 30°C (0.933 V) temperature gradients by the TEGs (Fig. 6.3B). Surprisingly, the PS-MEC fed with the VFA based anolyte performed similarly to TEG-MEC fed with an acetate based anolyte. The maximum current density increased to 0.22 mA cm$^{-2}$, 0.30 mA cm$^{-2}$, 0.29 mA cm$^{-2}$. The stability of the TEGs power to the MEC is likely the cause of this difference in performance [281].
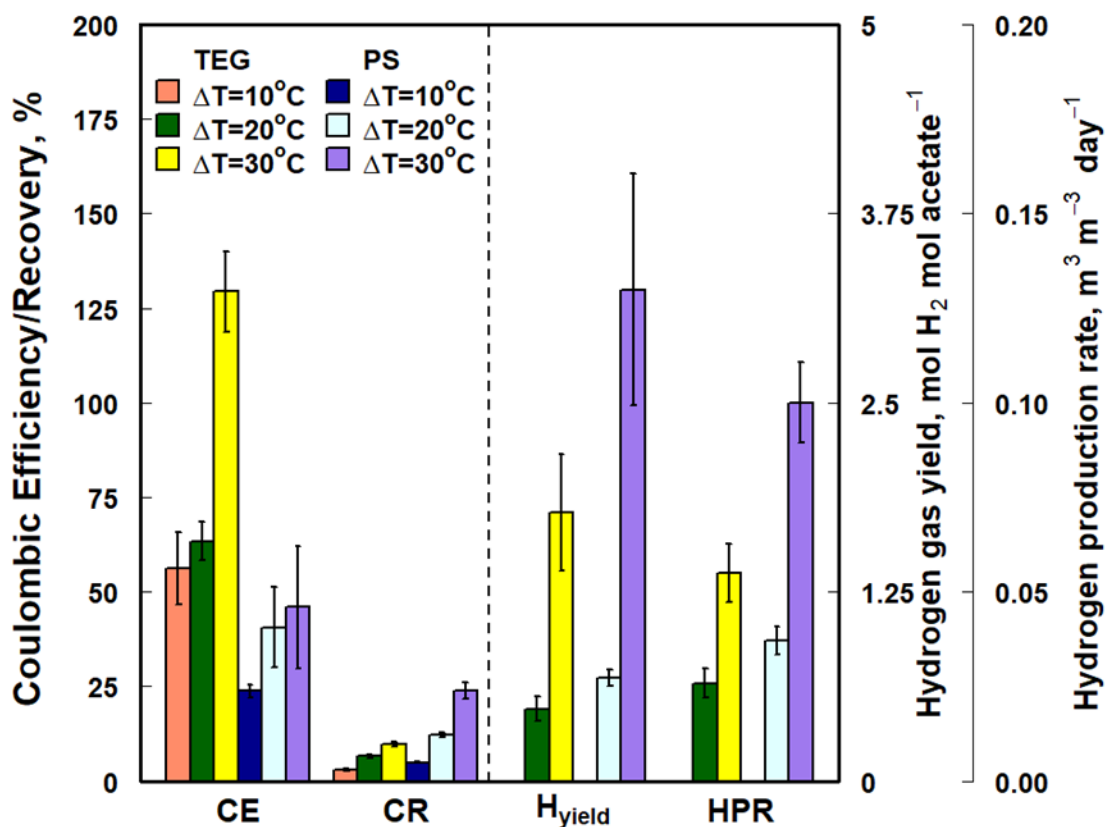


**Figure 6.4** Coulombic Efficiency (CE), Coulombic recovery (CR), H$_{yield}$ and hydrogen production rate (HPR) of TEG and PS powered MEC.

To further understand the implications of using the TEGs and PS as an energy source, Coulombic efficiency, Coulombic recovery, hydrogen yield and HPR (Fig. 6.4). The CE of the

TEG-MEC increased from $56.1 \pm 9.5\%$ to $129.3 \pm 30.4\%$ when the temperature gradient increased from 10°C to 30°C in the TEG cell. The PS had lower CEs ($23.7 \pm 1.8\%$ to $45.9 \pm 16.2\%$) compared to the TEG-MEC at the comparative voltages. This is mainly due to the higher consumption of acetate without correlating increases in current generation. The CR percentages reveal that potentially inhibition occurred with the TEG-MEC that did not occur in the PS-MEC system [186]. The CR for $\Delta T=10$°C, 20°C and 30°C TEG-MEC conditions were $2.9 \pm 0.3\%$, $6.5 \pm 0.3\%$, and $9.7 \pm 0.5\%$, respectively. The CR were higher ($4.9 \pm 1.8\%$, $12.1 \pm 0.7\%$, and $24.0 \pm 2.2\%$) for the PS-MEC system. This also suggests an arrest of methanogenic bacteria, which resulted in less organic removal in the TEG-MEC. For $H_{yield}$ and HPR, values could not be determined for the $\Delta T=10$°C conditions as expected with the low voltage (<0.4 V) output. The $H_{yield}$ increased 2.7 times for the TEG-MEC and 3.8 times for the PS-MEC. The HPR were smaller and similar to the TEG-MEC and PS-MEC as the temperature gradient increased. As the temperature increases, the difference in HPR may be smaller, suggesting that TEG-MEC at higher temperature gradients may be more favorable.

VFA composition in the effluent helped provide insight on favored organic sources in for microbes in the MEC. PS10 and TEG10 both had similar compositions in the effluent compared to the influent. This suggests that organic matter is not favored by microbes at low temperature gradients. Additionally, the low voltage did not suggest high microbial activity. However, analyzing the PS-MEC showed the acetate make up compared to the total VFA went from 67% to 19% to 14% for the PS10, PS20, and P30 conditions, respectively (Fig. 6.5). Similar trends were observed in previous studies for cases where similar voltages were supplied to the MEC [286]. This decrease is attributed to acetate oxidizing microbes being more active at <2.0V. The higher consumption of acetate also contributed to the higher production of hydrogen gas in the cathode.

The decrease in propionate and butyrate were due to the lower usage of longer chained VFAs as suggested in a previous study [287]. In the TEG-MEC, acetate was the least favored organic removed.
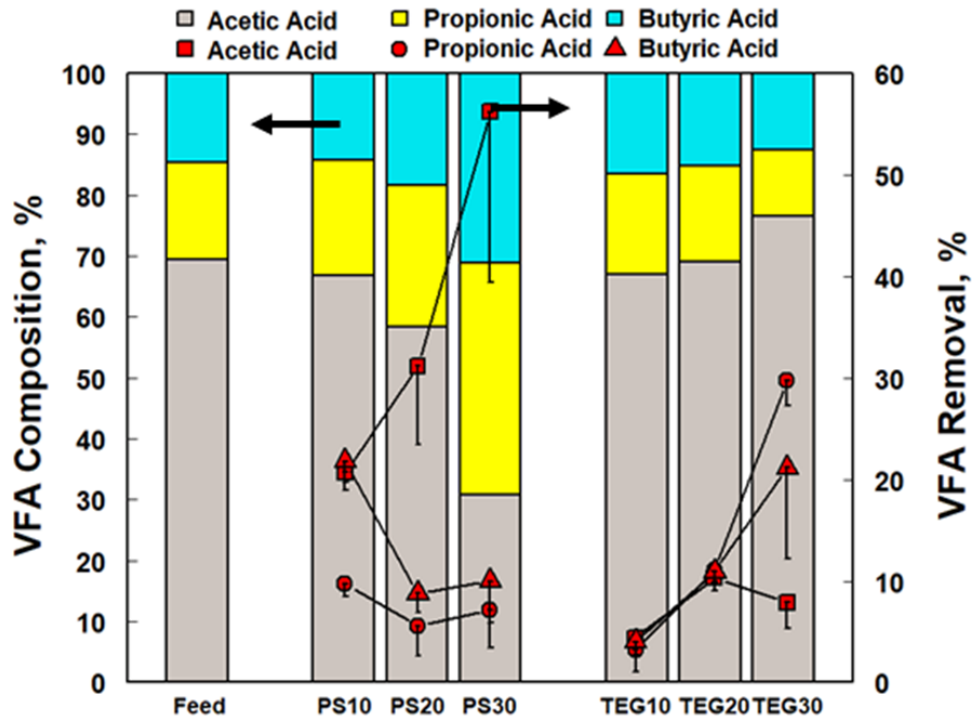


**Figure 6.5** Distribution of acetic, propionic, and butyric acid in MEC feed solution, effluent of TEG-MEC, and effluent of PS-MEC.

The removal of propionate ($3.2 \pm 0.5\%$, $11.0 \pm 1.1\%$, and $29.8 \pm 2.5\%$) and butyrate ($4.0 \pm 3.0\%$, $10.9 \pm 1.2\%$, and $21.2 \pm 9.0\%$) for the TEG10, TEG20, and TEG30 systems conditions increased. *Arcobacter* have been shown to directly use longer chained VFAs may grow with the use of TEGs as a power source [285]. There was a slight decrease in acetate removal between TEG20 and TEG30. The *Geobactor* microbes may have had more competition from the *Arcobacter* in the warmer conditions due to conduction across the TEGs. The pH levels of the anolyte also do not

suggest indirect consumption of propionic and butyrate that can be facilitated with carbon catalysis.

Microbial degradation and energy performance increased as the temperature gradient increased (Fig. 6.6). The maximum power density for $\Delta T=10°C$ was $0.07$ W m$^{-2}$ for the MEC without the TEGs connected. Increases in maximum power density were observed for $\Delta T=20°C$ ($61.2\%$ increase) and $\Delta T=30°C$ ($131.1\%$ increase). It is plausible that an increase in microbial activity is due to the temperature gradient increases in the TEG cells. This is an additional benefit that is not expected with the PS as the temperature will remain the same. When the TEG was connected to the MEC, the power density increased from $0.07$ W m$^{-2}$ to $0.25$ W m$^{-2}$ to $0.48$ W m$^{-2}$ as the heat source temperature increased. This shows how the addition of the TEG can improve the system. In addition, the internal resistance of the systems without the TEG decreased as the temperature increased. However, connecting the TEGs increased the temperature for $\Delta T=10°C$ ($214$ $\Omega$ to $416$ $\Omega$), $\Delta T=20°C$ ($151$ $\Omega$ to $324$ $\Omega$), $\Delta T=30°C$ ($116$ $\Omega$ to $336$ $\Omega$) conditions. For the $\Delta T=10°C$, the low voltage output of the TEGs was unable to overcome the high resistance. This is why the TEG-MEC system had a lower power density than the sole MEC systems. Overall, this suggests that fewer TEGs operating at a higher temperature would make the TEG-MEC system more efficient. Decreasing the resistance of the system would also promote electron transfer to the cathode chamber for hydrogen generation. An energy analysis was completed for the different PS and TEG conditions (Fig. 6.7). The power for recirculation rates was the same for each condition and only consumed $0.039$ kWh m$^{-3}$ during MEC treatment. The power source is the main consumer of energy in MECs as it went from $0.051$ kWh m$^{-3}$ to $1.390$ kWh m$^{-3}$ for PS10 to PS30. Since waste heat is free to the system it does not contribute to the financial feasibility considered for this energy analysis. This observation makes the TEG a more sustainable energy source compared to the PS.

Further consideration was given during the TEG tests. The TEG consumed 95% and 90% less energy than the PS for the same amount of hydrogen gas. This result shows that TEGs can be used to help
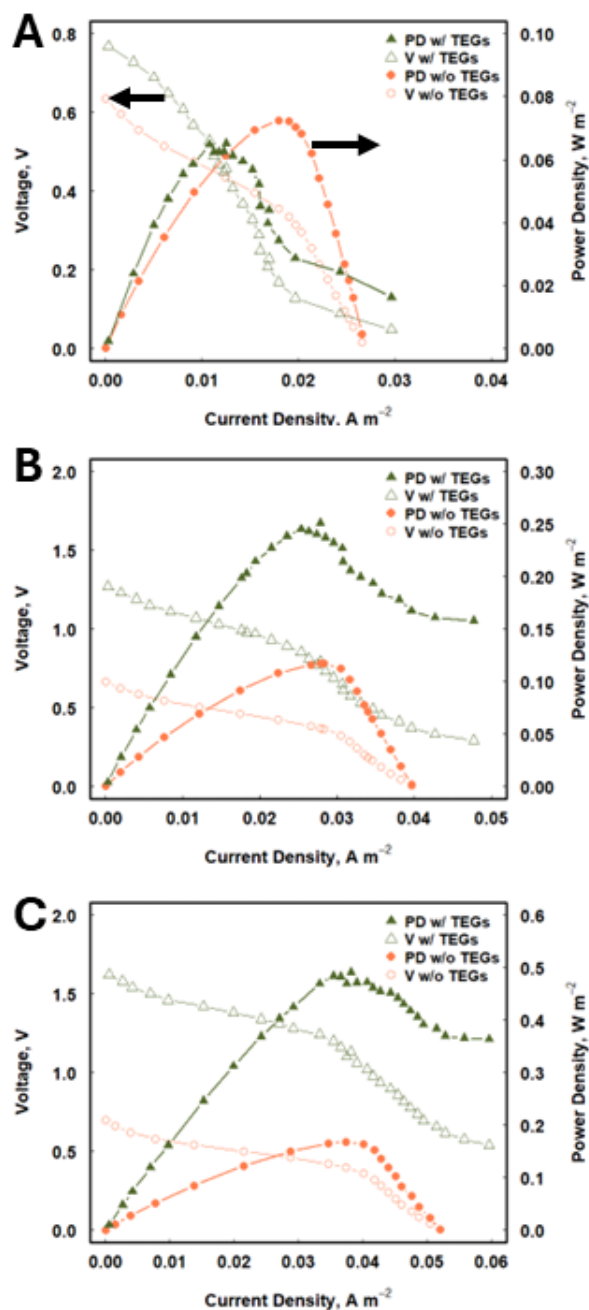


**Figure 6.6** Polarization curves for the TEG-MEC at (A) ΔT=10°C, (B), ΔT=20°C, and (C) ΔT=30°C.
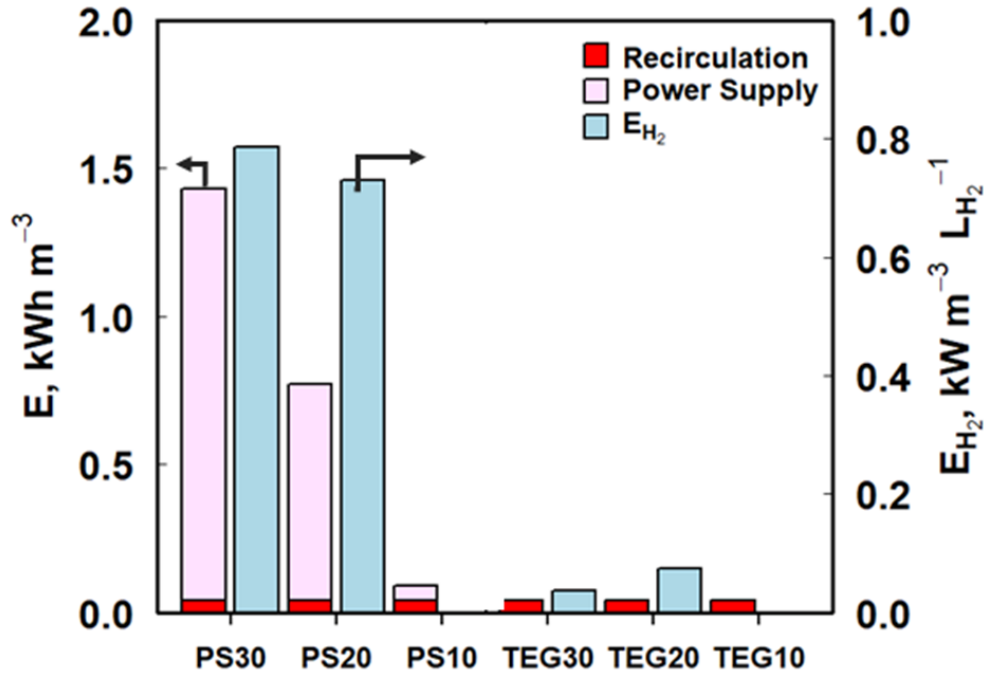
**Figure 6.7** Energy consumption and energy consumption for hydrogen gas generation for TEG-MEC and PS-MEC.

offset energy cost of MEC hydrogen production. placed on the amount of energy consumed per liter of hydrogen gas produced. The TEG20 and TEG30 conditions consumed 0.074 and 0.036 kW per liter of hydrogen gas, respectively.

## 6.4 Conclusion

In this study, TEGs were used as an alternative energy source to power a MEC treating a synthetic brewery wastewater. The TEG was characterized by adjusting the recirculation rate, the heat source/heat sink temperature gradient, and medium interfaces. Increasing the recirculating and temperature gradient yielded higher voltage output of the TEGs as conduction across the TEG was

decreased while maintaining temperature in the TEG cell. The TEG-MEC system consumed alkalinity as the temperature gradient increased, which resulted in microbial inhibition as the anolyte went towards acidic levels. The VFA fed MEC experienced a decrease in current generation compared to the acetate fed MEC. The polarization curves also showed that the maximum power density increase from 0.07 W m$^{-2}$ to 0.16 W m$^{-2}$ occurred because of increased activity of the microbes due to conduction from the heat source. Comparison analysis between the PS-MEC and TEG-MEC systems showed that while the PS experienced higher removal of organic matter and higher current generation, the TEG-MEC system is more efficient and energy friendly by using ~90% less energy for hydrogen production. Future studies should focus on decreasing the internal resistance of the system when using TEGs so that greater current densities can be achieved. The use of hot air should be explored to evaluate its robustness as an energy source.

# Chapter 7

# Perspectives

This dissertation used three objectives - (1) investigate forward osmosis as a pretreatment step for microbial fuel cell treatment, (2) explore membrane contactor integration with microbial fuel cell technology as a sustainable resource recovery method, and (3) investigate thermoelectric generators as an alternative power supply for microbial electrolysis cells - to show the promise coupling bioelectrochemical systems (BES) with other technologies has in terms of biological wastewater treatment and optimization of resource recovery from wastewater.

In Chapter 2, methods for removal and recovery of reverse fluxed solute from FO process were discussed. In Chapter 3, two draw solutes (NaCl and $NH_4HCO_3$) were investigated for use in a FO-MFC coupled system. Future work should investigate other draw solutes and their suitability for FO-MFC treatment. Focusing on $NH_4^+$ based draw solutes could provide insight into how nitrogen footprints could be decreased while increasing freshwater resources. Additionally, the use of the diluted draw solution should be considered. Direct use fertilizer is an approach that can continue to increase the sustainability of FO-MFC treatment. Magnetic particles can be investigated for sustainability since they are relatively recoverable compared to other inorganic salts. Membrane contactor was used in Chapter 4 to show its suitability for recovery of volatile fatty acids (VFA) and ammonium. In the future, different design modes (e.g., air gap, vacuum, and sweeping gas) should be investigated to determine if VFA and ammonium recovery can be increased. In order to improve modeling efforts, dynamic models need to be developed. These models should consider that all volatile and aqueous compounds have varied effects on solution vapor pressure based on factors such as temperature, pH, and mole ratio. Utilizing electrochemical

techniques to generate acids and bases could also decrease the resources necessary for MC operation. These electrochemical processes should be optimized so that MC does not lose its non-energy intensive characteristic. In Chapter 5, MC was shown to be a highly effective method of recovering ammonium from the cathode chamber of an MFC. Future work should consider additional variables that would improve the performance of both the MFC and MC. The energy consumption of the MFC+MC system should also optimize aeration to achieve maximum power output without sacrificing COD removal, ammonium removal and ammonium recovery. In Chapter 6, thermoelectric electric generators (TEGs) powered an MEC for more sustainable hydrogen gas generation. Future work should use hot air to mimic flue gas to investigate air as a heat source. Since TEGs are a bourgeoning technology in environmental systems, technoeconomic analysis and life cycle analysis studies should be completed to clarify the benefits and challenges of wastewater treatment systems powered by TEGs. Additionally, sustainable electrodes should be used to decrease the cost of MEC construction and operation.

In general, the future of biological wastewater treatment should be approached with innovative techniques. Emerging contaminants such as per- and polyfluorinated substances (PFAS), pharmaceuticals, and personal care products (PPCPs) have already been proven to negatively affect wastewater treatment and can negatively impact the environment. Specifically, exploration on the effects of PFAs and PPCPs on BES and coupled systems should be completed. The use of machine learning tools to help further explain coupled system effectiveness should also be considered. Large data sets based on findings from the literature and observations from experimental work can be used to test various algorithms (e.g., linear and logistic regression, K-Means, and random forest). It is expected that different systems will have different algorithms that predict outcomes. The effects of PFAs and PPCPs presence can also be determined using these

statistical and modeling tools. These efforts along with results from this dissertation will help the field identify problems that may arise, develop solutions to attenuate their effects, and achieve sustainable, advance wastewater treatment.

# References

1.  Jones, E.R., et al., *Country-level and gridded estimates of wastewater production, collection, treatment and reuse.* Earth Syst. Sci. Data, 2021. **13**(2): p. 237-254.

2.  Parida, V.K., et al., *Emerging contaminants in wastewater: A critical review on occurrence, existing legislations, risk assessment, and sustainable treatment alternatives.* Journal of Environmental Chemical Engineering, 2021. **9**(5): p. 105966.

3.  Gogoi, A., et al., *Occurrence and fate of emerging contaminants in water environment: A review.* Groundwater for Sustainable Development, 2018. **6**: p. 169-180.

4.  Mustafa, N., et al., *Anaerobic digestion of municipal wastewater sludges using anaerobic fluidized bed bioreactor.* Bioresource Technology, 2014. **172**: p. 461-466.

5.  Ray, H., F. Perreault, and T.H. Boyer, *Ammonia recovery and fouling mitigation of hydrolyzed human urine treated by nanofiltration and reverse osmosis.* Environmental Science: Water Research & Technology, 2022. **8**(2): p. 429-442.

6.  Kim, J., et al., *A comprehensive review of energy consumption of seawater reverse osmosis desalination plants.* Applied Energy, 2019. **254**: p. 113652.

7.  Li, Y., Y. Chen, and J. Wu, *Enhancement of methane production in anaerobic digestion process: A review.* Applied Energy, 2019. **240**: p. 120-137.

8.  Yang, E., et al., *Critical review of bioelectrochemical systems integrated with membrane-based technologies for desalination, energy self-sufficiency, and high-efficiency water and wastewater treatment.* Desalination, 2019. **452**: p. 40-67.

9.  McCarty, P.L., J. Bae, and J. Kim, *Domestic Wastewater Treatment as a Net Energy Producer–Can This be Achieved?* Environmental Science & Technology, 2011. **45**(17): p. 7100-7106.

10. Jadhav, G.S. and M.M. Ghangrekar, *Performance of microbial fuel cell subjected to variation in pH, temperature, external load and substrate concentration.* Bioresource Technology, 2009. **100**(2): p. 717-723.

11. Tenca, A., et al., *Evaluation of low cost cathode materials for treatment of industrial and food processing wastewater using microbial electrolysis cells.* International Journal of Hydrogen Energy, 2013. **38**(4): p. 1859-1865.

12. Bejjanki, D., et al., *Simultaneous bioelectricity generation and water desalination using Oscillatoria sp. as biocatalyst in photosynthetic microbial desalination cell.* Science of The Total Environment, 2021. **754**: p. 142215.

13. Huang, L., et al., *Complete cobalt recovery from lithium cobalt oxide in self-driven microbial fuel cell – Microbial electrolysis cell systems.* Journal of Power Sources, 2014. **259**: p. 54-64.

14. Mostafa, A., et al., *Bioelectrochemical system for enhancing anaerobic digestion of pharmaceutical-containing domestic wastewater.* Chemosphere, 2023. **339**: p. 139766.

15. Wang, G., et al., *Cost-efficient microbial electrosynthesis of hydrogen peroxide on a facile-prepared floating electrode by entrapping oxygen.* Bioresource Technology, 2021. **342**: p. 125995.

16. Ren, Z., T.E. Ward, and J.M. Regan, *Electricity Production from Cellulose in a Microbial Fuel Cell Using a Defined Binary Culture.* Environmental Science & Technology, 2007. **41**(13): p. 4781-4786.

17. Zhang, M., et al., *Increased power generation from cylindrical microbial fuel cell inoculated with P. aeruginosa.* Biosensors and Bioelectronics, 2019. **141**: p. 111394.

18. Ye, Y., et al., *Feasibility study on a double chamber microbial fuel cell for nutrient recovery from municipal wastewater.* Chemical Engineering Journal, 2019. **358**: p. 236-242.

19. Pepè Sciarria, T., et al., *Nutrient recovery and energy production from digestate using microbial electrochemical technologies (METs).* Journal of Cleaner Production, 2019. **208**: p. 1022-1029.

20. Hiegemann, H., et al., *An integrated 45L pilot microbial fuel cell system at a full-scale wastewater treatment plant.* Bioresource Technology, 2016. **218**: p. 115-122.

21. Logan, B.E., et al., *Microbial Fuel Cells: Methodology and Technology.* Environmental Science & Technology, 2006. **40**(17): p. 5181-5192.

22. Qin, M., et al., *Integrated experimental and modeling evaluation of energy consumption for ammonia recovery in bioelectrochemical systems.* Chemical Engineering Journal, 2017. **327**: p. 924-931.

23. Dong, H., et al., *Microbial fuel cell-based biosensor for monitoring anaerobic biodegradation of poly(3-hydroxybutyrate-co-4-hydroxybutyrate).* Polymer Degradation and Stability, 2023. **214**: p. 110409.

24. Pophali, A., S. Singh, and N. Verma, *Simultaneous hydrogen generation and COD reduction in a photoanode-based microbial electrolysis cell.* International Journal of Hydrogen Energy, 2020. **45**(48): p. 25985-25995.

25. Jeremiasse, A.W., et al., *Performance of metal alloys as hydrogen evolution reaction catalysts in a microbial electrolysis cell.* International Journal of Hydrogen Energy, 2011. **36**(17): p. 10482-10489.

26. Jafary, T., et al., *Clean hydrogen production in a full biological microbial electrolysis cell.* International Journal of Hydrogen Energy, 2019. **44**(58): p. 30524-30531.

27.    Yang, Y., et al., *Enhancing hydrogen production in microbial electrolysis cells by in situ hydrogen oxidation for self-buffering pH through periodic polarity reversal.* Journal of Power Sources, 2017. **347**: p. 21-28.

28.    Lu, L. and Z.J. Ren, *Microbial electrolysis cells for waste biorefinery: A state of the art review.* Bioresource Technology, 2016. **215**: p. 254-264.

29.    Onwuemezie, L. and H. Gohari Darabkhani, *Solar and wind assisted biohydrogen production from integrated anaerobic digestion and microbial electrolysis cell coupled with catalytic reforming.* Energy Conversion and Management, 2024. **305**: p. 118224.

30.    Strik, D.P.B.T.B., H.V.M. Hamelers, and C.J.N. Buisman, *Solar Energy Powered Microbial Fuel Cell with a Reversible Bioelectrode.* Environmental Science & Technology, 2010. **44**(1): p. 532-537.

31.    Islam, A.K.M.K., *Hydropower coupled with hydrogen production from wastewater: Integration of micro-hydropower plant (MHP) and microbial electrolysis cell (MEC).* International Journal of Hydrogen Energy, 2024. **49**: p. 1-14.

32.    Winfield, J., et al., *The overshoot phenomenon as a function of internal resistance in microbial fuel cells.* Bioelectrochemistry, 2011. **81**(1): p. 22-27.

33.    Kundu, A., et al., *An overview of cathode material and catalysts suitable for generating hydrogen in microbial electrolysis cell.* International Journal of Hydrogen Energy, 2013. **38**(4): p. 1745-1757.

34.    Foley, J.M., et al., *Life Cycle Assessment of High-Rate Anaerobic Treatment, Microbial Fuel Cells, and Microbial Electrolysis Cells.* Environmental Science & Technology, 2010. **44**(9): p. 3629-3637.

35.    Hou, Y., et al., *Microbial electrolysis cell with spiral wound electrode for wastewater treatment and methane production.* Process Biochemistry, 2015. **50**(7): p. 1103-1109.

36.    Gude, V.G., *Wastewater treatment in microbial fuel cells – an overview.* Journal of Cleaner Production, 2016. **122**: p. 287-307.

37.    Wang, H., et al., *Bioelectrochemical system platform for sustainable environmental remediation and energy generation.* Biotechnology Advances, 2015. **33**(3): p. 317-334.

38.    Zhang, Y. and I. Angelidaki, *Microbial electrolysis cells turning to be versatile technology: Recent advances and future challenges.* Water Research, 2014. **56**: p. 11-25.

39.    Zamora, P., et al., *Ammonia recovery from urine in a scaled-up Microbial Electrolysis Cell.* Journal of Power Sources, 2017. **356**: p. 491-499.

40.    Lutchmiah, K., et al., *Forward osmosis for application in wastewater treatment: A review.* Water Research, 2014. **58**: p. 179-197.

41. Reddy, A.S., V.P. Wanjari, and S.P. Singh, *Design, synthesis, and application of thermally responsive draw solutes for sustainable forward osmosis desalination: A review.* Chemosphere, 2023. **317**: p. 137790.

42. Li, X., Y. Lu, and Z. He, *Removal of reverse-fluxed ammonium by anammox in a forward osmosis system using ammonium bicarbonate as a draw solute.* Journal of Membrane Science, 2015. **495**: p. 424-430.

43. Sun, Y., et al., *Membrane fouling of forward osmosis (FO) membrane for municipal wastewater treatment: A comparison between direct FO and OMBR.* Water Research, 2016. **104**: p. 330-339.

44. Siagian, U.W.R., et al., *Membrane-based carbon capture technologies: Membrane gas separation vs. membrane contactor.* Journal of Natural Gas Science and Engineering, 2019. **67**: p. 172-195.

45. deMontigny, D., P. Tontiwachwuthikul, and A. Chakma, *Using polypropylene and polytetrafluoroethylene membranes in a membrane contactor for CO2 absorption.* Journal of Membrane Science, 2006. **277**(1): p. 99-107.

46. Dindore, V.Y., et al., *CO2 absorption at elevated pressures using a hollow fiber membrane contactor.* Journal of Membrane Science, 2004. **235**(1): p. 99-109.

47. Ashrafizadeh, S.N. and Z. Khorasani, *Ammonia removal from aqueous solutions using hollow-fiber membrane contactors.* Chemical Engineering Journal, 2010. **162**(1): p. 242-249.

48. Pan, X.-R., et al., *Recovery of high-concentration volatile fatty acids from wastewater using an acidogenesis-electrodialysis integrated system.* Bioresource Technology, 2018. **260**: p. 61-67.

49. Al-Juboori, R.A., et al., *Membrane contactor onsite piloting for nutrient recovery from mesophilic digester reject water: The effect of process conditions and pre-treatment options.* Separation and Purification Technology, 2022. **303**: p. 122250.

50. Zhang, Y., *Thermoelectric Advances to Capture Waste Heat in Automobiles.* ACS Energy Letters, 2018. **3**(7): p. 1523-1524.

51. Iezzi, B., et al., *Printed, metallic thermoelectric generators integrated with pipe insulation for powering wireless sensors.* Applied Energy, 2017. **208**: p. 758-765.

52. Aswal, D.K., R. Basu, and A. Singh, *Key issues in development of thermoelectric power generators: High figure-of-merit materials and their highly conducting interfaces with metallic interconnects.* Energy Conversion and Management, 2016. **114**: p. 50-67.

53. Rabari, R., S. Mahmud, and A. Dutta, *Effect of thermal conductivity on performance of thermoelectric systems based on Effective Medium Theory.* International Journal of Heat and Mass Transfer, 2015. **91**: p. 190-204.

54. Sargolzaeiaval, Y., et al., *Flexible thermoelectric generators for body heat harvesting – Enhanced device performance using high thermal conductivity elastomer encapsulation on liquid metal interconnects.* Applied Energy, 2020. **262**: p. 114370.

55. Kim, S., et al., *Gas-liquid membrane contactors for carbon dioxide separation: A review.* Chemical Engineering Journal, 2021. **411**: p. 128468.

56. Zhang, F., J. Li, and Z. He, *A new method for nutrients removal and recovery from wastewater using a bioelectrochemical system.* Bioresource Technology, 2014. **166**: p. 630-634.

57. Hassan, H., et al., *Microbial community and bioelectrochemical activities in MFC for degrading phenol and producing electricity: Microbial consortia could make differences.* Chemical Engineering Journal, 2018. **332**: p. 647-657.

58. Montpart, N., et al., *Hydrogen production in single chamber microbial electrolysis cells with different complex substrates.* Water Research, 2015. **68**: p. 601-615.

59. Zeppilli, M., et al., *Two-side cathode microbial electrolysis cell for nutrients recovery and biogas upgrading.* Chemical Engineering Journal, 2019. **370**: p. 466-476.

60. Wang, J. and X. Liu, *Forward osmosis technology for water treatment: Recent advances and future perspectives.* Journal of Cleaner Production, 2021. **280**: p. 124354.

61. Cath, T.Y., A.E. Childress, and M. Elimelech, *Forward osmosis: Principles, applications, and recent developments.* Journal of Membrane Science, 2006. **281**(1-2): p. 70-87.

62. Xie, M., et al., *Relating rejection of trace organic contaminants to membrane properties in forward osmosis: Measurements, modelling and implications.* Water Research, 2014. **49**: p. 265-274.

63. Klaassen, R., P. Feron, and A. Jansen, *Membrane contactor applications.* Desalination, 2008. **224**(1): p. 81-87.

64. Lee, S., et al., *Application of electrically conductive membrane contactor in the carbon dioxide stripping process for mitigation of fouling induced by flue gas.* Chemical Engineering Journal, 2023. **473**: p. 145425.

65. Uzkurt Kaljunen, J., et al., *Newly developed membrane contactor-based N and P recovery process: Pilot-scale field experiments and cost analysis.* Journal of Cleaner Production, 2021. **281**: p. 125288.

66. Marjani, A. and S. Shirazian, *Simulation of heavy metal extraction in membrane contactors using computational fluid dynamics.* Desalination, 2011. **281**: p. 422-428.

67. Kerber, J. and J.-U. Repke, *Mass transfer and selectivity analysis of a dense membrane contactor for upgrading biogas.* Journal of Membrane Science, 2016. **520**: p. 450-464.

68.     Lv, Y., et al., *Wetting of polypropylene hollow fiber membrane contactors.* Journal of Membrane Science, 2010. **362**(1): p. 444-452.

69.     Pourkiaei, S.M., et al., *Thermoelectric cooler and thermoelectric generator devices: A review of present and potential applications, modeling and materials.* Energy, 2019. **186**: p. 115849.

70.     Ouyang, Z. and D. Li, *Design of segmented high-performance thermoelectric generators with cost in consideration.* Applied Energy, 2018. **221**: p. 112-121.

71.     Champier, D., *Thermoelectric generators: A review of applications.* Energy Conversion and Management, 2017. **140**: p. 167-181.

72.     Jouhara, H., et al., *Thermoelectric generator (TEG) technologies and applications.* International Journal of Thermofluids, 2021. **9**: p. 100063.

73.     Zou, S., et al., *Modeling assisted evaluation of direct electricity generation from waste heat of wastewater via a thermoelectric generator.* Science of The Total Environment, 2018. **635**: p. 1215-1224.

74.     Castañeda, M., et al., *Thermoelectric generator using low-cost thermoelectric modules for low-temperature waste heat recovery.* Sustainability, 2023. **15**(4): p. 3681.

75.     Angelakis, A.N. and S.A. Snyder, *Wastewater treatment and reuse: Past, present, and future.* Water, 2015. **7**(9): p. 4887-4895.

76.     Garcia, X. and D. Pargament, *Reusing wastewater to cope with water scarcity: Economic, social and environmental considerations for decision-making.* Resources, Conservation and Recycling, 2015. **101**: p. 154-66.

77.     Sun, Y., et al., *Dynamic changes of the fouling layer in forward osmosis based membrane processes for municipal wastewater treatment.* Journal of Membrane Science, 2018. **549**: p. 523-532.

78.     Xinhua, W., et al., *Removal of cytostatic drugs from wastewater by an anaerobic osmotic membrane bioreactor.* Chemical Engineering Journal, 2018. **339**: p. 153-61.

79.     Corzo, B., et al., *Long-term evaluation of a forward osmosis-nanofiltration demonstration plant for wastewater reuse in agriculture.* Chemical Engineering Journal, 2018. **338**: p. 383-91.

80.     Gao, Y., et al., *Direct concentration of municipal sewage by forward osmosis and membrane fouling behavior.* Bioresource Technology, 2018. **247**: p. 730-735.

81.     Thiruvenkatachari, R., et al., *Application of integrated forward and reverse osmosis for coal mine wastewater desalination.* Separation and Purification Technology, 2016. **163**: p. 181-8.

82.     Cui, Y., et al., *Novel forward osmosis process to effectively remove heavy metal ions.* Journal of Membrane Science, 2014. **467**: p. 188-194.

83.     Phuntsho, S., et al., *Fertiliser drawn forward osmosis process: Pilot-scale desalination of mine impaired water for fertigation.* Journal of Membrane Science, 2016. **508**: p. 22-31.

84.     Kim, Y., et al., *Evaluation of fertilizer-drawn forward osmosis for coal seam gas reverse osmosis brine treatment and sustainable agricultural reuse.* Journal of Membrane Science, 2017. **537**: p. 22-31.

85.     Kim, J.E., S. Phuntsho, and H.K. Shon, *Pilot-scale nanofiltration system as post-treatment for fertilizer-drawn forward osmosis desalination for direct fertigation.* Desalination and Water Treatment, 2013. **51**(31-33): p. 6265-6273.

86.     Xie, M., et al., *Impact of organic and colloidal fouling on trace organic contaminant rejection by forward osmosis: Role of initial permeate flux.* Desalination, 2014. **336**(1): p. 146-152.

87.     Boo, C., et al., *Colloidal fouling in forward osmosis: Role of reverse salt diffusion.* Journal of Membrane Science, 2012. **390-391**: p. 277-284.

88.     Holloway, R.W., et al., *Mixed draw solutions for improved forward osmosis performance.* Journal of Membrane Science, 2015. **491**: p. 121-131.

89.     Zou, S., M. Qin, and Z. He, *Tackle reverse solute flux in forward osmosis towards sustainable water recovery: reduction and perspectives.* Water Research, 2019. **149**: p. 362-374.

90.     Lee, J., B. Kim, and S. Hong, *Fouling distribution in forward osmosis membrane process.* Journal of Environmental Sciences, 2014. **26**(6): p. 1348-1354.

91.     Tang, C.Y., et al., *Coupled effects of internal concentration polarization and fouling on flux behavior of forward osmosis membranes during humic acid filtration.* Journal of Membrane Science, 2010. **354**(1-2): p. 123-33.

92.     McCutcheon, J.R. and M. Elimelech, *Influence of concentrative and dilutive internal concentration polarization on flux behavior in forward osmosis.* Journal of Membrane Science, 2006. **284**(1-2): p. 237-247.

93.     Li, W., Y. Gao, and C.Y. Tang, *Network modeling for studying the effect of support structure on internal concentration polarization during forward osmosis: Model development and theoretical analysis with FEM.* Journal of Membrane Science, 2011. **379**(1): p. 307-321.

94.     Jeng Yih, L. and A.W. Mohammad, *Multiple-solute salts as draw solution for osmotic concentration of succinate feed by forward osmosis.* Journal of Industrial and Engineering Chemistry, 2017. **51**: p. 264-70.

95.     Sheng, L., et al., *Methane production in an anaerobic osmotic membrane bioreactor using forward osmosis: Effect of reverse salt flux.* Bioresource Technology, 2017. **239**: p. 285-93.

96.     Lu, Y., et al., *When bioelectrochemical systems meet forward osmosis: Accomplishing wastewater treatment and reuse through synergy.* Water, 2015. **7**(1): p. 38-50.

97.     Bowden, K.S., A. Achilli, and A.E. Childress, *Organic ionic salt draw solutions for osmotic membrane bioreactors.* Bioresource Technology, 2012. **122**: p. 207-216.

98.     Kuang, W., et al., *Investigation of internal concentration polarization reduction in forward osmosis membrane using nano-CaCO3particles as sacrificial component.* Journal of Membrane Science, 2016. **497**: p. 485-493.

99.     Jin, X., et al., *Boric Acid Permeation in Forward Osmosis Membrane Processes: Modeling, Experiments, and Implications.* Environmental Science & Technology, 2011. **45**(6): p. 2323-2330.

100.    Gang, C., et al., *Treatment of shale gas drilling flowback fluids (SGDFs) by forward osmosis: membrane fouling and mitigation.* Desalination, 2015. **366**: p. 113-20.

101.    Hamdan, M., et al., *Draw solutions for Forward Osmosis process: Osmotic pressure of binary and ternary aqueous solutions of magnesium chloride, sodium chloride, sucrose and maltose.* Journal of Food Engineering, 2015. **155**: p. 10-15.

102.    Corzo, B., et al., *Evaluation of draw solutions and commercially available forward osmosis membrane modules for wastewater reclamation at pilot scale.* Chemical Engineering Journal, 2017. **326**: p. 1-8.

103.    Long, Q., et al., *Synthesis and Application of Organic Phosphonate Salts as Draw Solutes in Forward Osmosis for Oil-Water Separation.* Environmental Science and Technology 2016. **50**(21): p. 12022-12029.

104.    Alejo, T., et al., *Advances in draw solutes for forward osmosis: hybrid organic-inorganic nanoparticles and conventional solutes.* Chemical Engineering Journal, 2017. **309**: p. 738-52.

105.    Nguyen, N.C., et al., *Optimising the recovery of EDTA-2Na draw solution in forward osmosis through direct contact membrane distillation.* Separation and Purification Technology, 2018. **198**: p. 108-112.

106.    Jui Shan, Y., W.A. Phillip, and M. Elimelech, *Coupled reverse draw solute permeation and water flux in forward osmosis with neutral draw solutes.* Journal of Membrane Science, 2012. **392-393**: p. 9-17.

107.    Qi, S., et al., *Highly efficient forward osmosis based on porous membranes-Applications and implications.* Environmental Science and Technology, 2015. **49**(7): p. 4690-4695.

108. Qiu, G., et al., *Direct and complete phosphorus recovery from municipal wastewater using a hybrid microfiltration-forward osmosis membrane bioreactor process with seawater brine as draw solution.* Environmental Science and Technology, 2015. **49**(10): p. 6156-6163.

109. Wang, X., et al., *Integration of micro-filtration into osmotic membrane bioreactors to prevent salinity build-up.* Bioresource Technology, 2014. **167**: p. 116-123.

110. Hu, T., et al., *Impacts of inorganic draw solutes on the performance of thin-film composite forward osmosis membrane in a microfiltration assisted anaerobic osmotic membrane bioreactor.* RSC Advances, 2017. **7**(26): p. 16057-16063.

111. Holloway, R.W., et al., *Long-term pilot scale investigation of novel hybrid ultrafiltration-osmotic membrane bioreactors.* Desalination, 2015. **363**: p. 64-74.

112. Qiu, G., et al., *Direct and complete phosphorus recovery from municipal wastewater using a hybrid microfiltration-forward osmosis membrane bioreactor process with seawater brine as draw solution.* Environmental science & technology, 2015. **49**(10): p. 6156-6163.

113. Luo, W., et al., *The role of forward osmosis and microfiltration in an integrated osmotic-microfiltration membrane bioreactor system.* Chemosphere, 2015. **136**: p. 125-132.

114. Qiu, G., et al., *Towards high through-put biological treatment of municipal wastewater and enhanced phosphorus recovery using a hybrid microfiltration-forward osmosis membrane bioreactor with hydraulic retention time in sub-hour level.* Bioresource Technology, 2016. **219**: p. 298-310.

115. Wenhai, L., et al., *Phosphorus and water recovery by a novel osmotic membrane bioreactor-reverse osmosis system.* Bioresource Technology, 2016. **200**: p. 297-304.

116. Wang, X., et al., *Development of a novel anaerobic membrane bioreactor simultaneously integrating microfiltration and forward osmosis membranes for low-strength wastewater treatment.* Journal of Membrane Science, 2017. **527**: p. 1-7.

117. Xie, M., et al., *Toward resource recovery from wastewater: extraction of phosphorus from digested sludge using a hybrid forward osmosis–membrane distillation process.* Environmental Science and Technology Letters, 2014. **1**(2): p. 191-195.

118. Zou, S., et al., *Nutrient-energy-water recovery from synthetic sidestream centrate using a microbial electrolysis cell - forward osmosis hybrid system.* Journal of Cleaner Production, 2017. **154**: p. 16-25.

119. Wu, Z., et al., *Forward osmosis promoted in-situ formation of struvite with simultaneous water recovery from digested swine wastewater.* Chemical Engineering Journal, 2018. **342**: p. 274-280.

120. Wu, S., et al., *Enhancing recovery of magnesium as struvite from landfill leachate by pretreatment of calcium with simultaneous reduction of liquid volume via forward osmosis.* Science of the Total Environment, 2018. **610-611**: p. 137-146.

121. Li, X., et al., *Long-term performance and microbial community characterization of an osmotic anammox system for removing reverse-fluxed ammonium.* Bioresource technology, 2016. **211**: p. 628-635.

122. Luo, W., et al., *Water extraction from mixed liquor of an aerobic bioreactor by forward osmosis: Membrane fouling and biomass characteristics assessment.* Separation and Purification Technology, 2015. **145**: p. 56-62.

123. Chang, H.-M., et al., *Osmosis membrane bioreactor–microfiltration with magnesium-based draw solute for salinity reduction and phosphorus recovery.* International Biodeterioration & Biodegradation, 2017. **124**: p. 169-175.

124. Wang, J., et al., *Performance of a novel fertilizer-drawn forward osmosis aerobic membrane bioreactor (FDFO-MBR): Mitigating salinity build-up by integrating microfiltration.* Water, 2017. **9**(1).

125. Bell, E.A., et al., *Produced water treatment using forward osmosis membranes: Evaluation of extended-time performance and fouling.* Journal of Membrane Science, 2017. **525**: p. 77-88.

126. Arkhangelsky, E., et al., *Combined organic–inorganic fouling of forward osmosis hollow fiber membranes.* Water Research, 2012. **46**(19): p. 6329-6338.

127. Kim, J.E., et al., *Environmental and economic impacts of fertilizer drawn forward osmosis and nanofiltration hybrid system.* Desalination, 2017. **416**: p. 76-85.

128. Guo, W., H.-H. Ngo, and J. Li, *A mini-review on membrane fouling.* Bioresource Technology, 2012. **122**: p. 27-34.

129. Yasukawa, M., et al., *Effect of molecular weight of draw solute on water permeation in forward osmosis process.* Industrial and Engineering Chemistry Research, 2015. **54**(33): p. 8239-8246.

130. An, X., et al., *Continuous juice concentration by integrating forward osmosis with membrane distillation using potassium sorbate preservative as a draw solute.* Journal of Membrane Science, 2019. **573**: p. 192-199.

131. Sahinkaya, E., et al., *Sulfate reduction and filtration performances of an anaerobic membrane bioreactor (AnMBR).* Chemical Engineering Journal, 2018. **349**: p. 47-55.

132. Matos, C.T., et al., *Nitrate removal in a closed marine system through the ion exchange membrane bioreactor.* Journal of Hazardous Materials, 2009. **166**(1): p. 428-434.

133. Cinperi, N.C., et al., *Treatment of woolen textile wastewater using membrane bioreactor, nanofiltration and reverse osmosis for reuse in production processes.* Journal of Cleaner Production, 2019. **223**: p. 837-848.

134. Ansari, A.J., et al., *Phosphorus recovery from digested sludge centrate using seawater-driven forward osmosis.* Separation and Purification Technology, 2016. **163**: p. 1-7.

135. Zhu, S., M. Li, and M. Gamal El-Din, *Forward osmosis as an approach to manage oil sands tailings water and on-site basal depressurization water.* Journal of Hazardous Materials, 2017. **327**: p. 18-27.

136. Perwitasari, D.S., et al., *Kinetics and morphology analysis of struvite precipitated from aqueous solution under the influence of heavy metals: Cu2+, Pb2+, Zn2+.* Journal of Environmental Chemical Engineering, 2018. **6**(1): p. 37-43.

137. Taddeo, R., et al., *Nutrient management via struvite precipitation and recovery from various agroindustrial wastewaters: Process feasibility and struvite quality.* Journal of Environmental Management, 2018. **212**: p. 433-439.

138. Nur, T., et al., *Struvite production using membrane-bioreactor wastewater effluent and seawater.* Desalination, 2018. **444**: p. 1-5.

139. Zeng, F., et al., *Struvite precipitation from anaerobic sludge supernatant and mixed fresh/stale human urine.* Chemical Engineering Journal, 2018. **344**: p. 254-261.

140. Zeng, C., et al., *Impact of feed water pH and membrane material on nanofiltration of perfluorohexanoic acid in aqueous solution.* Chemosphere, 2017. **183**: p. 599-604.

141. Shu, L., et al., *Why does pH increase with CaCl2 as draw solution during forward osmosis filtration.* Process Safety and Environmental Protection, 2016. **104**: p. 465-471.

142. Wang, X., V.W.C. Chang, and C.Y. Tang, *Osmotic membrane bioreactor (OMBR) technology for wastewater treatment and reclamation: Advances, challenges, and prospects for the future.* Journal of Membrane Science, 2016. **504**: p. 113-132.

143. Yang, Y., H. Song, and Z. He, *Mitigation of solute buildup by using a biodegradable and reusable polyelectrolyte as a draw solute in an osmotic membrane bioreactor.* Environmental Science: Water Research & Technology, 2019. **5**(1): p. 19-27.

144. Nawaz, M.S., et al., *Microbial toxity effects of reverse transported draw solute in the forward osmosis membrane bioreactor (FO-MBR).* Journal of Membrane Science, 2013. **429**: p. 323-329.

145. Kim, Y., et al., *Assessing the removal of organic micro-pollutants from anaerobic membrane bioreactor effluent by fertilizer-drawn forward osmosis.* Journal of Membrane Science, 2017. **533**: p. 84-95.

146. Qiu, G., et al., *The potential of hybrid forward osmosis membrane bioreactor (FOMBR) processes in achieving high throughput treatment of municipal wastewater with enhanced phosphorus recovery.* Water Research, 2016. **105**: p. 370-382.

147. Li, J.-Y., et al., *Membrane fouling of forward osmosis in dewatering of soluble algal products: Comparison of TFC and CTA membranes.* Journal of Membrane Science, 2018. **552**: p. 213-221.

148. Li, S., et al., *Impact of reverse nutrient diffusion on membrane biofouling in fertilizer-drawn forward osmosis.* Journal of Membrane Science, 2017. **539**: p. 108-115.

149. Beegle, J.R. and A.P. Borole, *Energy production from waste: Evaluation of anaerobic digestion and bioelectrochemical systems based on energy efficiency and economic factors.* Renewable and Sustainable Energy Reviews, 2018. **96**: p. 343-351.

150. Oliot, M., et al., *Ion transport in microbial fuel cells: Key roles, theory and critical review.* Applied Energy, 2016. **183**: p. 1682-1704.

151. Yang, Y., X. Yang, and Z. He, *Bioelectrochemically-assisted mitigation of salinity buildup and recovery of reverse-fluxed draw solute in an osmotic membrane bioreactor.* Water Research, 2018. **141**: p. 259-267.

152. Zhang, X., et al., *Factors affecting the efficiency of a bioelectrochemical system: a review.* RSC Advances, 2019. **9**(34): p. 19748-19761.

153. Marie, G., et al., *Impact of a high hydrostatic pressure pretreatment on the separation of bioactive peptides from flaxseed protein hydrolysates by electrodialysis with ultrafiltration membranes.* Separation and Purification Technology, 2019. **211**: p. 242-251.

154. Sadyrbaeva, T.Z., *Separation of copper(II) from palladium(II) and platinum(IV) by di(2-ethylhexyl)phosphoric acid-based liquid membranes during electrodialysis.* Journal of Membrane Science, 2006. **275**(1): p. 195-201.

155. Djouadi Belkada, F., et al., *Electrodialysis for fluoride and nitrate removal from synthesized photovoltaic industry wastewater.* Separation and Purification Technology, 2018. **204**: p. 108-115.

156. Mohammadi, T., A. Razmi, and M. Sadrzadeh, *Effect of operating parameters on Pb2+ separation from wastewater using electrodialysis.* Desalination, 2004. **167**: p. 379-385.

157. Tsiakis, P. and L.G. Papageorgiou, *Optimal design of an electrodialysis brackish water desalination plant.* Desalination, 2005. **173**(2): p. 173-186.

158. Sadrzadeh, M., A. Razmi, and T. Mohammadi, *Separation of monovalent, divalent and trivalent ions from wastewater at various operating conditions using electrodialysis.* Desalination, 2007. **205**(1): p. 53-61.

159.     Zou, S. and Z. He, *Electrodialysis recovery of reverse-fluxed fertilizer draw solute during forward osmosis water treatment.* Chemical Engineering Journal, 2017. **330**: p. 550-558.

160.     Belashova, E., et al., *Impact of cation-exchange membrane scaling nature on the electrochemical characteristics of membrane system.* Separation and Purification Technology, 2017. **189**: p. 441-448.

161.     Ren, M., et al., *Concentration and treatment of ceric ammonium nitrate wastewater by integrated electrodialysis-vacuum membrane distillation process.* Chemical Engineering Journal, 2018. **351**: p. 721-731.

162.     Zhang, Y., et al., *Selectrodialysis: Fractionation of divalent ions from monovalent ions in a novel electrodialysis stack.* Separation and Purification Technology, 2012. **88**: p. 191-201.

163.     Gil, G.-C., et al., *Operational parameters affecting the performannce of a mediator-less microbial fuel cell.* Biosensors and Bioelectronics, 2003. **18**(4): p. 327-334.

164.     Li, M., et al., *Microbial fuel cell (MFC) power performance improvement through enhanced microbial electrogenicity.* Biotechnology Advances, 2018. **36**(4): p. 1316-1327.

165.     Ge, Z. and Z. He, *Long-term performance of a 200 liter modularized microbial fuel cell system treating municipal wastewater: treatment, energy, and cost.* Environmental Science: Water Research & Technology, 2016. **2**(2): p. 274-281.

166.     Zou, S. and Z. He, *Efficiently "pumping out" value-added resources from wastewater by bioelectrochemical systems: A review from energy perspectives.* Water Research, 2018. **131**: p. 62-73.

167.     Cai, T., et al., *Application of advanced anodes in microbial fuel cells for power generation: A review.* Chemosphere, 2020. **248**: p. 125985.

168.     Chakraborty, I., et al., *Waste-derived biochar: Applications and future perspective in microbial fuel cells.* Bioresource Technology, 2020. **312**: p. 123587.

169.     Singh, S.K., C. Sharma, and A. Maiti, *A comprehensive review of standalone and hybrid forward osmosis for water treatment: Membranes and recovery strategies of draw solutions.* Journal of Environmental Chemical Engineering, 2021. **9**(4): p. 105473.

170.     Rood, B., et al., *Forward osmosis with an algal draw solution to concentrate municipal wastewater and recover resources.* Water Environment Research, 2020. **92**(5): p. 689-697.

171.     Cai, Y. and X.M. Hu, *A critical review on draw solutes development for forward osmosis.* Desalination, 2016. **391**: p. 16-29.

172.     Kim, J.E., et al., *Techno-economic assessment of fertiliser drawn forward osmosis process for greenwall plants from urban wastewater.* Process Safety and Environmental Protection, 2019. **127**: p. 180-188.

173. Zou, S. and Z. He, *Enhancing wastewater reuse by forward osmosis with self-diluted commercial fertilizers as draw solutes.* Water Research, 2016. **99**: p. 235-243.

174. Ly, Q.V., et al., *Characteristics and influencing factors of organic fouling in forward osmosis operation for wastewater applications: A comprehensive review.* Environment International, 2019. **129**: p. 164-184.

175. Suwaileh, W., et al., *Forward osmosis membranes and processes: A comprehensive review of research trends and future outlook.* Desalination, 2020. **485**: p. 114455.

176. Ang, W.L., et al., *Forward osmosis research trends in desalination and wastewater treatment: A review of research trends over the past decade.* Journal of Water Process Engineering, 2019. **31**: p. 100886.

177. Qin, M. and Z. He, *Resource recovery by osmotic bioelectrochemical systems towards sustainable wastewater treatment.* Environmental Science: Water Research & Technology, 2017. **3**(4): p. 583-592.

178. Zhang, F., K.S. Brastad, and Z. He, *Integrating Forward Osmosis into Microbial Fuel Cells for Wastewater Treatment, Water Extraction and Bioelectricity Generation.* Environmental Science & Technology, 2011. **45**(15): p. 6690-6696.

179. Qin, M., et al., *Understanding electricity generation in osmotic microbial fuel cells through integrated experimental investigation and mathematical modeling.* Bioresource Technology, 2015. **195**: p. 194-201.

180. Liu, J., et al., *Integrating microbial fuel cells with anaerobic acidification and forward osmosis membrane for enhancing bio-electricity and water recovery from low-strength wastewater.* Water Research, 2017. **110**: p. 74-82.

181. Ismail, Z.Z. and M.A. Ibrahim, *Desalination of oilfield produced water associated with treatment of domestic wastewater and bioelectricity generation in microbial osmotic fuel cell.* Journal of Membrane Science, 2015. **490**: p. 247-255.

182. Yuan, H., I.M. Abu-Reesh, and Z. He, *Enhancing desalination and wastewater treatment by coupling microbial desalination cells with forward osmosis.* Chemical Engineering Journal, 2015. **270**: p. 437-443.

183. Yuan, H., I.M. Abu-Reesh, and Z. He, *Mathematical modeling assisted investigation of forward osmosis as pretreatment for microbial desalination cells to achieve continuous water desalination and wastewater treatment.* Journal of Membrane Science, 2016. **502**: p. 116-123.

184. Song, Y.-H., et al., *Nutrients removal and recovery from anaerobically digested swine wastewater by struvite crystallization without chemical additions.* Journal of Hazardous Materials, 2011. **190**(1): p. 140-149.

185.    Achilli, A., T.Y. Cath, and A.E. Childress, *Selection of inorganic-based draw solutions for forward osmosis applications.* Journal of Membrane Science, 2010. **364**(1-2): p. 233-41.

186.    Wang, Z. and Z. He, *Demystifying terms for understanding bioelectrochemical systems towards sustainable wastewater treatment.* Current Opinion in Electrochemistry, 2020. **19**: p. 14-19.

187.    Oh, S.-H., et al., *Nanoparticle charge affects water and reverse salt fluxes in forward osmosis process.* Desalination, 2018. **438**: p. 10-18.

188.    Tansel, B., et al., *Significance of hydrated radius and hydration shells on ionic permeability during nanofiltration in dead end and cross flow modes.* Separation and Purification Technology, 2006. **51**(1): p. 40-47.

189.    Zhang, L., et al., *Simultaneous electricity generation and nitrogen and carbon removal in single-chamber microbial fuel cell for high-salinity wastewater treatment.* Journal of Cleaner Production, 2020. **276**: p. 123203.

190.    Lee, J., E. Kim, and S. Hwang, *Effects of inhibitions by sodium ion and ammonia and different inocula on acetate-utilizing methanogenesis: Methanogenic activity and succession of methanogens.* Bioresource Technology, 2021. **334**: p. 125202.

191.    Qin, M. and Z. He, *Self-supplied ammonium bicarbonate draw solute for achieving wastewater treatment and recovery in a microbial electrolysis cell-forward osmosis-coupled system.* Environmental Science & Technology Letters, 2014. **1**(10): p. 437-441.

192.    Qin, M., et al., *Passive separation of recovered ammonia from catholyte for reduced energy consumption in microbial electrolysis cells.* Chemical Engineering Journal, 2018. **334**: p. 2303-2307.

193.    Ferby, M., S. Zou, and Z. He, *Reduction of reverse solute flux induced solute buildup in the feed solution of forward osmosis.* Environmental Science: Water Research & Technology, 2020. **6**(3): p. 423-435.

194.    Kondusamy, D. and A.S. Kalamdhad, *Pre-treatment and anaerobic digestion of food waste for high rate methane production – A review.* Journal of Environmental Chemical Engineering, 2014. **2**(3): p. 1821-1830.

195.    Li, W., et al., *Two-phase anaerobic digestion of municipal solid wastes enhanced by hydrothermal pretreatment: Viability, performance and microbial community evaluation.* Applied Energy, 2017. **189**: p. 613-622.

196.    Aghapour Aktij, S., et al., *Feasibility of membrane processes for the recovery and purification of bio-based volatile fatty acids: A comprehensive review.* Journal of Industrial and Engineering Chemistry, 2020. **81**: p. 24-40.

197. González-García, I., et al., *Improved anaerobic digestion of swine manure by simultaneous ammonia recovery using gas-permeable membranes.* Water Research, 2021. **190**: p. 116789.

198. Liu, Y., et al., *The roles of free ammonia (FA) in biological wastewater treatment processes: A review.* Environment International, 2019. **123**: p. 10-19.

199. Lu, Y., et al., *Effect of pH on volatile fatty acid production from anaerobic digestion of potato peel waste.* Bioresource Technology, 2020. **316**: p. 123851.

200. Chen, Y., J.J. Cheng, and K.S. Creamer, *Inhibition of anaerobic digestion process: A review.* Bioresource Technology, 2008. **99**(10): p. 4044-4064.

201. Yenigün, O. and B. Demirel, *Ammonia inhibition in anaerobic digestion: A review.* Process Biochemistry, 2013. **48**(5): p. 901-911.

202. Shi, X., et al., *Effects of free ammonia on volatile fatty acid accumulation and process performance in the anaerobic digestion of two typical bio-wastes.* Journal of Environmental Sciences, 2017. **55**: p. 49-57.

203. Peng, X., et al., *Long-term high-solids anaerobic digestion of food waste: Effects of ammonia on process performance and microbial community.* Bioresource Technology, 2018. **262**: p. 148-158.

204. Xie, M., et al., *Membrane-based processes for wastewater nutrient recovery: Technology, challenges, and future direction.* Water Research, 2016. **89**: p. 210-221.

205. Fortunato, L., et al., *Textile dye wastewater treatment by direct contact membrane distillation: Membrane performance and detailed fouling analysis.* Journal of Membrane Science, 2021. **636**: p. 119552.

206. Xu, B. and Z. He, *Ammonia recovery from simulated anaerobic digestate using a two-stage direct contact membrane distillation process.* Water Environment Research, 2021. **93**(9): p. 1619-1626.

207. Wang, X., et al., *Simultaneous recovery of ammonium and phosphorus via the integration of electrodialysis with struvite reactor.* Journal of Membrane Science, 2015. **490**: p. 65-71.

208. Chalmers Brown, R., et al., *Overcoming nutrient loss during volatile fatty acid recovery from fermentation media by addition of electrodialysis to a polytetrafluoroethylene membrane stack.* Bioresource Technology, 2020. **301**: p. 122543.

209. Ray, H., F. Perreault, and T.H. Boyer, *Rejection of nitrogen species in real fresh and hydrolyzed human urine by reverse osmosis and nanofiltration.* Journal of Environmental Chemical Engineering, 2020. **8**(4): p. 103993.

210.    Babin, A., et al., *A closer look on the development and commercialization of membrane contactors for mass transfer and separation processes.* Separation and Purification Technology, 2019. **227**: p. 115679.

211.    Park, H.J., et al., *Experimental Study on the Selective Removal of SO2 from a Ship Exhaust Gas Stream Using a Membrane Contactor.* Industrial & Engineering Chemistry Research, 2019. **58**(32): p. 14897-14905.

212.    Ravishankar, H., et al., *Silicone membrane contactor for selective volatile fatty acid and alcohol separation.* Process Safety and Environmental Protection, 2021. **148**: p. 125-136.

213.    Licon Bernal, E.E., et al., *Valorization of ammonia concentrates from treated urban wastewater using liquid–liquid membrane contactors.* Chemical Engineering Journal, 2016. **302**: p. 641-649.

214.    Yesil, H., B. Calli, and A.E. Tugtas, *A hybrid dry-fermentation and membrane contactor system: Enhanced volatile fatty acid (VFA) production and recovery from organic solid wastes.* Water Research, 2021. **192**: p. 116831.

215.    Tugtas, A.E., *Recovery of volatile fatty acids via membrane contactor using flat membranes: Experimental and theoretical analysis.* Waste Management, 2014. **34**(7): p. 1171-1178.

216.    Darestani, M., et al., *Hollow fibre membrane contactors for ammonia recovery: Current status and future developments.* Journal of Environmental Chemical Engineering, 2017. **5**(2): p. 1349-1359.

217.    Reig, M., et al., *Study of the operational parameters in the hollow fibre liquid-liquid membrane contactors process for ammonia valorisation as liquid fertiliser.* Separation and Purification Technology, 2021. **255**: p. 117768.

218.    Vecino, X., et al., *Liquid fertilizer production by ammonia recovery from treated ammonia-rich regenerated streams using liquid-liquid membrane contactors.* Chemical Engineering Journal, 2019. **360**: p. 890-899.

219.    Rezakazemi, M., S. Shirazian, and S.N. Ashrafizadeh, *Simulation of ammonia removal from industrial wastewater streams by means of a hollow-fiber membrane contactor.* Desalination, 2012. **285**: p. 383-392.

220.    Rongwong, W. and S. Sairiam, *A modeling study on the effects of pH and partial wetting on the removal of ammonia nitrogen from wastewater by membrane contactors.* Journal of Environmental Chemical Engineering, 2020. **8**(5): p. 104240.

221.    He, L., et al., *Enhanced ammonia resource recovery from wastewater using a novel flat sheet gas-permeable membrane.* Chemical Engineering Journal, 2020. **400**: p. 125338.

222.    Serra-Toro, A., et al., *Ammonia recovery from acidogenic fermentation effluents using a gas-permeable membrane contactor.* Bioresource Technology, 2022. **356**: p. 127273.

223. Reyhanitash, E., S.R.A. Kersten, and B. Schuur, *Recovery of Volatile Fatty Acids from Fermented Wastewater by Adsorption.* ACS Sustainable Chemistry & Engineering, 2017. **5**(10): p. 9176-9184.

224. Zeng, Q., et al., *Emerging electrochemistry-based process for sludge treatment and resources recovery: A review.* Water Research, 2022. **209**: p. 117939.

225. Yan, Z., et al., *Application of membrane distillation to anaerobic digestion effluent treatment: Identifying culprits of membrane fouling and scaling.* Science of The Total Environment, 2019. **688**: p. 880-889.

226. Wang, H., et al., *Membrane fouling mitigation in different biofilm membrane bioreactors with pre-anoxic tanks for treating mariculture wastewater.* Science of The Total Environment, 2020. **724**: p. 138311.

227. Varjani, S., *Prospective review on bioelectrochemical systems for wastewater treatment: Achievements, hindrances and role in sustainable environment.* Science of The Total Environment, 2022. **841**: p. 156691.

228. Sathe, S.M., et al., *A novel bio-electro-Fenton process for eliminating sodium dodecyl sulphate from wastewater using dual chamber microbial fuel cell.* Bioresource Technology, 2021. **341**: p. 125850.

229. Ferby, M., S. Zou, and Z. He, *Effects of draw solutes on an integrated forward osmosis— Microbial fuel cell system treating a synthetic wastewater.* Water Environment Research, 2022. **94**(11): p. e10802.

230. Hidayat, A.R.P., et al., *Recent development of double chamber microbial fuel cell for hexavalent chromium waste removal.* Journal of Environmental Chemical Engineering, 2022. **10**(3): p. 107505.

231. Uddin, M.J., Y.-K. Jeong, and W. Lee, *Microbial fuel cells for bioelectricity generation through reduction of hexavalent chromium in wastewater: A review.* International Journal of Hydrogen Energy, 2021. **46**(20): p. 11458-11481.

232. Chen, T., et al., *Ammonia-rich solution production from coal gasification gray water using Chemical-free Flow-Electrode capacitive deionization coupled with a monovalent cation exchange membrane.* Chemical Engineering Journal, 2022. **433**: p. 133780.

233. Dalu, T., et al., *River nutrient water and sediment measurements inform on nutrient retention, with implications for eutrophication.* Science of The Total Environment, 2019. **684**: p. 296-302.

234. Yahampath Arachchige Don, C.D.Y. and S. Babel, *Comparing the performance of microbial fuel cell with mechanical aeration and photosynthetic aeration in the cathode chamber.* International Journal of Hydrogen Energy, 2021. **46**(31): p. 16751-16761.

235. Quan, X.-c., Y.-p. Quan, and K. Tao, *Effect of anode aeration on the performance and microbial community of an air–cathode microbial fuel cell.* Chemical Engineering Journal, 2012. **210**: p. 150-156.

236. Zhang, G., D.-J. Lee, and F. Cheng, *Treatment of domestic sewage with anoxic/oxic membrane-less microbial fuel cell with intermittent aeration.* Bioresource Technology, 2016. **218**: p. 680-686.

237. Srivastava, P., et al., *Low-power energy harvester from constructed wetland-microbial fuel cells for initiating a self-sustainable treatment process.* Sustainable Energy Technologies and Assessments, 2021. **46**: p. 101282.

238. Li, M., et al., *Enhanced bioenergy recovery and nutrient removal from swine wastewater using an airlift-type photosynthetic microbial fuel cell.* Energy, 2021. **226**: p. 120422.

239. Zhang, D.-X., et al., *A tartrate-EDTA-Fe complex mediates electron transfer and enhances ammonia recovery in a bioelectrochemical-stripping system.* Environmental Science and Ecotechnology, 2022. **11**: p. 100186.

240. Park, Y., et al., *Understanding complete ammonium removal mechanism in single-chamber microbial fuel cells based on microbial ecology.* Science of The Total Environment, 2021. **764**: p. 144231.

241. Kuntke, P., et al., *Ammonium recovery and energy production from urine by a microbial fuel cell.* Water Research, 2012. **46**(8): p. 2627-2636.

242. Koffi, N.D.J. and S. Okabe, *Bioelectrochemical anoxic ammonium nitrogen removal by an MFC driven single chamber microbial electrolysis cell.* Chemosphere, 2021. **274**: p. 129715.

243. Merino-Jimenez, I., et al., *Enhanced MFC power production and struvite recovery by the addition of sea salts to urine.* Water Research, 2017. **109**: p. 46-53.

244. Hao, P., et al., *Gas/gas membrane contactors – An emerging membrane unit operation.* Journal of Membrane Science, 2014. **462**: p. 131-138.

245. Ahmad, N.A., et al., *CO2 removal using membrane gas absorption with PVDF membrane incorporated with POSS and SAPO-34 zeolite.* Chemical Engineering Research and Design, 2017. **118**: p. 238-247.

246. Zhu, Y., et al., *Review of ammonia recovery and removal from wastewater using hydrophobic membrane distillation and membrane contactor.* Separation and Purification Technology, 2024. **328**: p. 125094.

247. Xu, P., et al., *Hydrophilic membrane contactor for improving selective removal of SO2 by NaOH solution.* Separation and Purification Technology, 2020. **250**: p. 117134.

248. Rossi, R., et al., *Evaluation of Electrode and Solution Area-Based Resistances Enables Quantitative Comparisons of Factors Impacting Microbial Fuel Cell Performance.* Environmental Science & Technology, 2019. **53**(7): p. 3977-3986.

249. Yap, K.-L., et al., *Crucial roles of aeration and catalyst on caffeine removal and bioelectricity generation in a double chambered microbial fuel cell integrated electrocatalytic process.* Journal of Environmental Chemical Engineering, 2021. **9**(1): p. 104636.

250. Hiegemann, H., et al., *Inhibition of microbial fuel cell operation for municipal wastewater treatment by impact loads of free ammonia in bench- and 45L-scale.* Science of The Total Environment, 2018. **624**: p. 34-39.

251. Si, Z., D. Han, and J. Xiang, *Experimental investigation on the mechanical vapor recompression evaporation system coupled with multiple vacuum membrane distillation modules to treat industrial wastewater.* Separation and Purification Technology, 2021. **275**: p. 119178.

252. Sharma, A., et al., *Factors affecting hydrogen production in microbial electrolysis cell (MEC): A review.* International Journal of Hydrogen Energy, 2024. **61**: p. 1473-1484.

253. Kadier, A., et al., *A comprehensive review of microbial electrolysis cells (MEC) reactor designs and configurations for sustainable hydrogen gas production.* Alexandria Engineering Journal, 2016. **55**(1): p. 427-443.

254. Escapa, A., et al., *Performance of a continuous flow microbial electrolysis cell (MEC) fed with domestic wastewater.* Bioresource Technology, 2012. **117**: p. 55-62.

255. Shen, R., et al., *Microbial electrolysis treatment of post-hydrothermal liquefaction wastewater with hydrogen generation.* Applied Energy, 2018. **212**: p. 509-515.

256. Ndayisenga, F., et al., *Thermophilic-operating environment promotes hydrogen-producing microbial growth in a lignocellulose-fed DF-MEC system for enhanced biohydrogen evolution.* Process Safety and Environmental Protection, 2022. **167**: p. 213-224.

257. Lu, Y.R. and P.A. Nikrityuk, *Steam methane reforming driven by the Joule heating.* Chemical Engineering Science, 2022. **251**: p. 117446.

258. Wang, X., et al., *Ni/Fe based electrocatalyst for highly-efficient anion exchange membrane water electrolysis.* Journal of Power Sources, 2024. **591**: p. 233819.

259. Hasibar, B., et al., *Increasing biohydrogen production with the use of a co-culture inside a microbial electrolysis cell.* Biochemical Engineering Journal, 2020. **164**: p. 107802.

260. Sarmin, S., et al., *Significant improvement of power generation through effective substrate-inoculum interaction mechanism in microbial fuel cell.* Journal of Power Sources, 2021. **484**: p. 229285.

261. Cui, W., et al., *Hydrogen production in single-chamber microbial electrolysis cell under high applied voltages.* Science of The Total Environment, 2021. **780**: p. 146597.

262. Liu, H., et al., *Configuration and rapid start-up of a novel combined microbial electrolytic process treating fecal sewage.* Science of The Total Environment, 2020. **705**: p. 135986.

263. Gil-Carrera, L., et al., *Microbial electrolysis cell scale-up for combined wastewater treatment and hydrogen production.* Bioresource Technology, 2013. **130**: p. 584-591.

264. Guerrero-Sodric, O., J.A. Baeza, and A. Guisasola, *Exploring key operational factors for improving hydrogen production in a pilot-scale microbial electrolysis cell treating urban wastewater.* Chemical Engineering Journal, 2023. **469**: p. 144001.

265. Liang, D., et al., *Efficient hydrogen recovery with CoP-NF as cathode in microbial electrolysis cells.* Applied Energy, 2020. **264**: p. 114700.

266. Ghasemi, B., et al., *Introducing an affordable catalyst for biohydrogen production in microbial electrolysis cells.* Journal of Bioscience and Bioengineering, 2020. **129**(1): p. 67-76.

267. Carlotta-Jones, D.I., et al., *Improved hydrogen gas production in microbial electrolysis cells using inexpensive recycled carbon fibre fabrics.* Bioresource Technology, 2020. **304**: p. 122983.

268. Jaziri, N., et al., *A comprehensive review of Thermoelectric Generators: Technologies and common applications.* Energy Reports, 2020. **6**: p. 264-287.

269. Xu, S., et al., *High-Performance PEDOT:PSS Flexible Thermoelectric Materials and Their Devices by Triple Post-Treatments.* Chemistry of Materials, 2019. **31**(14): p. 5238-5244.

270. Liu, K., et al., *High-performance and integrated design of thermoelectric generator based on concentric filament architecture.* Journal of Power Sources, 2018. **393**: p. 161-168.

271. Yuan, Z., et al., *Screen-printed radial structure micro radioisotope thermoelectric generator.* Applied Energy, 2018. **225**: p. 746-754.

272. Chen, L. and J. Lee, *Efficiency enhancement of an industrial-scale thermoelectric generator system by periodically inputting thermal power.* Energy Conversion and Management, 2016. **119**: p. 75-80.

273. Shen, Z.-G., L.-L. Tian, and X. Liu, *Automotive exhaust thermoelectric generators: Current status, challenges and future prospects.* Energy Conversion and Management, 2019. **195**: p. 1138-1173.

274. Luo, D., Z. Sun, and R. Wang, *Performance investigation of a thermoelectric generator system applied in automobile exhaust waste heat recovery.* Energy, 2022. **238**: p. 121816.

275.     Yuan, D., et al., *Technology method and functional characteristics of road thermoelectric generator system based on Seebeck effect.* Applied Energy, 2023. **331**: p. 120459.

276.     Mytafides, C.K., et al., *High-Power All-Carbon Fully Printed and Wearable SWCNT-Based Organic Thermoelectric Generator.* ACS Applied Materials & Interfaces, 2021. **13**(9): p. 11151-11165.

277.     Meng, F., L. Chen, and F. Sun, *A numerical model and comparative investigation of a thermoelectric generator with multi-irreversibilities.* Energy, 2011. **36**(5): p. 3513-3522.

278.     Liu, A., et al., *Enhancing the performance of TEG system coupled with PCMs by regulating the interfacial thermal conduction.* Energy Reports, 2020. **6**: p. 1942-1949.

279.     Kidegho, G., et al., *Evaluation of thermal interface materials in mediating PV cell temperature mismatch in PV–TEG power generation.* Energy Reports, 2021. **7**: p. 1636-1650.

280.     Jain, A. and Z. He, *Improving hydrogen production in microbial electrolysis cells through hydraulic connection with thermoelectric generators.* Process Biochemistry, 2020. **94**: p. 51-57.

281.     Jain, A. and Z. He, *Powering microbial electrolysis cells by electricity generation from simulated waste heat of anaerobic digesters using thermoelectric generators.* International Journal of Hydrogen Energy, 2020. **45**(7): p. 4065-4072.

282.     Chen, Y., et al., *H2 production by the thermoelectric microconverter coupled with microbial electrolysis cell.* International Journal of Hydrogen Energy, 2016. **41**(48): p. 22760-22768.

283.     Sun, M., et al., *An MEC-MFC-Coupled System for Biohydrogen Production from Acetate.* Environmental Science & Technology, 2008. **42**(21): p. 8095-8100.

284.     Wang, Y.-Z., et al., *Influence of initial anolyte pH and temperature on hydrogen production through simultaneous saccharification and fermentation of lignocellulose in microbial electrolysis cell.* International Journal of Hydrogen Energy, 2017. **42**(36): p. 22663-22670.

285.     Yan, Y., et al., *Spatially heterogeneous propionate conversion towards electricity in bioelectrochemical systems.* Journal of Power Sources, 2020. **449**: p. 227557.

286.     Lim, S.S., et al., *Impact of applied cell voltage on the performance of a microbial electrolysis cell fully catalysed by microorganisms.* International Journal of Hydrogen Energy, 2020. **45**(4): p. 2557-2568.

287.     Yang, N., H. Hafez, and G. Nakhla, *Impact of volatile fatty acids on microbial electrolysis cell performance.* Bioresource Technology, 2015. **193**: p. 449-455.

# Appendix A: Supplementary Material for Reduction of Reverse Solute Flux Induced Solute Buildup in the Feed Solution of Forward Osmosis (Chapter 2)

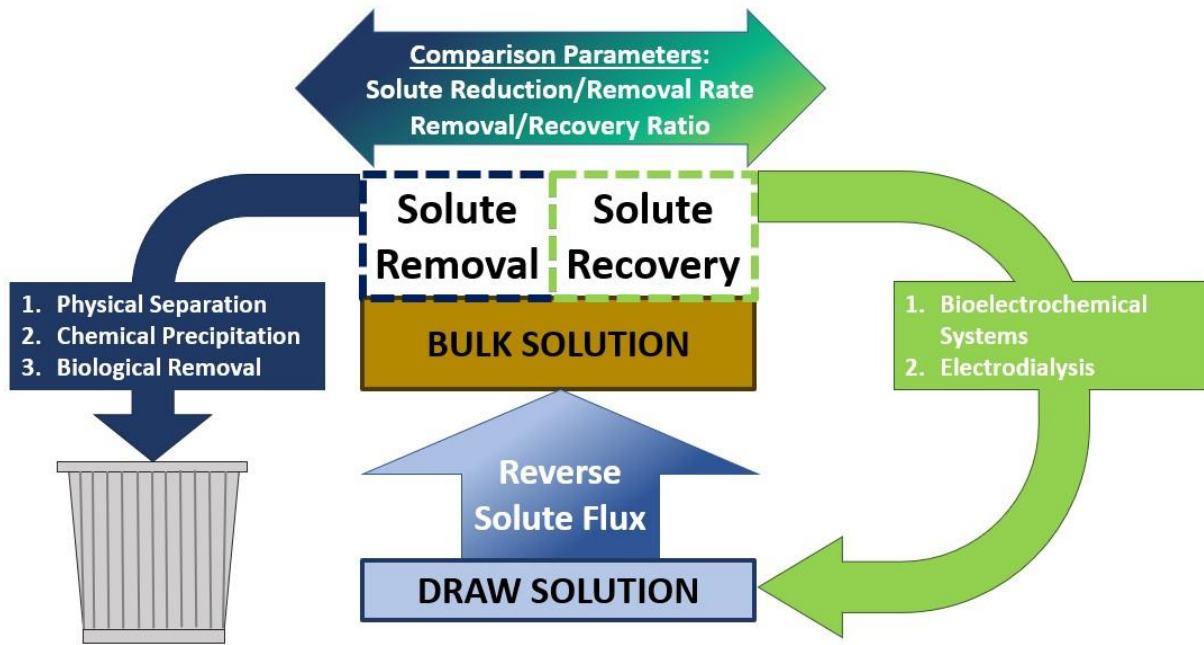Total Pages: 4 excluding cover page

Total Figures: 1

Total Tables: 2

**Figure A.1**    Graphical Abstract

***Solute Buildup and Concentrating Effect***

Solute buildup ($SBU$) (g m$^{-2}$ h$^{-1}$) is used to quantify the solute concentration due to accumulation cause by RSF and can be calculated using Eq. (A.1)

$$SBU = \frac{(n_{f,F} - n_{i,F}) \times MW}{A \times t}$$

(A.1)

where $n_{i,F}$ and $n_{f,F}$ represent the DS in the feed solution's initial and final mole, respectively; and MW is the molecular weight of the solute [173].

The concentrating effect (*CE*) quantitatively describes the effect of water recovery on the solute concentration, if already present, in the feed solution (Eq. (A.2)):

$$CE = \frac{V_{recovered} \times C_{i,F}}{A \times t}$$

(A.2)

Note that CE (g m$^{-2}$ h$^{-1}$) utilizes the amount of recovered water - $V_{recovered}$ (L) and the initial concentration of the feed solution - $C_{i,F}$ (g L$^{-1}$) to find a rate with both the membrane's structural parameter and time. These two variables can be used to determine the movement of solute ($J_s$) across the membrane by subtracting the *SBU* from the *CE*, unless DI water is used as the feed solution resulting in $J_s$ = *SBU* [89].

***Additional Information on Mass Balances***

***Physical Separation Case Study***

In order to showcase the use of the two proposed parameters- solute removal/recovery rate (SRR) and removal/recovery ratio (ReR), a mass balance was completed on the osmotic membrane bioreactor (OMBR) of a previous study [123]. The data used to generate Figure 3A was both calculated and provided (Table A.1).

**Table A.1** Mass balance variable used for physical separation case study

| Mass Balance Variable* | Value |
| --- | --- |
| Average Water Flux | 3.5 LMH |
| Average Reverse Salt Flux | 0.03 g m$^{-2}$ h$^{-1}$ |
| Salinity Accumulation | 0.06 mS cm$^{-1}$ day$^{-1}$ |
| Mg$^{2+}$ Removal | 4.06 mg L$^{-1}$ |

\* Variables are either directly reported or calculated based on the data in the study

The salinity accumulation in the OMBR was determined as described by Eq. (A.3).

$$Accumulation = \frac{(TDS_f - TDS_i) * V}{\Delta t} = \frac{(EC_f * \alpha - EC_i * \alpha) * V}{\Delta t}$$ (A.3)

Where $EC_f$ and $EC_i$ represent the final and initial electrical conductivity (mS cm$^{-1}$), respectively; $\Delta t$ (days) represents the operation time; $\alpha$ is the conversion factor between conductivity and TDS; $TDS_f$ and $TDS_i$ represent the final and initial TDS (g L$^{-1}$) concentration; $V$ is the bioreactor's feed solution volume. MF flux used in the SRR calculation was estimated using a study that investigated MF flux rates compared to FO flux [124]. The draw solution concentration was considered in this assumption as well.

*Chemical Precipitation Case Study*

For the chemical precipitation case study, the information was both calculated and provided to generate Figure 2.4A (Table A.2). The mass balance was based off a previous FO study [119].

**Table A.2** Mass balance variable used for chemical separation case study

| Mass Balance Variable* | Value |
| --- | --- |
| Draw Solution Molarity (MgCl$_2$) | 0.5 M |
| Average Water Flux | 2.32 L m$^{-2}$ h$^{-1}$ |
| Average Reverse Salt Flux | 1.55 g m$^{-2}$ h$^{-1}$ |
| Struvite Precipitation | 0.39 g m$^{-2}$ h$^{-1}$ |

*  Variables are either directly reported or calculated based on the data in the study

This case study presented many of the details necessary to compare to other DS precipitation studies. The RSF was converted to more widely used units ($g\ m^{-2}\ h^{-1}$) to determine the other parameters. In the paper, the authors reported that ~25% of the DS precipitated as struvite. The struvite composition was determined using scanning electron microscopy-energy dispersive spectroscopy. In addition to struvite, it was reported that a portion of the $Mg^{2+}$ precipitated as $Mg(OH)_2$. With struvite being the precipitate of interest, the SRR would be calculated using Eq. (A.4).

$$SRR = \frac{C_{Mg,struvite} * V_{feed}}{A * \Delta t}$$

(A.4)

Where $C_{Mg,struvite}$ (m) is the concentration of magnesium precipitated as struvite, $V_{feed}$ is the volume of the concentrated feed solution. However, not enough information was provided to make this distinction and resulted in a slightly higher ReR. Based on information provided by the authors, the amount of reversed fluxed $Mg^{2+}$ that precipitated as struvite was assumed to be the ReR (0.25). The assumed ReR did not include $Mg^{2+}$ that was naturally present in the digested swine wastewater (feed). Moreover, removal techniques rely heavily on a precipitate being formed over the chemical purity. This caused us to consider calculating the SRR for this case study by manipulating the ReR parameter (Eq. A.5).

$$SRR = ReR * RSF$$

(A.5)

In the event that more information is provided, the ReR can be denoted if a particular precipitate is desired. This would suggest that future research could present ReR that determine how much of the reverse fluxed DS precipitated as one compound compared to another. For example, distinction between $Mg(OH)_2$ and struvite could help determine what operation conditions exist

[147]

when comparing removal efficacies between different studies that use $MgCl_2$ as a DS. This same concept would apply to other DS and precipitates, as well.

# Appendix B: Supplementary Material for Effects of Draw Solutes on an Integrated Forward Osmosis - Microbial Fuel Cell System Treating a Synthetic Wastewater (Chapter 3)

Total Pages: 4 excluding cover page
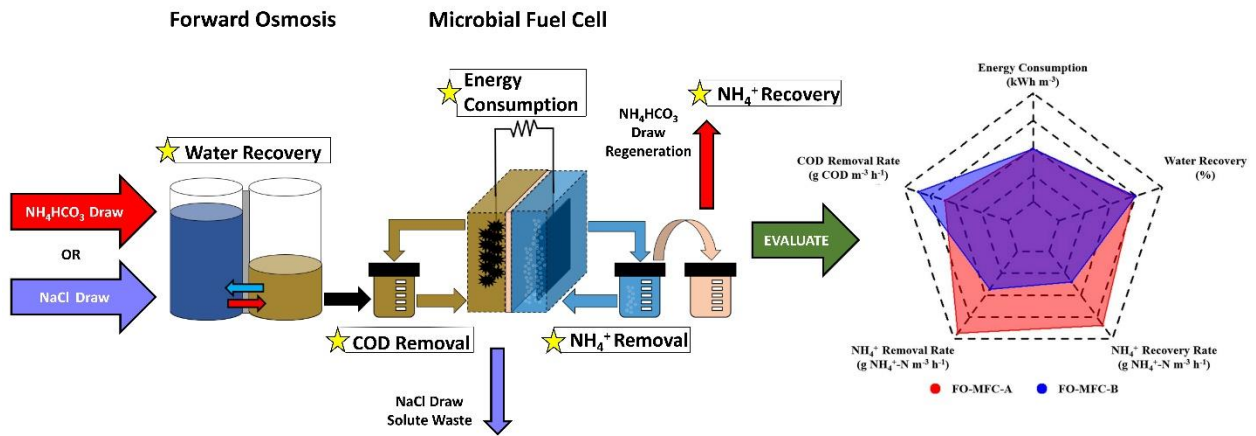
Total Figures: 3

Total Tables: 1



**Figure B.1**  Graphical Abstract

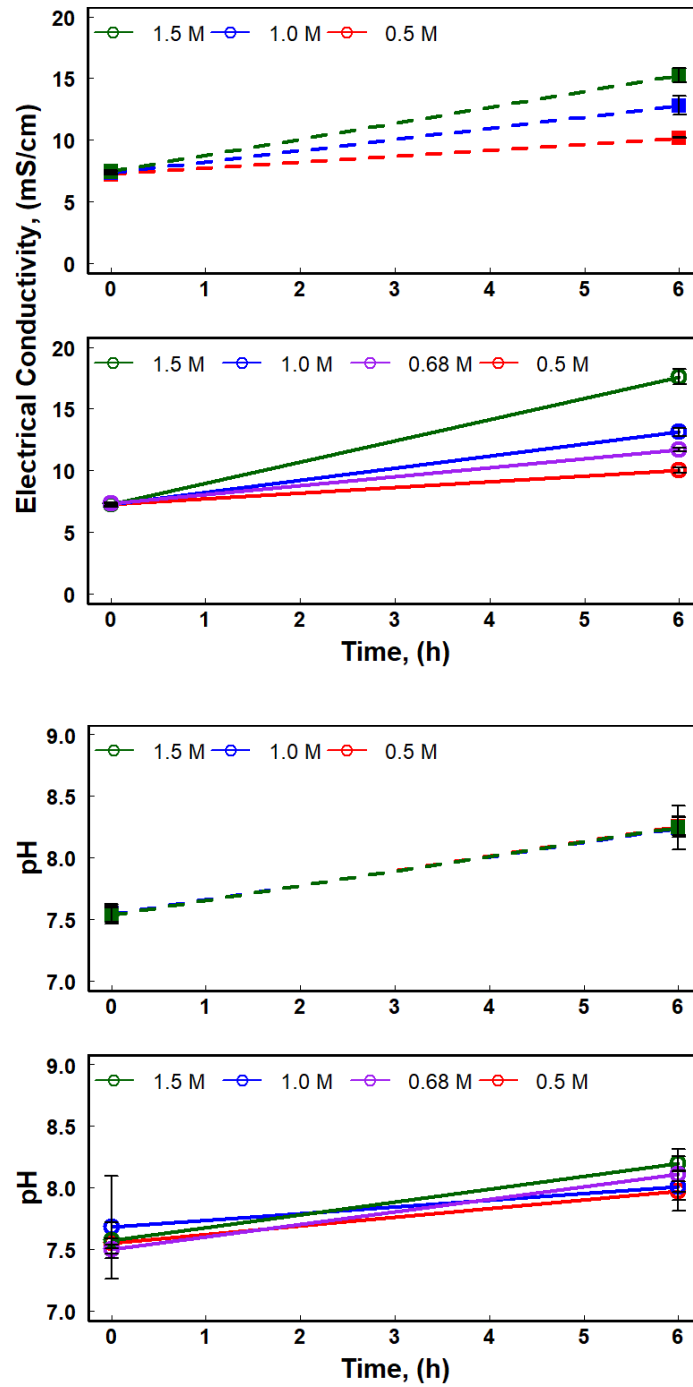*Initial and Final Electrical Conductivity and pH During FO Treatment*



**Figure B.2.** Electrical Conductivity and pH of feed solutions for $NH_4HCO_3$ and NaCl draw solution test.

*Statistical Comparison of Water Flux for NH₄HCO₃ and NaCl Draw Solutions*

**Table B.1** P-values for FO tests

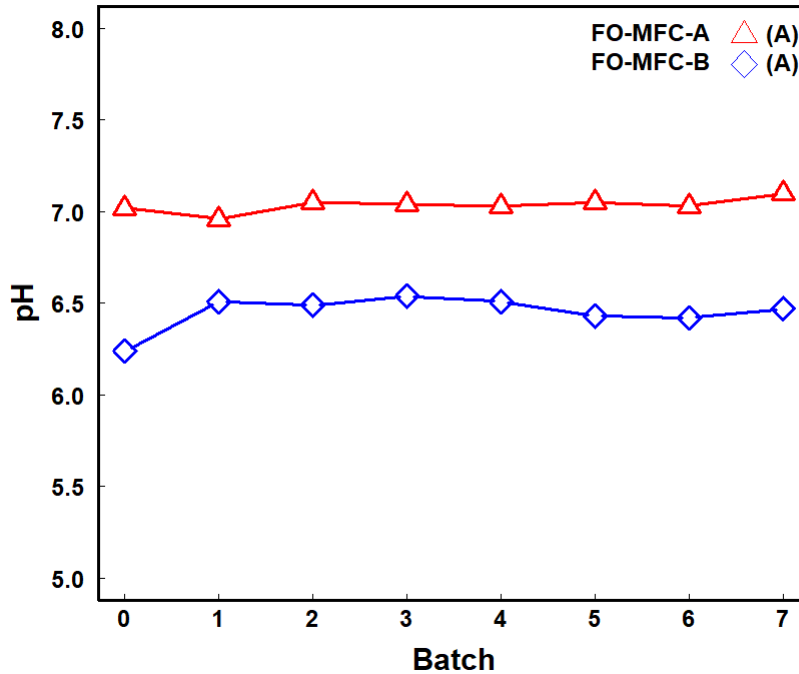| | 0.5 M NH4HCO3 | 1.0 M NH4HCO3 | 1.5 M NH4HCO3 | 0.5 M NaCl | 1.0 M NaCl | 1.5 M NaCl |
|---|---|---|---|---|---|---|
| 1.0 M NH4HCO3 | 3.2E-03 | - | - | - | - | - |
| 1.5 M NH4HCO3 | 3.0E-05 | 3.5E-03 | - | - | - | - |
| 0.5 M NaCl | 6.4E-04 | 1.6E-02 | 4.8E-04 | - | - | - |
| 1.0 M NaCl | 8.0E-05 | 1.1E-02 | 7.3E-01 | 1.5E-06 | - | - |
| 1.5 M NaCl | 6.3E-04 | 1.8E-03 | 1.5E-03 | 2.9E-05 | 4.8E-05 | - |
| 0.68 M NaCl | 3.5E-03 | 1.0E+00 | 3.6E-03 | 5.1E-04 | 1.0E-04 | 1.8E-05 |

*Anolyte pH during MFC treatment*



**Figure B.3.** Anolyte pH for 7 batch operation from FO-MFC-A and FO-MFC-B system.

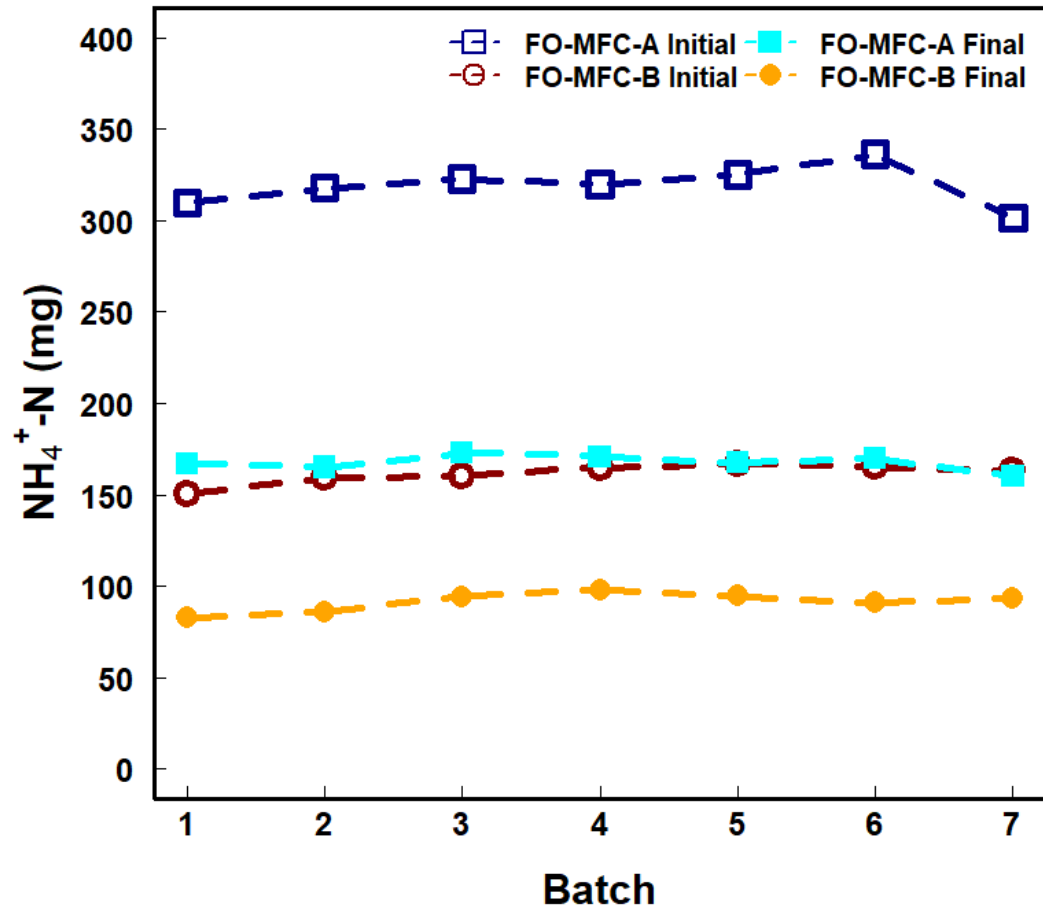*Initial and final Absolute mass of NH$_4^+$-N in anolyte for each batch*



**Figure B.4.** Initial and final NH$_4^+$-N mass in 7 batch operation from FO-MFC-A and FO-MFC-B system.

# Appendix C. Supplementary Material for Recovery of both Volatile Fatty Acids and Ammonium from Simulated Wastewater: Performance of Membrane Contactor and Understanding the Effects of Osmotic Distillation (Chapter 4)

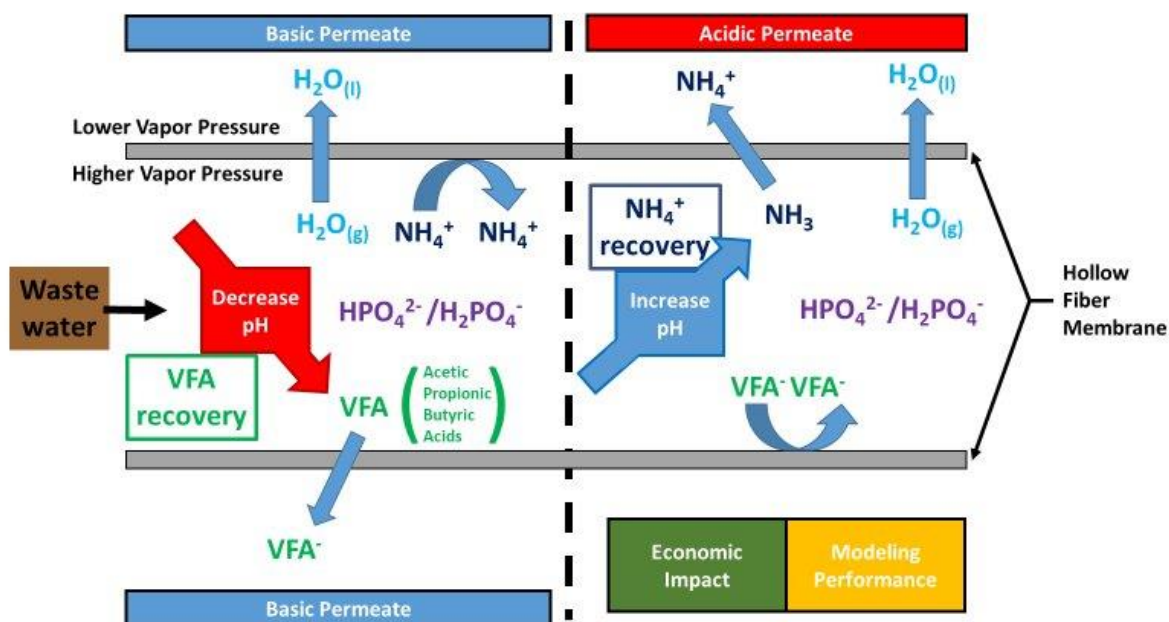Total pages: 5 excluding cover page

Total Figures: 4

Total Tables: 1
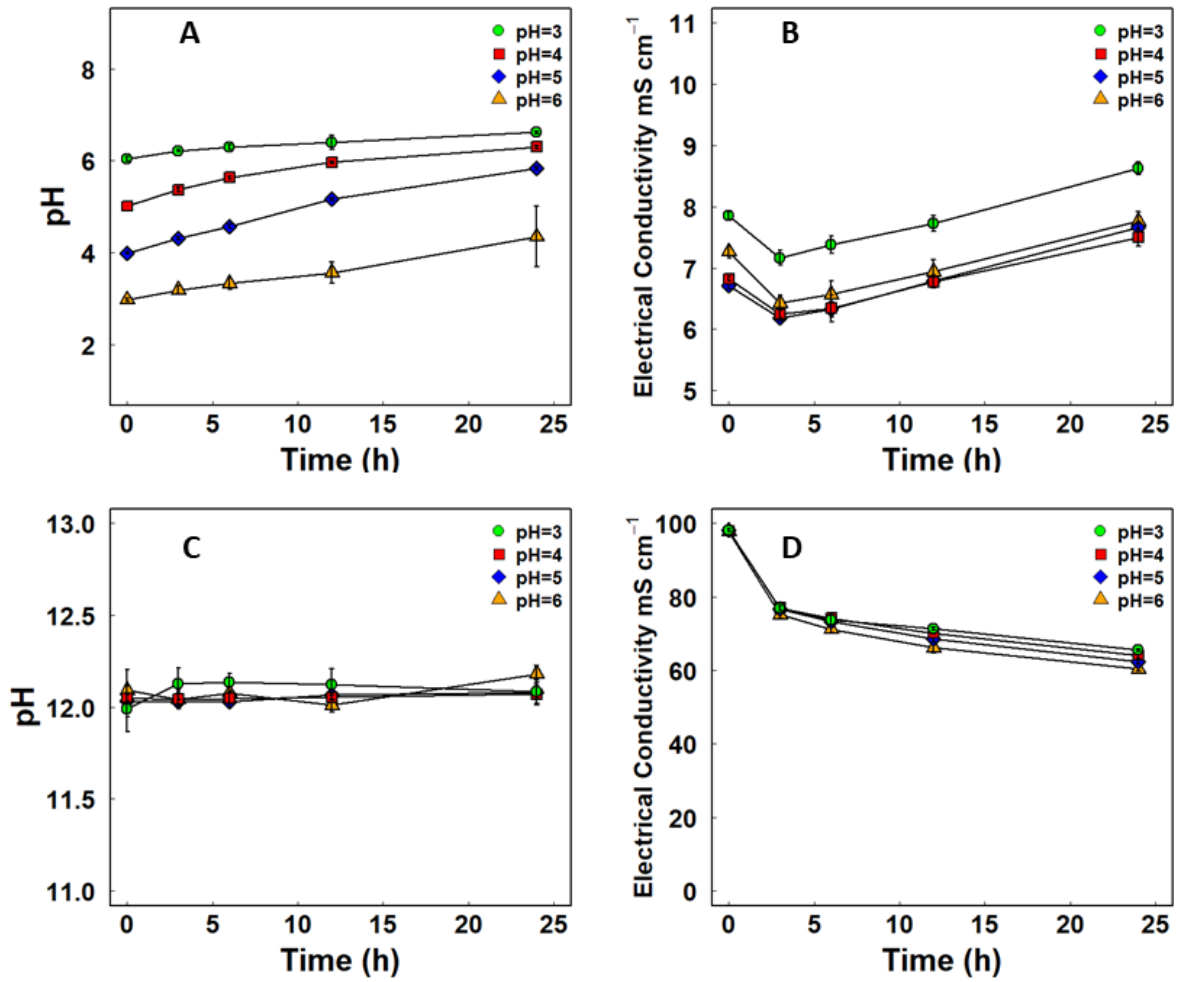


**Figure C.1** Graphical Abstract

**Figure C.2** (A-B) Feed pH and electrical conductivity data for VFA membrane contactor recovery and (C-D) permeate pH and electrical conductivity data for VFA membrane contactor recovery tests when the pH was adjusted from 3 to 6 and the permeate was maintained at 0.5 M NaOH.
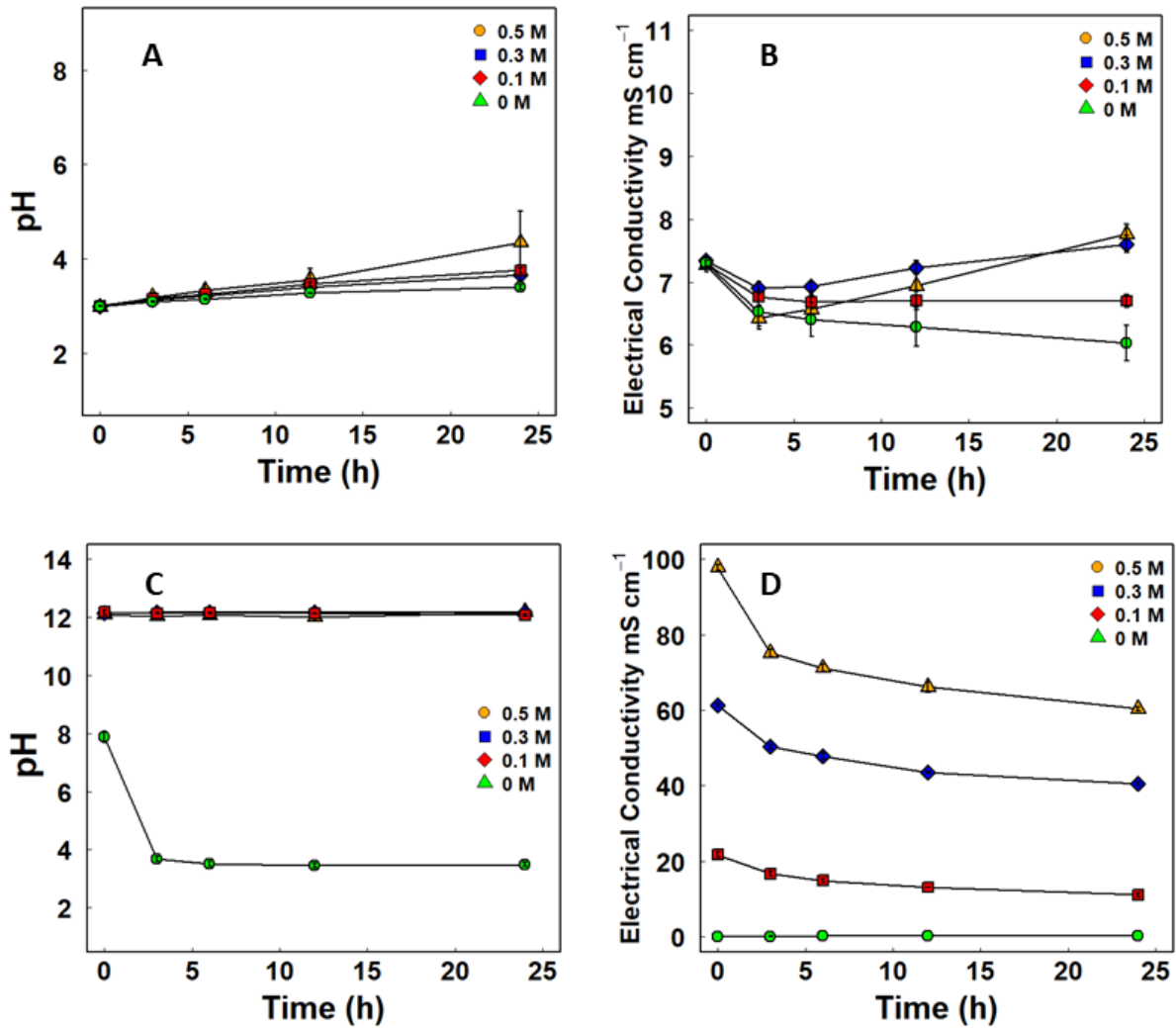
**Figure C.3** (A-B) Feed pH and electrical conductivity data for VFA membrane contactor recovery and (C-D) permeate pH and electrical conductivity data for VFA membrane contactor recovery tests when the permeate was adjusted from 0 M to 0.5 M NaOH and the feed pH=3 was maintained.
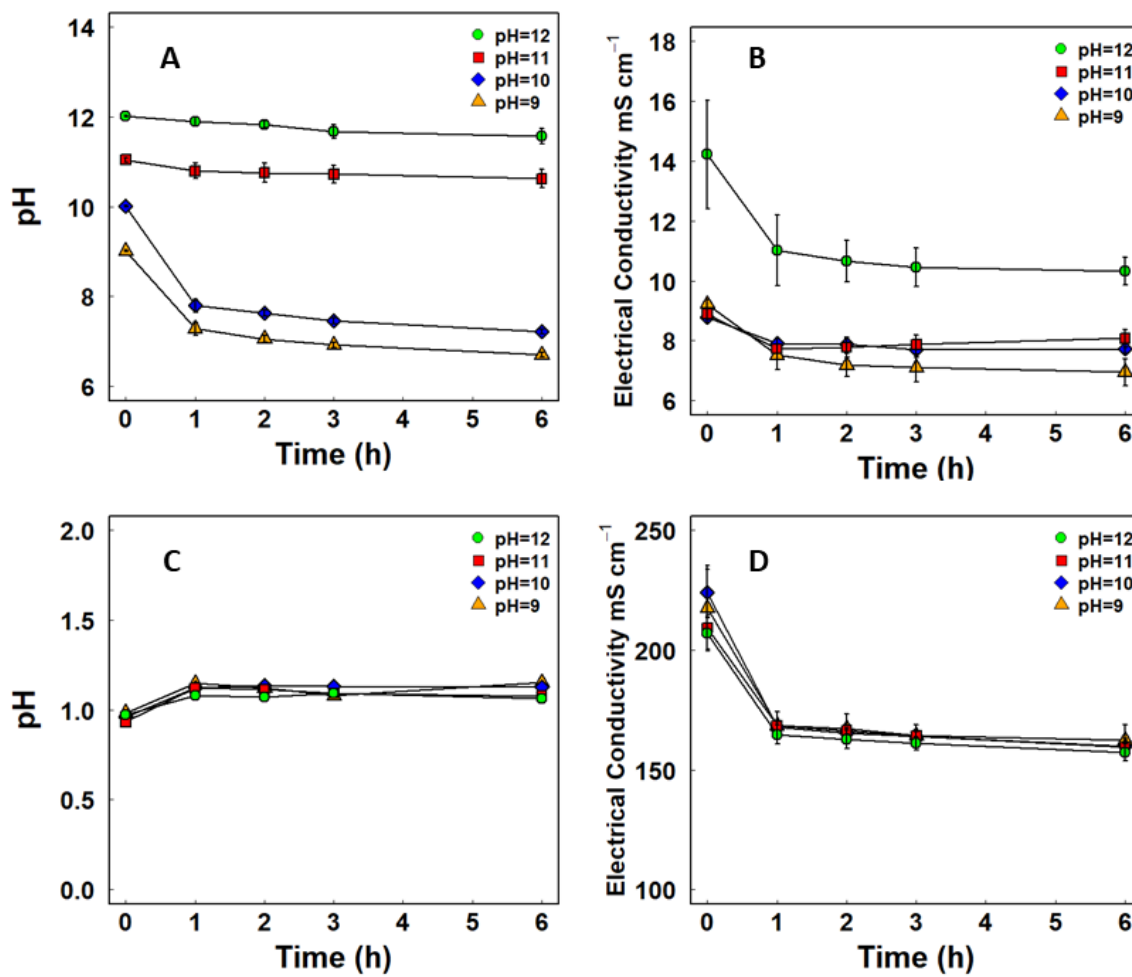
**Figure C.4** (A-B) Feed pH and electrical conductivity data for $NH_4^+$ membrane contactor recovery and (C-D) permeate pH and electrical conductivity data for $NH_4^+$ membrane contactor recovery tests when the pH was adjusted from 9 to 12 and the permeate was maintained at 0.5 M $H_2SO_4$.
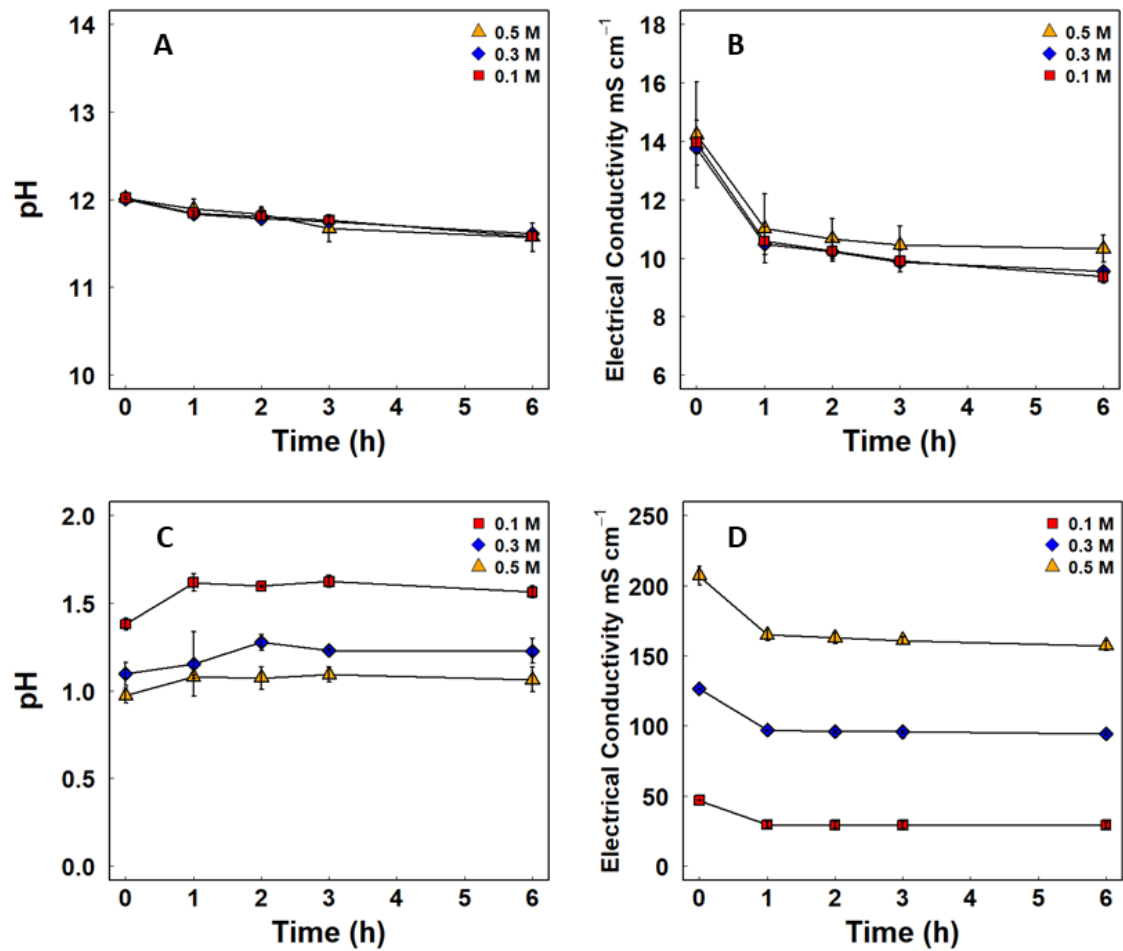
**Figure C.5** (A-B) Feed pH and electrical conductivity data for $NH_4^+$ membrane contactor recovery and (C-D) permeate pH and electrical conductivity data for $NH_4^+$ membrane contactor recovery tests when the permeate was adjusted from 0.1 M to 0.5 M $H_2SO_4$ and the feed pH=12 was maintained.

**Table C.1.** Cost for combined VFA and NH$_4^+$ recovery system based on acid and base cost for pH adjustment in each operation condition. For NH$_4^+$ recovery, Ai-iii represent the strength of the absorption solution strength from 0.1M – 0.5M H$_2$SO$_4$ and pi-iv represents the initial feed pH from 9-12. For VFA recovery, Ai-iv represent the strength of the absorption solution strength from 0M – 0.5M NaOH and pi-iv represents the initial feed pH from 3-6.

NH$_4^+$ recovery

| VFA recovery | | Ai | Aii | Aiii | pi | pii | piii | piv |
|---|---|---|---|---|---|---|---|---|
| | | 0.46 | 0.37 | 0.27 | 0.35 | 0.39 | 0.42 | 0.46 |
| Ai | 0.70 | 1.16 | 1.07 | 0.97 | 1.06 | 1.10 | 1.12 | 1.16 |
| Aii | 0.43 | 0.89 | 0.80 | 0.69 | 0.78 | 0.82 | 0.84 | 0.89 |
| Aiii | 0.15 | 0.61 | 0.52 | 0.41 | 0.50 | 0.54 | 0.56 | 0.61 |
| Aiv | 0.01 | 0.47 | 0.38 | 0.27 | 0.36 | 0.40 | 0.42 | 0.47 |
| pi | 0.70 | 1.16 | 1.07 | 0.97 | 1.06 | 1.10 | 1.12 | 1.16 |
| pii | 0.70 | 1.16 | 1.07 | 0.97 | 1.05 | 1.09 | 1.12 | 1.16 |
| piii | 0.71 | 1.17 | 1.08 | 0.97 | 1.06 | 1.10 | 1.12 | 1.17 |
| piv | 0.73 | 1.19 | 1.10 | 1.00 | 1.08 | 1.12 | 1.15 | 1.19 |

Color scale: 1.75 — 1.00 — 0.25